The Role of Variable Oceanographic and Environmental Conditions on Acoustic Tracking Effectiveness

by

Jeannette Bedard
B.Sc., Royal Roads Military College, 1994
M.Sc., University of Victoria, 2011

A Dissertation Submitted in Partial Fulfillment of the
Requirements for the Degree of

DOCTOR OF PHILOSOPHY

in the School of Earth and Ocean Sciences

Supervisory Committee

The Role of Variable Oceanographic and Environmental Conditions on Acoustic Tracking Effectiveness

by

Jeannette Bedard
B.Sc., Royal Roads Military College, 1994
M.Sc., University of Victoria, 2011

Supervisory Committee

Dr. Svein Vagle, Co-supervisor
(School of Earth and Ocean Sciences)

Dr. Stan Dosso, Co-Supervisor
(School of Earth and Ocean Sciences)

Dr. Richard Dewey, Departmental Member
(School of Earth and Ocean Sciences)

Dr. David Atkinson, Outside Member
(Department of Geography)

ABSTRACT

Examining fish behaviour through acoustic tracking is a technique being employed more and more. Typically, research using this method focuses on detections without fully considering the influence of both the physical and acoustic environment. Here we link the aquatic environment of Cumberland Sound with factors influencing the detection effectiveness of fish tracking equipment and found multi-path signal interference to be a major issue while seasonal variabilty had little impact. Cumberland Sound is a remote Arctic embayment, where three species of deep-water fish are currently tracked, that can be considered as two separate layers. Above the 300 m deep sill, the cold Baffin Island Current follows a geostrophic pattern, bending into the sound along the north shore, circulating before leaving along the south shore. The warm deep water is replenished from the recirculated arm of the West Greenland Current occasionally flowing over the sill and down to a stable depth. This influx of water prevents deep water hypoxia, allowing the deep-dwelling fish populations in the sound to thrive. To complement the work done in Cumberland Sound, a year-long study of the underwater soundscape of another Arctic coastal site, Cambridge Bay, Nunavut, was conducted over 2015. Unlike other Arctic locations considered to date, this site was louder when covered in ice with the loudest times occurring in April. Sounds of anthropogenic origin were found to dominate the soundscape with ten times more snowmobile traffic on ice than open water boat traffic.

Contents

List of Tables

List of Figures

ACKNOWLEDGEMENTS

Thank you to my supervisors Svein Vagle and Stan Dosso, for providing guidance and feedback throughout this project.

My thanks goes out to all who those have helped me complete this dissertation with whom this project may not have been possible. In particular, I would like to thank: David Atkinson, Iva Peklova, Kevin Hedges, Nigel Hussey, Aaron Fisk, Nick Hall-Patch, Mike Dempsey, Sarah Zimmerman, Jenifer Jackson, Bill Williams, Rob Cooke, Caitlin O'Neil, Emma Murowinski, Marlene Jefferies and Richard Dewey.

I would like to thank the Captain and crew of the R/V Nuliajuk, Ocean Networks Canada as well as the Ocean Tracking Network project.

Thanks also to my husband Gavin, for putting up with me working in the office for hours on end, and for providing guidance and a sounding board when required. I would also like to thank my daughter Anna for her patience and understanding whilst doing my work at home. And to my friends Alana, Christine and Amy for forcing me to occasionally do something fun.

Chapter 1

Introduction

Arctic marine ecosystems experience extremes in light and dark, heat and cold, ice cover and open water in addition to the tidal forces shared by more southern locations. These rhythms combine to create habitats where the link between biological processes and the physical environment are strong (Dayton et al., 1994). Even subtle hydrographic changes to that environment can profoundly impact the animals that reside there (Carmack and Wassmann, 2006). In addition to these physical forces, the underwater acoustic environment, or soundscape, also impacts how ecosystems function (Staaterman et al., 2013). For Arctic sites, times of ice cover versus open water can dramatically alter the local soundscape (Kinda et al., 2013).

Because direct observations of aquatic animals are difficult to obtain, especially at sites experiencing ice cover, implanting passive acoustic tags into these animals is a method gaining in popularity. This technique is providing new information about how animals live in their aquatic environments (Hussey et al., 2015; Lennox et al., 2017), which is especially important in polar ecosystems where climate change is occurring more rapidly and the animals that live there are more vulnerable due to their slow growth and low fecundity (Thomas et al., 2008).

By tagging these animals and recording detections, more information can be obtained beyond simple presence and absence. Multiple detections of the same animal can provide data on movement allowing inferences to be made about animal behaviours such as habitat use and predator/prey dynamics (Kessel et al., 2013). However, understanding the limitations of this technique puts the resulting data into context and prevents incorrect conclusions (Payne et al., 2010; Kessel et al., 2013). One major limitation is the detection range of the receivers which is variable and impacted by both the equipment and the local environment.

The objective of this thesis is to gain a better understanding of the link between Arctic coastal oceanography and soundscapes and the impact on the range of passive detection of acoustically-tagged fish. To achieve this, three main questions are posed and addressed:

1. What are the oceanographic processes that define the underwater environment in an Arctic coastal embayment?
2. What sounds dominate the underwater soundscape of the site?
3. How do the oceanography and soundscape impact acoustic tag function in the local environment?

By answering these questions, biological behaviour recorded by the acoustic tags can be put into context with the physical and acoustic environment. In this study in situ data collection, water sampling and acoustic ray-tracing modelling are used to obtain results.

1.1 Study Sites

The original intent of this research project was to consider all three questions at a single site, Cumberland Sound, a large embayment on the east coast of Baffin Island (Figure 1.1). The work was started as part of a cross-discipline team within the Ocean Tracking Network (OTN) (Cooke et al., 2011). Biologists addressing questions around habitat use for three species of fish were included in addition to oceanographers. However, at the end of the first year (summer 2012) all moored equipment was removed at the request of the local Inuit community, before any underwater acoustic recordings were made. Unfortunately, only a single year of mooring data was collected (2011-2012). Surface-based measurements were not part of the ban, allowing collection to continue resulting in three years of summer data (2011-2013).

As a result of being unable to collect acoustic data in Cumberland Sound, the soundscape component of this work was performed in Cambridge Bay (Figure 1.1), another Arctic coastal site. Cambridge Bay has an underwater platform collecting data as part of the Ocean Networks Canada (ONC) array. This platform hosts a variety of oceanographic instruments measuring aspects of the local environment as well as a continuously-recording hydrophone. Data from 2015 were chosen, because

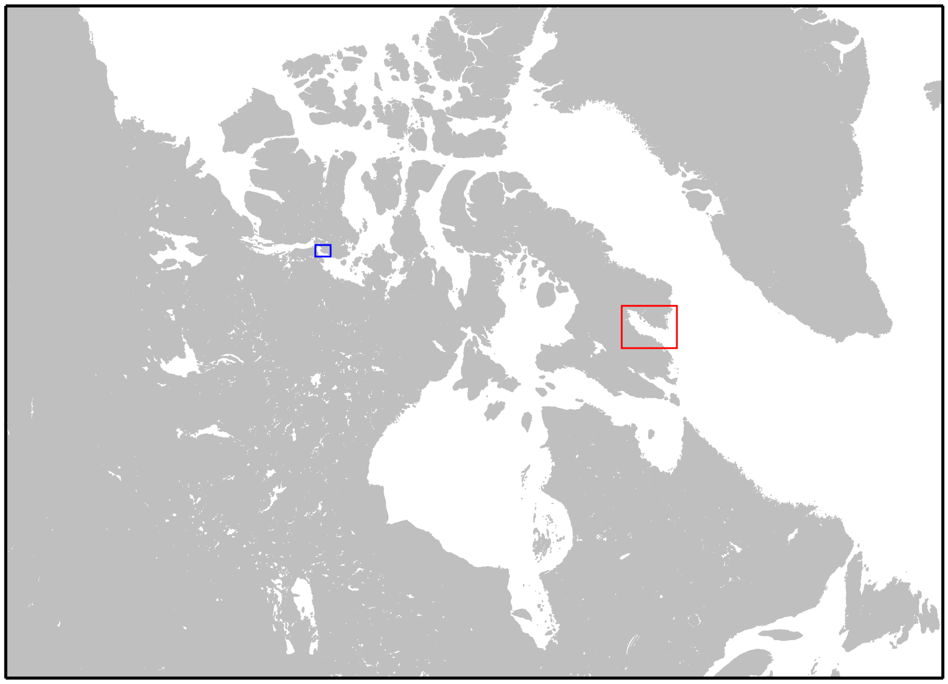

Figure 1.1: Relative locations of study sites. Red box is Cumberland Sound and blue box is Cambridge Bay.

the acoustic data were nearly complete (the exception being September 2015) and that year coincided with an acoustic range test of the same acoustic tags used in Cumberland Sound. The original intent of moving to this site was to expand the evaluation of range tests to a very shallow (∼9 m water depth) location. However, the range test data set proved to be unusable as it was heavily contaminated by a nearby ship running a 50 kHz sonar from May until September. This range test was abandoned and a shift was made to consider the soundscape instead.

Unfortunately, Cumberland Sound and Cambridge Bay are fundamentally different sites with only seasonal ice cover and their position within the Canadian Arctic Archipelago (CAA) in common. Cumberland Sound is a large embayment heavily influenced by outside water. The sound is ∼80 km wide by ∼250 km long with a 300 m deep sill and maximum depths of over 1400 m. In comparison Cambridge Bay is more complex in shape. Near the study site it is ∼4 km wide by ∼3 km long, with maximum depths of only 86 m.

There is an ongoing anthropogenic presence at both of these sites involving fishing activity and vehicle use. In Cumberland Sound, Greenland halibut (*Reinhardtius* *hippoglossodies*) is a fish species of commercial interest with population dynamics that are only beginning to be understood (Peklova et al., 2012). While in Cambridge Bay, vehicle noise at times dominates the aquatic environment which, in general, has been shown to have a negative effect on the fauna (Williams et al., 2015).

1.2 Outline of Thesis

This thesis is based on three papers written to address each of the questions posed above. Details of the methodologies used are presented in each paper.

1. The first paper (Chapter 2) discusses the outside influences on the water column of Cumberland Sound. This is the first oceanographic work in this location where even the bathymetry is not fully known. The water column in the sound is divided into two layers: the water above the 300 m deep sill, and the water below. Two different mechanisms are presented that bring in different water masses. The first is geostrophic flow cycling through the upper layer and the second is seasonal, intermittent deep water replenishment that prevents the bottom waters from becoming hypoxic. Local processes that contribute to mixing within the sound are also presented. This paper has been published as Bedard et al. (2015).

2. The second paper (Chapter 3) examines the variability in detection ranges of passive acoustic tags in an Arctic embayment. Three year-long range tests were performed with acoustic fish tags in Cumberland Sound, with tags programmed to transmit at known intervals deployed at a variety of ranges from receivers. Results from these range tests are linked with factors influencing the detection effectiveness using a simple ray tracing model. Multi-path interference is found to be a major issue impacting detections while seasonal variability is not an issue at this site. This paper will be submitted to Animal Biotelemetry.

3. The final paper (Chapter 4) presents results from a year-long study of the soundscape in Cambridge Bay. Unlike other Arctic locations considered to date, this site is louder when covered in ice with the loudest times occurring in April. Sounds of anthropogenic origin are found to dominate the soundscape with roughly ten times more snowmobile traffic on ice than open-water boat

traffic. Precipitation, wind and ice noise are the other major contributors and non-human biological sources are not found to be significant.

The following chapters were written as stand-alone papers with their own introduction, methods, results, discussion and conclusion sections.

Chapter 2

Outside influences on the water column of Cumberland Sound, Baffin Island

Cumberland Sound, host to a commercially viable fish population in the deepest depths, is a large embayment on the southeast coast of Baffin Island that opens to Davis Strait. Conductivity, temperature and depth profiles were collected during three summer field seasons (2011-2013) and two moorings were deployed during 2011-2012. Within the sound, salinity increases with increasing depth while water temperature cools reaching a minimum of -1.49 °C at roughly 100 m. Below 100 m, the water becomes both warmer and saltier. Temperature-salinity curves for each year followed a similar pattern, but the entire water column in Cumberland Sound cooled from 2011 to 2012, then warmed through the summer of 2013. Even though the sound's maximum depth is over a kilometre deeper than its sill, water in the entire sound is well oxygenated. A comparison of water masses within the sound and in Davis Strait shows that, above the sill, the sound is flooded with cold Baffin Island Current water following an intermittent geostrophic flow pattern entering the sound along the north coast and leaving along the south. Below the sill, replenishment is infrequent and includes water from both the Baffin Island Current and the West Greenland Current. Deep water replenishment occurred more frequently on spring tides, especially in the fall of 2011. Although the sound's circulation is controlled by outside currents, internal water modifying processes occur such as estuarine flow and wind-driven mixing.

2.1 Introduction

The tight link between physical and biological processes found in Arctic aquatic ecosystems (Dayton et al., 1994) creates an environment where even subtle hydrographic changes can profoundly impact local biological activity (Carmack and Wassmann, 2006). Located on the cusp of the Arctic Circle, Cumberland Sound's benthic ecosystem is especially vulnerable to change. Currents containing water from both the Pacific and Atlantic Oceans cross the sound's mouth (Jones et al., 2003), while its shallow sill is poised to cut off most of the water column. However, a kilometre below the depth of the sill, a permanent population of Greenland Halibut (*Reinhardtius hippoglossoides*) reside (Peklova et al., 2012). These fish are harvested in the only community-run commercial Greenland Halibut fishery in Nunavut, providing needed economic support to the small Inuit community of Pangnirtung. In addition, this fishery is being used as a model to create similar fisheries in other northern communities. As we will show, Cumberland Sound is periodically renewed by intrusions of dense, mixed shelf water supplying oxygen to support the Greenland Halibut and their associated ecosystem. The sound's renewal dynamics depend on the temperature and salinity of the currents passing across Cumberland Sound's mouth. As these currents change with our changing climate (Steiner et al., 2013), the sound's ecosystem will also change.

Previous observations of physical water properties within Cumberland Sound are sparse: a naturalist from the Smithsonian spent a winter there in 1877-78 (Kumlien, 1879) observing the flora and fauna while taking meteorological measurements, and in 1952, Dunbar (1958) sampled temperature and salinity at three stations across the mouth of the sound. Dunbar found a temperature minimum around 100 m and no evidence of geostrophic flow in and out of the sound. Since 1952, no further sampling has been reported. Even though no oxygen measurements have been previously reported in Cumberland Sound, based on the existence of a bottom dwelling population of Greenland Halibut in the sound (Peklova et al., 2012), we can assume that the deepest regions are not hypoxic. However, oxygen levels may be low, as Greenland Halibut have been found in regions with 18–25% oxygen saturation and can survive down to 15% in laboratory studies (Dupont-Prinet et al., 2013).

Cumberland Sound opens to southwestern Davis Strait (Figure 2.1) where roughly equal quantities of Pacific- and Atlantic-origin water transit heading south (Jones et al. 2003; Lique et al. 2010). Several properties distinguish these water masses.

Pacific origin water is colder and fresher than the warmer, saltier Atlantic origin water (Jones et al., 2003). Additionally, Pacific origin water contains less nitrate than Atlantic water creating different relationships between nitrate and phosphate, a ratio which is conserved and can be used to identify a water mass origins (Jones et al., 1998). Due to higher sea levels in the Pacific, water flows from the Pacific across the Arctic Ocean to the Atlantic (Carmack, 2007). Once in the Arctic Ocean, Pacific water flows east along the north coast of North America (Rudels 2012; Hu and Myers 2013), before passing through the Canadian Arctic Archipelago's (CAA) maze of channels (Prinsenberg and Bennett 1989; Jones et al. 2003; McLaughlin et al. 2004; Michel et al. 2006; Rudels 2012). This flow exits into Baffin Bay, a large body of water between northern Baffin Island, southern Ellesmere Island and the west coast of Greenland, joining the cyclonic flow pattern within the bay (Tang et al. 2004; Cuny et al. 2005).

Once in Baffin Bay, Pacific and Arctic Ocean origin water mix, becoming 'Arctic Water' (AW) (Cuny et al. 2005; Curry et al. 2014). AW ($\theta \leq 2$ °C and S ≤ 33.7 g kg^{-1}) remains in the surface layer (< 300 m) incorporating winter cooling remnants in a temperature minimum around 100 m (Tang et al., 2004). On the Greenland side of Baffin Bay, denser Atlantic-origin water moves away from the coast, sliding beneath the colder, but lighter AW (Bacle et al., 2002) becoming Transitional Water (TrW) ($\theta > 2$ °C and S > 33.7 g kg^{-1}) (Cuny et al. 2005; Curry et al. 2014). With an interface around 300 m, these two layers flow south, hugging Baffin Island, as the Baffin Island Current (BIC). Some of the southward flowing BIC water recirculates north of Davis Strait (e.g. Myers and Ribergaard 2013; Gladish et al. 2015). The BIC ultimately crosses Cumberland Sound's mouth (Tang et al., 2004; Curry et al., 2014) (Figure 2.1).

Flowing north along the Greenland coast through Davis Strait into Baffin Bay, is the West Greenland Current (WGC). This current carries two distinct water masses flowing side-by-side (Curry et al., 2014). Arctic origin 'West Greenland Shelf Water' (WGSW) ($\theta < 7$ °C and S < 34.1 g kg^{-1}) flows along the Greenland coast. Adjacent to the WGSW along the West Greenland slope, flows West Greenland Irmiger Water (WGIW) ($\theta > 2$ °C and S > 34.1 g kg^{-1}) of Atlantic origin. At the southern edge of Davis Strait the WGC splits, with one part continuing north through the strait and the other part turning westward (Cuny et al. 2002; Fratantoni and Pickart 2007; Myers et al. 2009) (Figure 2.1). The westward arm crosses Davis Strait before circulating southward adjacent to the BIC roughly 100 km away from Cumberland Sound's mouth

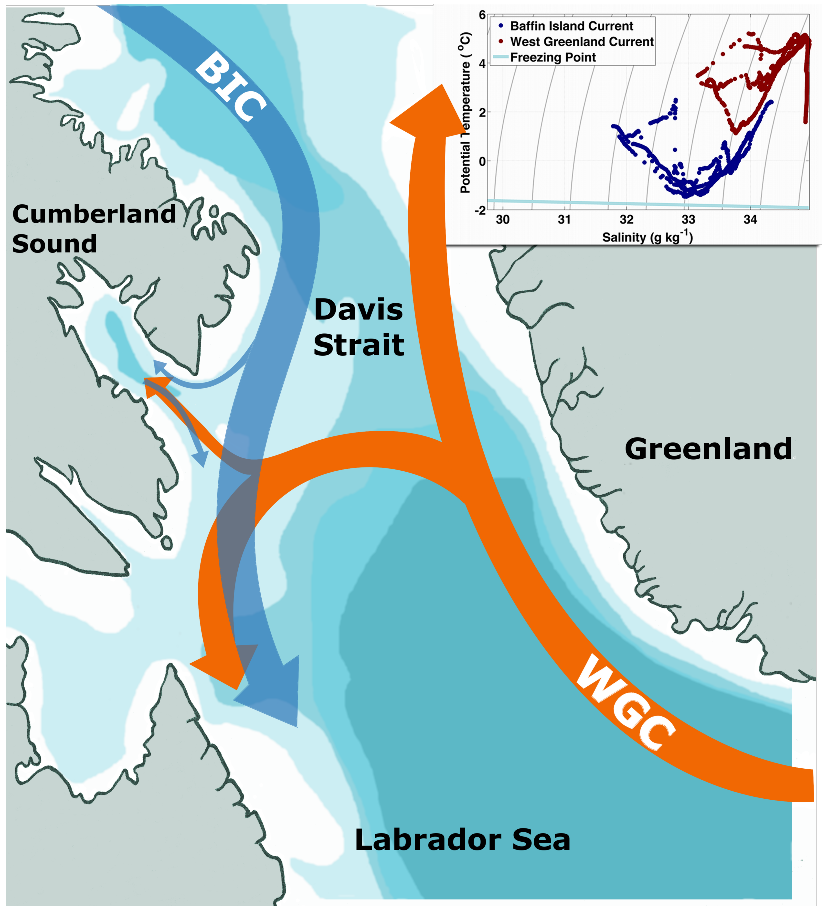

Figure 2.1: A diagram showing the origin of water in Cumberland Sound. The Baffin Island Current (BIC) in blue for the mid-depth layer and the West Greenland Current (WGC) in orange for the deep layer based on Curry et al.(2014), arrows entering Cumberland Sound are proposed in this paper. Rough 200, 500, 1000 and 2000 m isobaths are included. Inset plot shows temperature-salinity characteristics for both the BIC (blue) and WGC (red) from data collected in the fall of 2011.

(Cuny et al. 2002; Fratantoni and Pickart 2007; Myers et al. 2009).

The BIC and WGC's velocity, temperature and salinity vary on an annual basis (Curry et al., 2014). The BIC follows a seasonal cycle with peak currents in October-November and flow reversals in the winter (Curry et al., 2014). In the Arctic Water (AW) layer of the BIC, salinity reaches a maximum in May and a minimum in January while temperature reaches a maximum in August and a minimum in April (Curry et al., 2014). AW density ranges from roughly 1025 to 1027.2 kg m^{-3}. The West Greenland Irminger Water (WGIW) water mass in the WGC also follows a seasonal pattern with maximum currents occurring between October and December and a density range of 1027.3 to 1027.8 kg m^{-3}. Salinity peaks twice, once between

October and January and the second time between March and May. The WGIW reaches a temperature maximum in late fall and a minimum over the summer. At the front between the AW in the BIC and WGIW in the WGC, the WGC is always denser. Although significant inter-annual variability has been observed in both the BIC and WGC, no clear inter-annual trends have been identified (Curry et al., 2014). Both currents flow past the mouth of Cumberland Sound, and have the potential to influence water within the sound.

The objectives of this paper are: (a) to identify the origins of the water in Cumberland Sound and (b) to describe the physical water properties in the sound. In Section 2 we describe the physical setting, data collection, meteorological and ice conditions of the sound. In Section 3, the sound is split into above and below sill layers to discuss the origins and physical processes influencing each layer. In Section 4, possible consequences of long term changes are discussed.

2.2 Data and Methods

2.2.1 Study Site

Cumberland Sound is a coastal body of water on the south coast of Baffin Island roughly 80 km wide and 250 km long following a northwest-southeast axis (Figure 2.2). At the southeast end, Cumberland Sound opens into Davis Strait. At the mouth, the sill is part of the Baffin Island Shelf and reaches ∼300 m in depth, and half of the sounds total volume is below the sill depth. The steepest bathymetry occurs along the north coast where the sounds depth drops from the coast to ∼150 m in 17 km (slope of 0.07). Within the sound there are two deep, muddy-bottomed pockets, one reaching ∼800 m and the other ∼1400 m with a 300 m deep ridge separating them. Although there are no major rivers, several seasonal small rivers along with glacier runoff empty into the sound. Small islands litter the periphery of the sound and several fjords open out into it. Like Frobisher Bay and Hudson Strait to the south, Cumberland Sound has very strong tides. The tides have a 6 m range and are dominated by semi-diurnal oscillations (M2) modulated by the spring-neap cycle (Webtide Model, Hannah et al. 2008). At the sound's mouth barotropic tidal velocities reach 0.18 m s^{-1}, and exceed 0.2 m s^{-1} in the narrow channels between the islands and the coast (Webtide Model, Hannah et al. 2008).

Cumberland Sound is far enough north to experience complete winter ice cover,

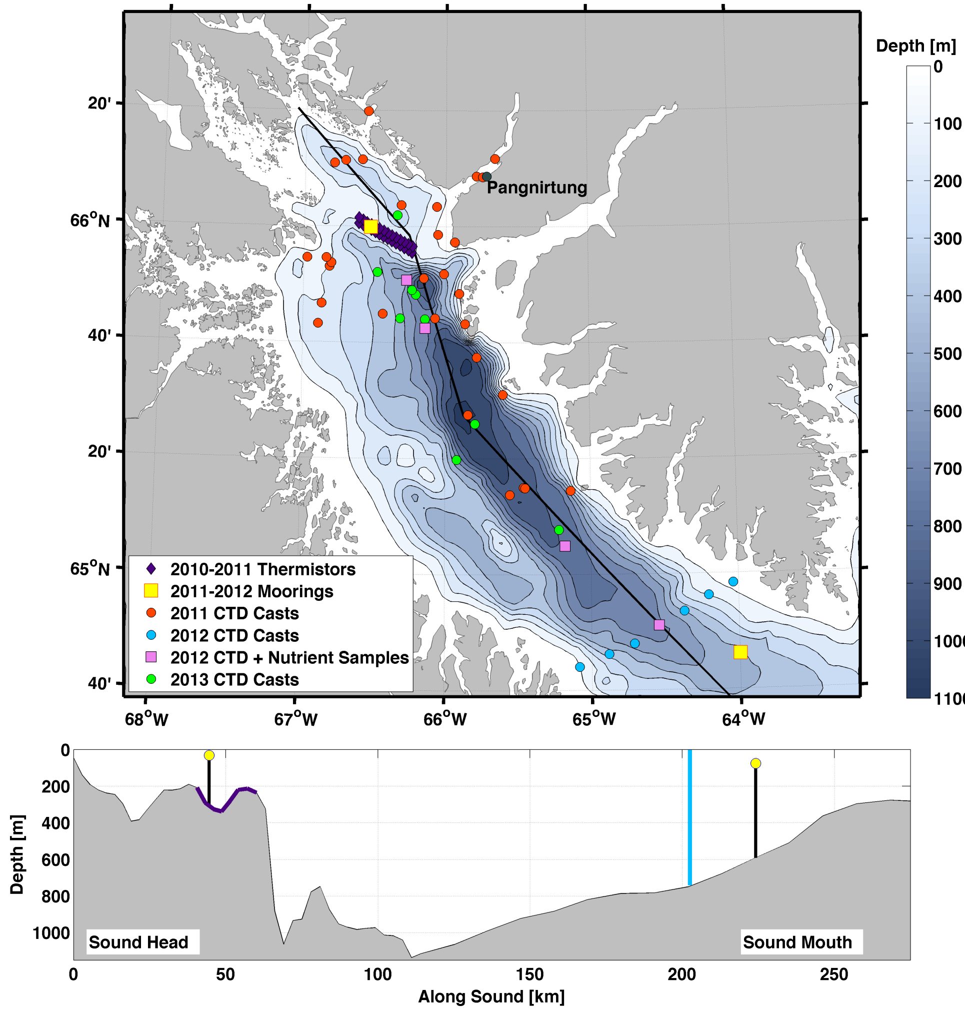

Figure 2.2: (top) Cumberland Sound bathymetry from the International Bathymetric Chart of the Arctic Ocean (IBCAO) and locations where data were collected. (bottom) An along-sound depth profile shown as a black line on the top plot from inland at the sound's head on the left to the mouth opening into Davis Strait on the right on the same IBCAO grid. Black lines with yellow circles mark the mooring locations. Dark blue line marks where bottom thermistors were deployed and blue line is the location of the cross-mouth profiles.

however, within the sound, regions of open water typically remain all winter (Figure 2.3a). On average, January open water area is ∼34 km^2, less than 1% of the total area of the sound (Barber and Massom, 2007). Ice cover above the two mooring sites during 2011-2012 was very similar (Figure 2.3a). Weekly ice cover proportions from the Canadian Ice Service archives (http://www.ec.gc.ca/glaces-ice/) indicate that the sound had 50% ice cover over the entire sound by 28 November 2011 and 90% by December 5$^{\text{th}}$. By 19 December 2011, fast ice began forming along the shores

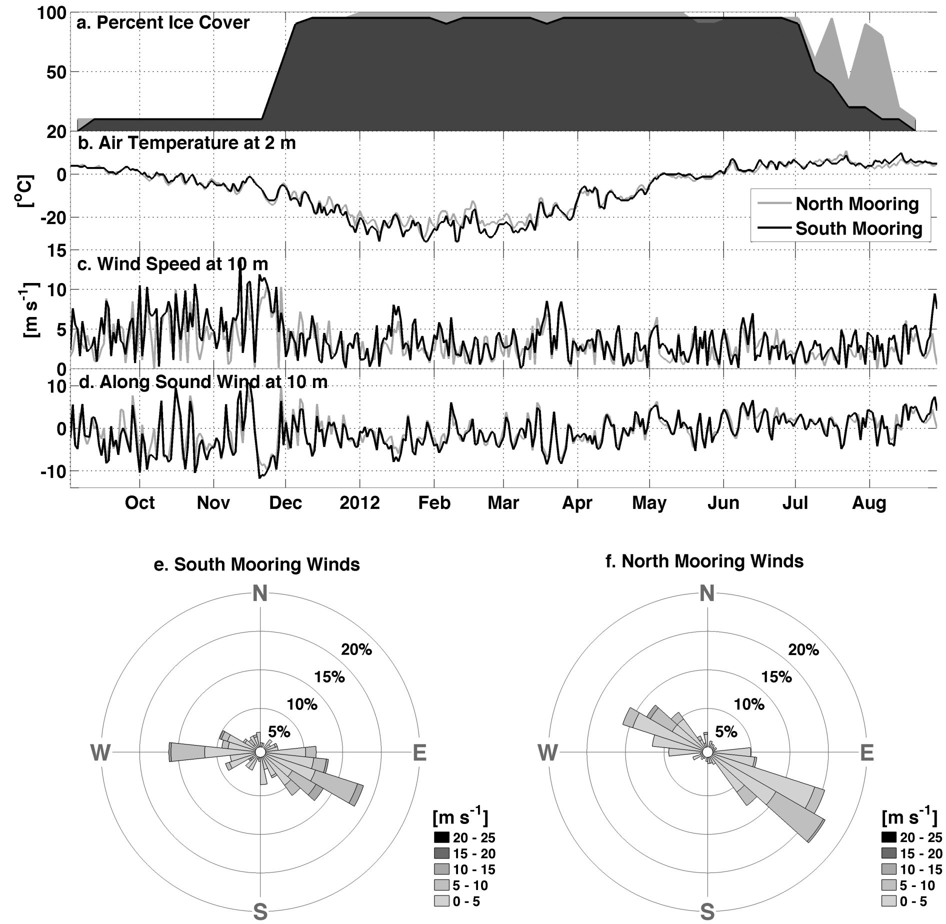

Figure 2.3: Ice and meteorology over 2011-2012 at the two mooring sites. The North Mooring is in grey and the South Mooring is in black. All meteorological data from NCEP reanalysis. The horizontal axis grid is by month. (a) Percent ice cover from the Canadian Ice Service weekly ice charts. (b) Daily average air temperature at 2 m. (c) Daily average wind speeds at 10 m. (d) Along-sound wind speed. (e and f) Wind roses for each mooring site showing that most winds blow along sound rather than across it.

of the sound and by early January 2012, the sound contained primarily fast ice. In May 2012 an open area formed midway along the south shore and cycled open and closed until the sound became ice free. In the same month, at the north end of the sound, areas of reduced ice cover appeared then closed by early June. Ice began retreating in July leaving the sound mostly ice free by late August.

Daily mean composites of wind and air temperature were obtained from NOAA's National Centre for Atmospheric Prediction (NCEP) North American Regional Reanalysis Composites (Kalnay et al., 1996). Air temperature was taken at 2 m and wind

Year	Date Range	Number of Casts	Instrument
2011	23 July-26 August	44	Seabird SBE 19 CTD with a SBE-43 DO sensor
2012	17 August-20 September	31	Seabird SBE 19 CTD
2013	13 August-3 September	9	RBR XR-620 CTD with JFE Alex Co.Ltd Rinko DO sensor

Table 2.1: For each year, CTD Cruise dates, number of casts and instruments used.

velocity at 10 m (Figure 2.3). Air temperature in Davis Strait was generally higher, resulting in warmer air in the sound during periods with southerly winds. Northerly winds off of the land mass of Baffin Island were typically colder. In Cumberland Sound, winds predominately blew along the axis of the sound (Figure 2.3e and f) and the wind directions were similar at both mooring sites. The u and v components of the wind were rotated 160° into an along-sound and across-sound coordinate system where positive values indicate wind blowing into the sound (Figure 2.3d). Since, the along-sound winds were significantly stronger than cross-sound ones, the cross-sound winds are ignored. The wind blew predominately out of the sound (Northerly winds) from September 2011 until mid April 2012. From mid April until August 2012, the wind blew on average into the sound (Southerly winds). Although, the winds followed this pattern over long time scales, on a daily basis there was significant variability in direction. The strongest winds were found in the fall, switching direction every few days.

2.2.2 Temperature, Salinity and Depth Profiles

Ship-based conductivity, temperature and depth (CTD) profiles were collected as part of the Ocean Tracking Network (OTN) project each summer from 2011 to 2013. CTD cast locations and instruments used for each year can be found in Figure 2.2 and sampling dates and instruments are listed in Table 2.2. A different CTD instrument was used each year and each instrument's sensors were calibrated at the beginning of each field season. The CTD instrument also included a dissolved oxygen sensor in 2011 and 2013, in both years these sensors were calibrated before and after use. In 2012, two cross-mouth transects were performed a month apart (17 Aug 2012 and 20 Sept 2012) along the same line Dunbar (1958) sampled in 1952. The same seven stations were sampled on each transect with an average spacing between stations of 9 km. Both transects took 6 hours to complete and were done on opposite phases of the tide. Additional CTD data were collected for Labrador Sea directly out from Cumberland Sound (transect shown in Figure 2.5b) by the University of Washington using a a Seabird 911+ instrument.

Conductivity, temperature and depth data from 2011 and 2012 were processed the same way. First, CTD corrections were made using the Seabird software, then upcasts and downcast were separated out. The upcasts and downcasts were compared and found to be almost the same. In 2011, the downcast data were used. In 2012 the upper 50 m of CTD data was bad because the pump was not on. These data were removed and replaced with data from the upcasts. In 2013, CTD casts were taken at fish survey locations (Figure 2.2) with an instrument limited to depths above 740 m. A preset conductivity threshold was programmed to start and stop the instrument which resulted in frequent missed sampling in the upper layers. Up and down casts were compared and found to be very similar. To compensate for missed upper layer samples, up-casts were used. Each years data were averaged into 1-m bins from which potential temperature, salinity and density were calculated. The mean of each 1-m depth bin was taken to create an average cast for each year.

2.2.3 Moorings

In the summer of 2010, OTN acoustic fish tagging began and lines of acoustic receiver moorings were deployed in Cumberland Sound at the northern end of the sound (Figure 2.2). Eleven RBR TR-1050 thermistors set to sample every minute were attached on the bottom of these moorings. These moorings ranged in depth between 178 and 385 m and were recovered during the 2011 field season.

Two dedicated oceanographic moorings were deployed from 2011-2012 (Figure 2.2), mooring locations and composition are listed in Table 2. One mooring was deployed at the north, inland end of the sound in close proximity to the line of thermistors from 2010-2011. This site, referred to as the ‘north mooring’, was situated between two deep pockets that are known fish habitats. Water depth was 272 m and the float extended to 32 m below the surface. At the mouth of the sound, the south mooring was deployed to sample water entering the sound from Davis Strait. This mooring sat at a depth of 475 m with the float 75 m below the surface. Both moorings were recovered in the summer of 2012. The conductivity temperature (CT) sensor

Mooring	Date Range	Location	Instrument	Depth [m]
Bottom Thermistors	17 Aug 2010-10 July 2011	65.96°N 66.38°W	RBR TR-1050 thermistor	178
		65.97°N 66.38°W	RBR TR-1050 thermistor	188
		65.97°N 66.35°W	RBR TR-1050 thermistor	223
		65.98°N 66.41°W	RBR TR-1050 thermistor	229
		65.94°N 66.29°W	RBR TR-1050 thermistor	232
		65.95°N 66.32°W	RBR TR-1050 thermistor	237
		65.95°N 66.26°W	RBR TR-1050 thermistor	271
		65.96°N 66.32°W	RBR TR-1050 thermistor	275
		65.93°N 66.26°W	RBR TR-1050 thermistor	291
		65.92°N 66.24°W	RBR TR-1050 thermistor	374
		65.95°N 66.35°W	RBR TR-1050 thermistor	385
North Mooring	24 Aug 2011-1 Sept 2012	65.99°N 66.53°W	RBR XR-420 CT+	32
			RBR TR-1050 thermistor	57
			RBR TR-1050 thermistor	82
			RBR TR-1050 thermistor	107
			RBR TR-1050 thermistor	157
			RBR TR-1050 thermistor	182
			RBR TR-1050 thermistor	207
			RBR TR-1050 thermistor	232
			RBR DO-1050	272
South Mooring	1 Sept 2011-2 Sept 2012	64.77°N 63.99°W	RBR XR-420 CT+	75
			RBR TR-1050 thermistor	57
			RBR TR-1050 thermistor	100
			RBR TR-1050 thermistor	125
			RBR TR-1050 thermistor	150
			RBR TR-1050 thermistor	175
			RBR TR-1050 thermistor	225
			RBR XR-420 CT+	275
			RBR TR-1050 thermistor	325
			RBR TR-1050 thermistor	375
			RBR DO-1050	475

Table 2.2: Mooring deployment dates, locations, instruments and depths for the 2010-2011 bottom thermistors, which were each on their own mooring, and the 2011-2012 North and South Moorings. Note: RBR XR-420 CT+ on the North Mooring at 32 m failed 3 Feb 2012

on the north mooring failed 3 February 2012 for unknown reasons. All instruments were from RBR Ltd. and programmed to sample every minute. Accuracy for the temperature sensors was ±0.002 °C, for the conductivity sensors ±0.003 mS cm^{-1} and for the dissolved oxygen sensor ±2%.

2.2.4 Nutrients

Water samples were collected at four sites along the length of the sound in August 2012 (Figure 2.2). At each site, duplicate samples were taken at the surface, 100 m, 200 m and 400 m using a horizontal acrylic water sampler. The samples were frozen for transport to the Institute of Ocean Sciences in Sidney, B.C. Each sample was analyzed for nitrate+nitrite, phosphate and silicate using a Three Channel Technicon Autoanalyzer, only the nitrate+nitrite and phosphate are used here. For the nitrate+nitrite the duplicate difference mean was 0.90 μm l^{-1} and standard deviation was 0.68 μm l^{-1}. For the phosphate the duplicate difference mean was 0.14 μm l^{-1} and standard deviation was 0.24 μm l^{-1}. Duplicate results were averaged together.

2.3 Results

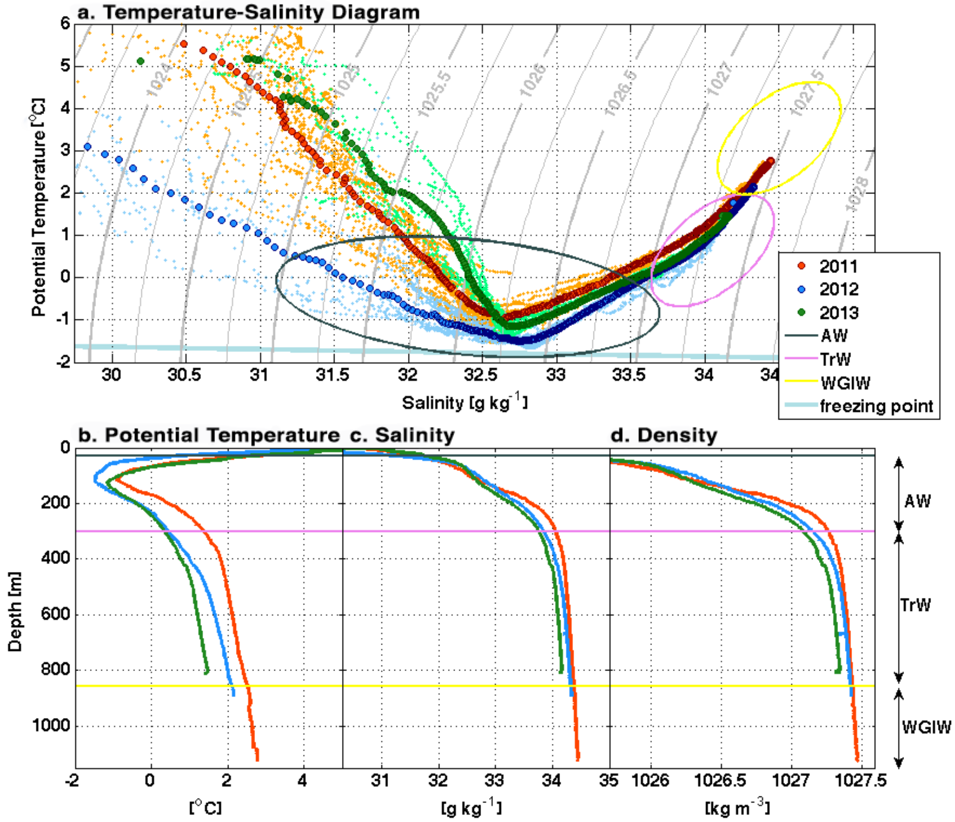

Figure 2.4: (a) Temperature-salinity diagram where red is 2011, blue is 2012 and green is 2013. Darker markers are average profiles and light blue line is the freezing point of water. Grey lines are potential density. Water masses from Davis Strait (Curry et al., 2014) are marked as ellipses, dark grey is Arctic Water (AW), light purple is Transitional Water (TrW), yellow is West Greenland Irmiger Water (WGIW). (b) to (d) are average potential temperature, salinity and density profiles from 2011-2013. Water masses from (a) are marked along the right side of (d).

Between 2011 and 2013, Cumberland Sound's water column changed, however each year there were shared features (Figure 2.4). The water reached a near freezing temperature minimum around 100 m, a typical characteristic of Arctic waters (Melling, 2002). Below the temperature minimum, water became warmer and saltier with depth, creating an upturn in the temperature-salinity curve (Figure 2.4a) implying different origin water intruded into the sound (Dunbar, 1958). Bottom density did not exceed 1027.5 kg m^{-3} (Figure 2.4a and d), which will be important when considering bottom water renewal. From 2011 to 2013 the water column cooled and freshened at all depths. At 800 m, the result was water cooled by ~1 °C and freshened by $\sim$0.2 g kg^{-1} (Figure 2.4b and c).

Even though Cumberland Sound's deepest region is more than a kilometre below the sill, the sound is not isolated at any depth from the surrounding waters traversing Davis Strait. On the temperature-salinity diagram (Figure 2.4a) ovals indicating water masses from Davis Strait are included from Curry et al. (2014). Within Cumberland Sound, water with properties similar to AW, TrW and WGIW are found (Figure 2.4a). Above the sill ($\sim$300 m) the sound is directly linked to outside water, while below the sill, there is a pool of water only occasionally replenished. Since these two layers are subject to different processes, the sill, which is really the Baffin Island Shelf, is used to separate the sound into upper and lower layers.

2.3.1 Water above Cumberland Sound's sill

Above the sill, Cumberland Sound is flooded with water from the BIC. This is demonstrated by the potential temperature contours shown in Figure 2.5a. Cold BIC water flows southward along the $\sim$100 km wide shelf that forms the sound's sill (Figure 2.5a). Within the sound, below the $\sim$25 m deep warmer layer at the surface, water of similar temperature as the BIC extends across the entire above-sill layer (Figure 2.5a). Temperature-salinity profiles show that although water in the sound is slightly warmer and fresher than water of the same depth in the BIC (Figure 2.5b), in general, the above sill water in Cumberland Sound matches the AW layer of the BIC suggesting an ongoing interaction with the BIC. Additional evidence of AW water within the sound is found in the nutrient ratios (Figure 2.6).

Arctic Water is composed of a combination of Pacific and Atlantic origin waters. Although biological processes modify nutrient concentrations (Cooper et al., 1999), the nutrient levels between Pacific and Atlantic waters are different enough to allow the identification of water mass origins across the Arctic to the Labrador Sea (Jones et al., 1998). Here, nitrate and phosphate ratios are used to infer the origins of the above sill layer in Cumberland Sound (Figure 2.6). Pacific and Atlantic ratios are included as lines in Figure 2.6. Values that fall on these lines suggest a water mass composed of that origin water, while values in between the lines imply mixing occurred. For comparison, nutrient relationships from Davis Strait, north of Cumberland Sound are included (Jones et al., 2003). In the BIC, the fraction of Pacific origin water ranged from 30 to 60%, decreasing with depth (Jones et al., 2003). Above the sill, Cumberland Sound contains 40% Pacific water, similar to Davis Strait (Jones

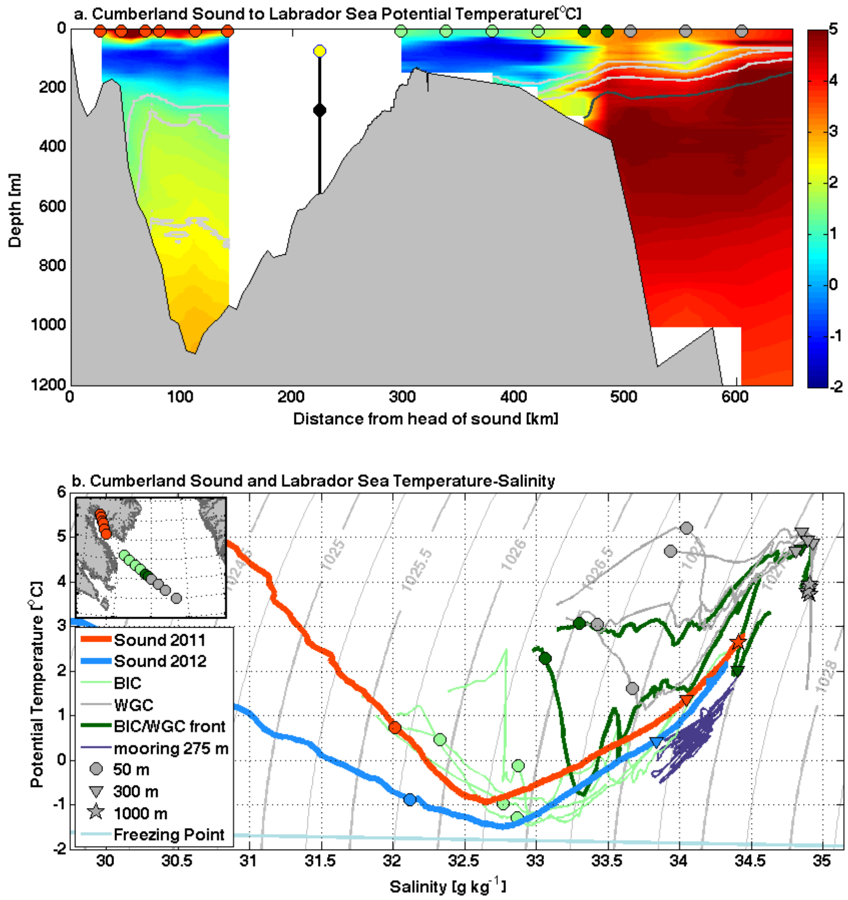

Figure 2.5: (a) Potential temperature from 2011 where dots along the top indicate CTD cast locations. Light grey isopycnals are 1027.2, 1027.3 and 1027.4 kg m^{-3}, black isopycnal is 1027.5 kg m^{-3}. South mooring is marked and the black dot is the CT instrument depth. (b) Temperature-salinity diagram with colour coded 2011 CTD casts (see inset map). Average Cumberland Sound 2011 CTD profile in red and 2012 CTD profile in blue. Depths are indicated with markers.

et al., 2003), providing further evidence that the upper layer of the sound is filled with AW from the BIC.

Geostrophic Flow

In this section geostrophic flow is considered as the mechanism bringing BIC water into the above-sill layer of Cumberland Sound. The relatively wide width of the sound compared to the Rossby radius suggests a component of the south-moving BIC water enters the sound. The first-mode baroclinic Rossby radius (L_r) is:

$$L_r = NHf^{-1} \tag{2.1}$$

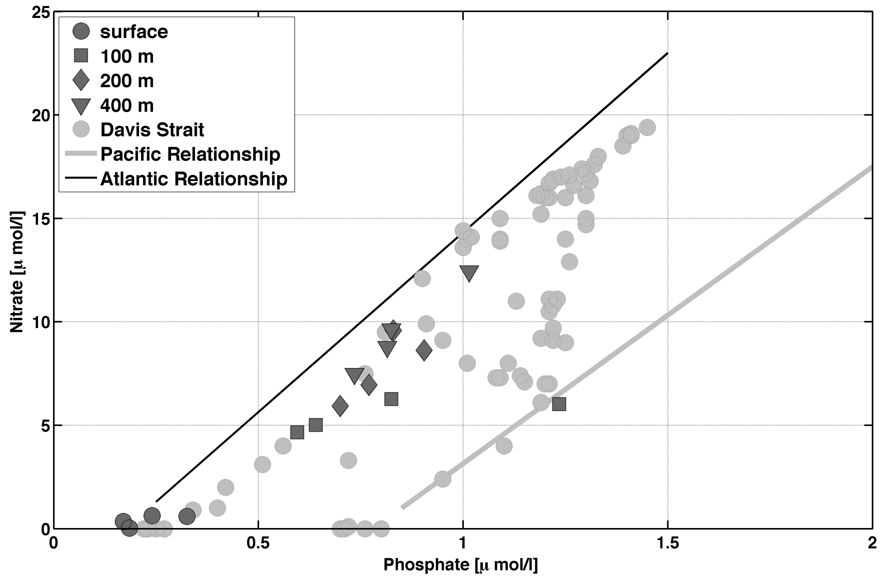

Figure 2.6: Nitrate-phosphate relationship for Cumberland Sound from stations in Figure 2.2 in dark grey where shapes denoted depth to 400 m. Light grey dots from Davis Strait north of Cumberland Sound taken from Jones et al. (2003). Known relationships between these nutrients are included for the Atlantic (solid black line) and Pacific (solid grey line) (Jones et al., 2003).

where N is the buoyancy frequency ($N = 5.4 \text{ x } 10^{-3} \text{ s}^{-1}$), H is the depth ($H =$ 300 m, approximate depth of the sill) and f is the Coriolis ($f = 1.3 \text{ x } 10^{-4} \text{ s}^{-1}$). Here, only the lowest mode Rossby radius was considered. For the mouth of Cumberland Sound, the Rossby radius was 12 km, or approximately 1/6 of the width of the sound.

Using density profiles from the two 2012 cross-mouth transects, flow patterns in and out of Cumberland Sound were deduced (Figure 2.7). For each transect, geostrophic flow was calculated assuming no net transport through the section which required small bottom flows of 0.007 m s^{-1} for the first transect and 0.002 m s^{-1} for the second. Transect 1 followed the expected pattern where a component of the BIC entered the sound along the north shore and exited along the south shore. Mid-sound, currents were very weak. By transect 2, a month later, the flow pattern through the mouth of the sound changed dramatically, now water flowed into the sound along the south shore, and flow out was concentrated in the top 100 m centre-sound. Below 100 m, little water movement occurred. Further evidence of this variability was found in 1952 when Dunbar (1958) looked for a geostropic flow pattern but did not observe one at the time of his cross-mouth transect. However, the three stations

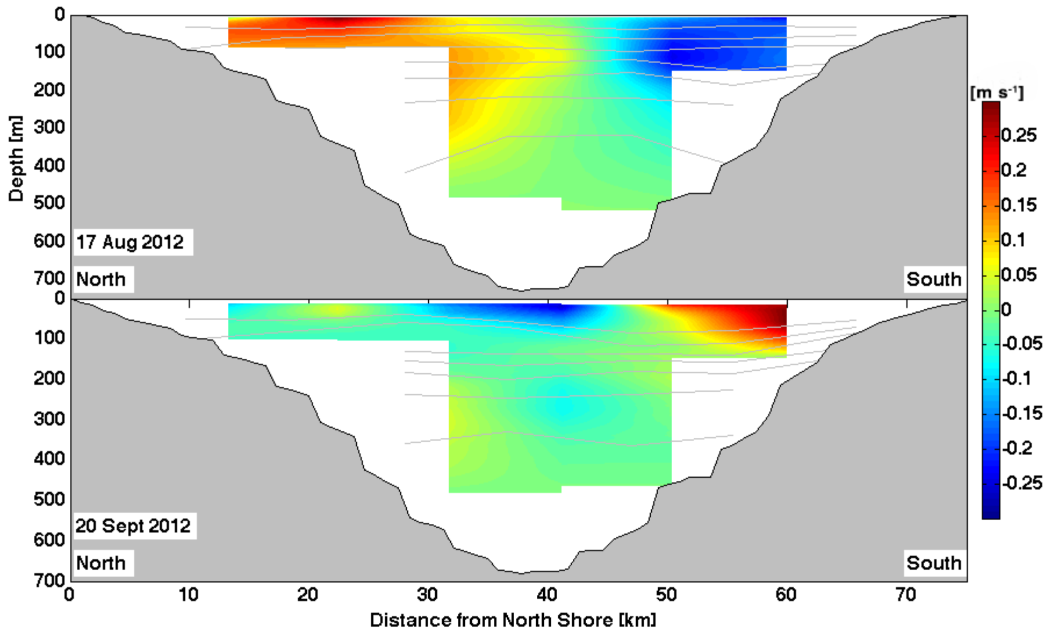

Figure 2.7: Geostrophic velocities at the mouth of Cumberland Sound calculated from cross-mouth CTD transects. The north shore is on the left so the reader looks out of the sound towards Davis Strait. Positive is flow into the sound and negative is flow out. Grey lines are isopycnals starting at 1025.75 kg m^{-3} increasing by 0.25 kg m^{-3} to 1027.25 kg m^{-3}.

Dunbar used were roughly 25 km apart; greater than the Rossby Radius, making it possible a geostrophic flow pattern was missed. The observed changing flow patterns demonstrates variability in how water enters and leaves the sound, but does not quantify the frequency of any specific pattern. However, from the two transects, we conclude for at least some of the time, the BIC enters the sound.

Using the geostrophic velocities, a rough residence time for the above-sill layer can be computed. Here we assume that the transport through the sound's mouth is constant, that the water circulates around the entire sound and that there is no interaction below the sill. The International Bathymetric Chart of the Arctic Ocean (IBCAO) was used to calculate the volume of the above-sill layer and the volume of water entering the sound was taken from transect 1 (Figure 2.7). Residence time can be defined by system capacity volume divided by the volume transport, for the above-sill layer of Cumberland Sound this works out to roughly 30 days if the transect 1 flow pattern was constant. Since, we have already determined there is variability in the flow pattern through the sound's mouth, we can only say that the residence time for this layer is on the order of months.

Internal Structure of Cumberland Sound

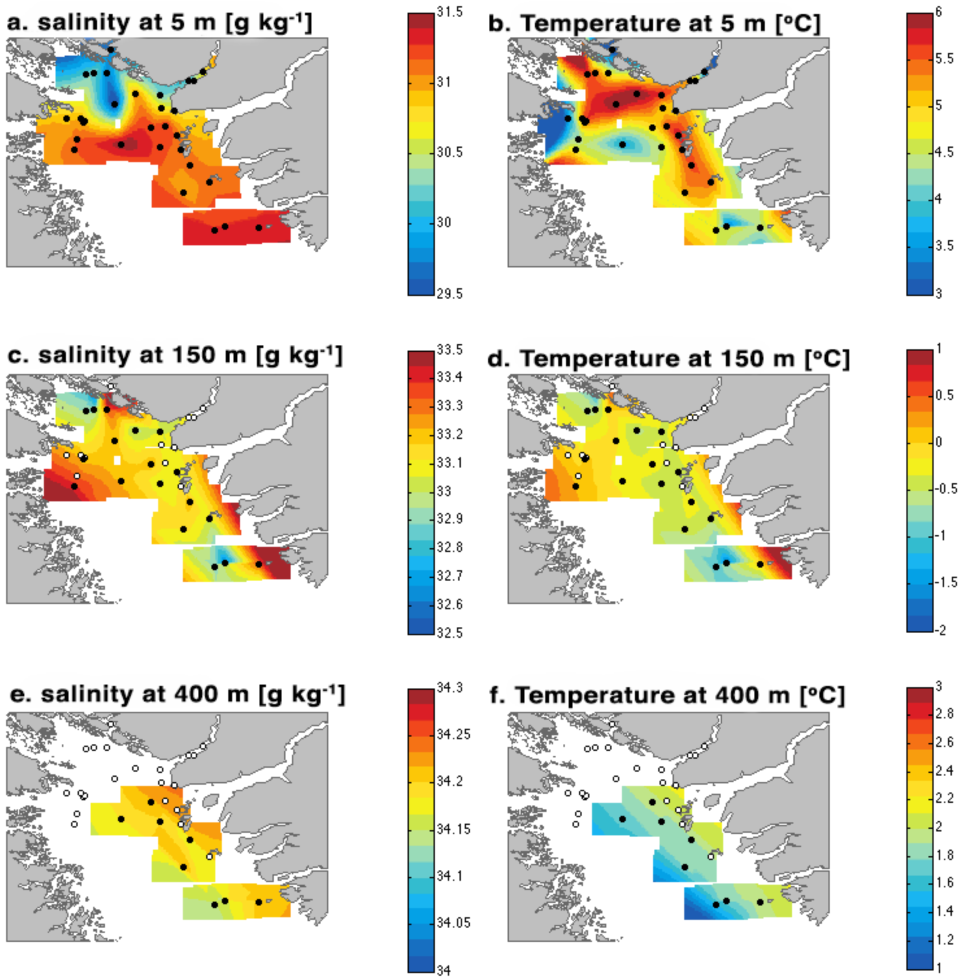

Figure 2.8: 2011 CTD data interpolated into horizontal layers with different ranges used on each panel to highlight features at that depth. Locations of CTD casts used for each depth are indicated by black dots and the CTD casts too shallow to include are indicated by white dots. Displayed are 20x20 km boxes around each used CTD cast.

In addition to the outside influence from water masses in Davis Strait, lateral mapping of the sound's water properties indicates estuarine circulation also occurs. The 2011 data will be discussed since CTD casts that year had the widest horizontal coverage of the sound. Near the surface, water was fresher towards the sound's head, forming a plume with a sharp gradient adjacent to Pangnirtung Fjord (Figure 2.8a). For most of the fresh water plume, water was warmer than that outside the plume except the northernmost, inland CTD cast taken at the mouth of a seasonal river where water was more than a degree colder (Figure 2.8b). As this surface water flowed away from the source it is possibly warmed by contact with the atmosphere. The plume's presence suggests fresh water from glacier runoff and small seasonal rivers plays a role in driving water movement outwards from the head of the sound.

At 150 m, below the sound's temperature minimum, lower salinity water was observed along the north coast compared to centre sound (Figure 2.8c). This lower salinity water was also colder towards the mouth of the sound (Figure 2.8d). A pocket of higher salinity, warmer water was found under the surface freshwater plume at the sound's head suggesting estuarine flow may occur in this region drawing up deeper warm water to replace that pushed out by the surface freshwater plume. At 400 m, water was nearly uniform in salinity, with water along the north coast only ~0.05 g kg^{-1} saltier (Figure 2.8e). This more saline water was also warmer (Figure 2.8f). The gradients of different water along the north coast at both 150 m and 400 m suggest an influx of outside water followed the isobaths and modified within the sound. The less saline, colder water along the coast at 150 m is likely AW and the slightly more saline and warmer water found in the same location at 400 m could be TrW.

The spatial plots in Figure 2.8 show the two moorings were situated in different oceanographic regimes. The north mooring was directly beneath the fresh water plume in the path of possible estuarine flow. At the mouth of the sound, the south mooring was in the path of outside water entering the sound. To determine how related observations at the two moorings were, coherence was calculated between thermistors located at similar depths at each mooring (not shown) (Bendat and Piersol, 2010). The coherence function evaluates how similar two different functions are. Temperature data was interpolated into hourly increments then coherence was calculated over 21, 42, 85 and 120 days to find common frequencies. Significant coherence (>0.6) only occurred at tidal frequencies, confirming the moorings experienced different regimes.

North Mooring Temperature and Salinity Structure

Over 2010-2011 near bottom water on-average warmed over the year (not shown), then in 2011-2012 water cooled, with the warmest temperatures observed in September 2011 and coldest in May 2012 (2011-2012 shown in Figure 2.9e). The opposite changes over these two years suggests that an annual cycle of warming and cooling following the seasons did not occur in Cumberland Sound. The most notable difference between the two years was the average wind direction. Over the fall of 2010, winds

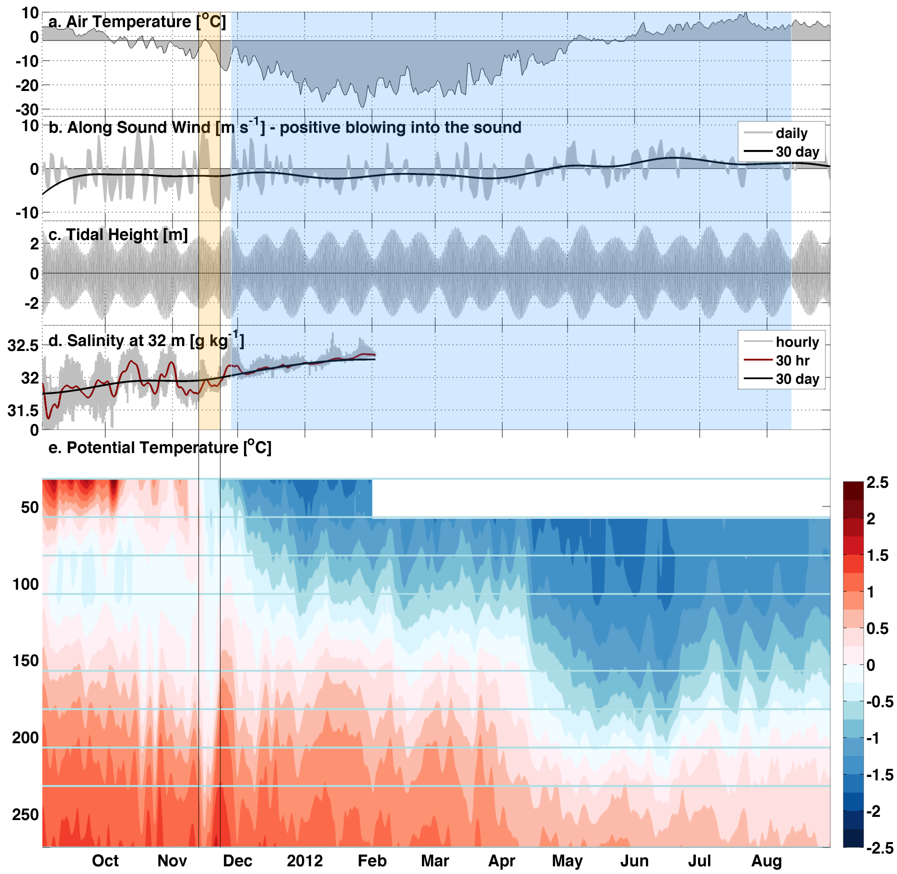

Figure 2.9: Time-series plots from the North Mooring where blue shaded area indicates time of 90% ice cover. Orange highlighted area indicates a wind mixing event. (a) NCEP reanalysis daily averaged air temperature at 2 m with a horizontal line at the freezing point of 32 g kg^{-1} salinity water. (b) NCEP reanalysis daily average winds at 10 m rotated along the sound. (c) tidal height from the Webtide model. (d) mooring salinity at 32 m, raw data is in grey, red line has a 30 hour filter applied and black line has a 30 day filter applied. (e) mooring potential temperature time series. A 30 hour filter has been applied to all the data. Grey lines indicate instrument depths.

on average blew into the sound, bringing in warmer air from Davis Strait, keeping air temperatures above the freezing point of water for salinity 32 g kg^{-1} (1.75 °C) until the end of November 2010. Ice did not reach 50% cover until mid-February 2011. During the fall of 2011, winds on average blew out of the sound bringing cold air from the mountainous terrain on Baffin Island over the sound. This year, ice formed much earlier. By December 2011, this region of the sound experienced 90% ice cover (Figure 2.3a).

Over 2011-2012 temperature decreased at the north mooring, most rapidly in November 2011 and March 2012 (Figure 2.9e). Between these times the water column only slightly cooled. Since the only salinity measurements were taken at 32 m on an instrument that failed in February, the focus will be on Fall 2011. From September 2011 to February 2012, salinity increased at 32 m by ~0.5 g kg^{-1} mostly over two separate time-frames (Figure 2.9d). The first salinity increase occurred between 4 September and 10 October 2011 when water temperatures were above 1.5 °C and the warmest in the water column (Figure 2.9e). This suggests the salinity increase during this time period was not the result of ice formation, therefore another process must have been responsible.

Between 13 and 16 November 2011, a mixing event occurred that rapidly cooled the top ~182 m by ~1 °C (highlighted in orange on Figure 2.9). This event was likely wind driven and is the only observation of a surface process influencing deeper layers. On 13 November 2011, wind reversed from blowing out of the sound and began blowing into the sound bringing in warmer air from Davis Strait (Figure 2.9b). As the wind speed increased, air temperature increased above the freezing point, but still colder than the surface water, prompting cooling by ~0.5 °C. In the top 182 m, the water appeared homogeneous in temperature suggesting the breakdown of stratification. By 15 November 2011, well mixed, cold water reached a depth of 232 m, while the upper layers continued to cool. One day later, this cooling reached the bottom and surface layers cooled by ~1 °C, renewing the whole water column. On 18 November 2011, wind reversed again, now blowing out of the sound, and the air temperature rapidly dropped well below the freezing point (Figure 2.9a).

Salinity increased more rapidly starting around 20 November 2011 and levelled off by 22 January 2012 (Figure 2.9d). During this time, temperatures at the same depth approached the freezing point. At the surface, ice cover reached 90% by 3 December 2011 (Figure 2.3a), suggesting the second salinity increase may have been influenced by brine rejection from ice formation.

2.3.2 Water below Cumberland Sound's sill

Cumberland Sound's sill cuts off the lower layer from direct interaction with water masses in Davis Strait. Down to the deepest pockets in potentially isolated regions of the sound lives a population of Greenland Halibut (Peklova et al., 2012). Therefore deep water renewal must occur often enough to prevent hypoxia. As hypoxia threshold definitions vary (Hofmann et al., 2011), here a mid-value of 20% dissolved oxygen (DO) saturation will be used which is within the range that Greenland Halibut have

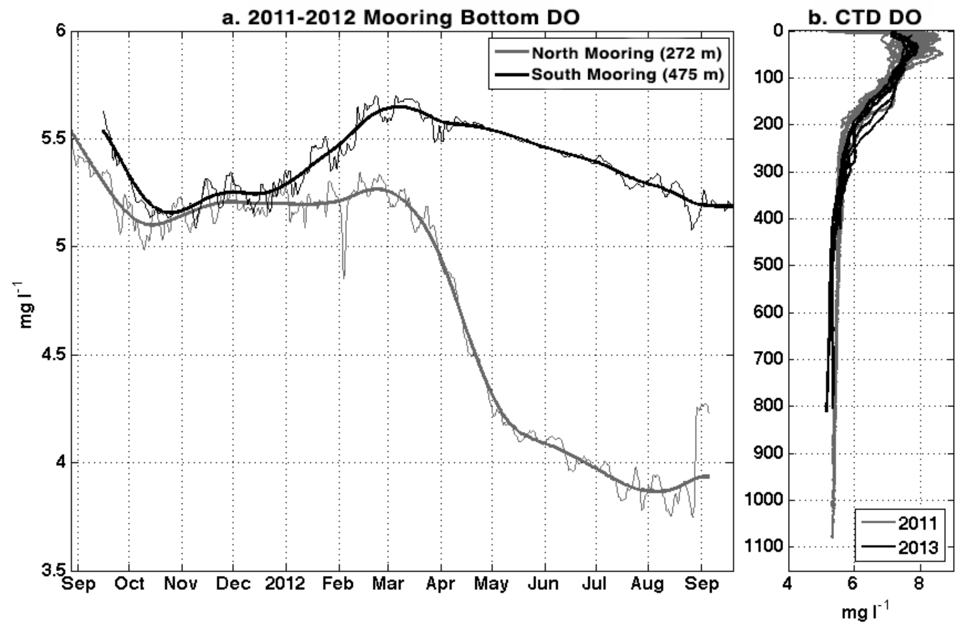

Figure 2.10: (a) Dissolved oxygen from the bottom of the two moorings, north mooring is grey and south mooring is black. North mooring sensor was at 272 m and the south mooring's was at 475 m. The darker line is a 30 day low pass filter applied to this data, while the lighter weight line is a 30 hour filter. (b) Dissolved Oxygen from CTD casts taken in 2011 in grey and from 2013 in black.

been found elsewhere (Dupont-Prinet et al., 2013). For Cumberland Sound's bottom temperatures, 20% DO saturation corresponds to an oxygen concentration of roughly 3 mg l^{-1}. The deepest (1127 m) DO measurement, taken in 2011, was well above this hypoxia threshold (Figure 2.10b). Dissolved oxygen measurements were taken again in 2013 to a depth of ~800 m. Although there was more variability this year, values were similar to those observed in 2011.

At both mooring sites bottom DO concentrations decreased throughout 2011-2012 (Figure 2.10a), likely due to a combination of respiration and decomposition as biological activity continued beneath the ice in limited daylight. Some influx of oxygenated water likely occurred in February and March 2012, possibly through an intrusion of outside water. Alternately, convection or deep mixing might play a role at the north mooring location. Assuming the observed decrease typical of DO use in Cumberland Sound, below sill renewal must occur to replenish the oxygen. To roughly estimate how long oxygen in the deep pockets of Cumberland Sound could last without renewal, the 0.3 mg l^{-1} DO decrease over 2011-2012 at the bottom of the south mooring (475 m) (Figure 2.10a) was assumed to mirror deep water oxygen changes. By continuing to decrease DO without renewal, bottom water would become hypoxic in four years. Therefore, to maintain Cumberland Sound's ecosystem, deep water must be replenished at intervals shorter than four years.

Below the sill, the sound collects incursions of water from the strait. This region has characteristics similar to TrW water from the lower layer of the BIC, however this water is not warm or dense enough to be the sole source of the deepest waters. On the other side of the BIC, warmer, dense water is found in the WGIW component of the WGC. WGIW water reaches 5 °C, much warmer than Cumberland Sound's deep water maximum measured temperature of 2.9 °C. Thus, at the same salinity, the deepest temperatures in the sound were warmer than the BIC (region shown in light green, Figure 2.5b) but not as warm as the WGC (region shown in grey, Figure 2.5b), implying the deep water is a mixture of these two water types.

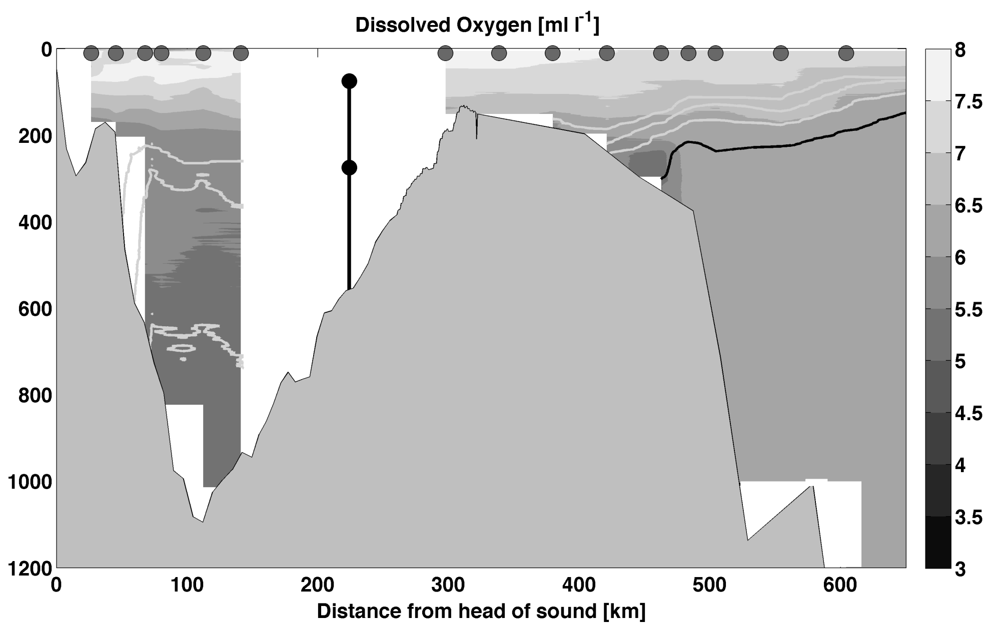

Figure 2.11: Contour plot of dissolved oxygen along Cumberland Sound and out into the Labrador Sea. Light grey isopycnals are 1027.2, 1027.3 and 1027.4 kg m^{-3}, black isopycnal is 1027.5 kg $^{-3}$ South mooring at ∼230 km is marked and the black dot is the CT instrument depth. Dots along the top indicate cast location following the same scheme as Figure 2.5.

The front between the cold BIC and warm recirculated arm of the WGC possibly creates the water destined to become Cumberland Sound deep water. In September 2011, this front was located roughly 100 km across the sill of the sound (Figure 2.5a) and contained a sharp temperature gradient over the entire water column while density increased from the BIC into the WGC. On the WGC side of the front, water denser than 1027.5 kg m^{-3} was observed at a depth of 300 m (isopycnal denoted in black on Figure 2.5b) roughly 100 km away from the sound. This water was denser than the water observed within Cumberland Sound. Therefore, the sound's deep water likely originates from the sound side of the 1027.5 kg m^{-3} isopycnal where BIC and WGC waters interact. Across the sill into the Labrador Sea, DO levels are generally greater that those found below the sill within the sound (Figure 2.11). There is a pocket of lower DO found near the bottom across the sill at the interface between the BIC and WGC (below dark green dots on Figure 2.11) providing further evidence the below sill water in the sound originates from this region.

South Mooring Temperature and Salinity Temporal Structure

Like the north mooring, the water column at the south mooring decreased in temperature over 2011-2012 (Figure 2.12e). Concurrently, the water column freshened, which was more pronounced at 75 m (decrease by 0.39 g kg^{-1}) than at 275 m (decrease by 0.18 g kg^{-1}) (Figure 2.12d). These changes are consistent with changes in average CTD casts observed between summer 2011 and 2012 (Figure 2.4). On a seasonal timescale, the whole water column cooled in the late fall, lasting from late November 2011 until January 2012, however the bottom waters still remained warmer than those above, suggesting an outside influence or moving front between water masses rather than a wind mixing event like that observed at the north mooring (Figure 2.9). This fall-to-winter cooling also corresponds to the lowest temperatures in the TrW layer of the BIC flowing across the mouth of the sound (Curry et al., 2014) and is likely a combination of both outside influence and local mixing. After this time, water below sill depth warmed while the upper layer remained cool, perhaps in response to the lower temperatures in the AW layer of the BIC that occur at this time (Curry et al., 2014). Another cooling event occurs in mid-July 2012 which was contrary to the general timing of maximum temperatures in the BIC observed June-August (Curry et al., 2014).

The most striking feature of this time series are the fluctuations found in both the temperature and salinity (Figure 2.12d and e). Spectral analysis indicates that the most energetic periods correspond to tidal frequencies and are dominated by the spring-neap and M2 tides. To check if these fluctuations were the result of mooring movement, the mooring was modelled using the Mooring Design and Dynamics Mat-

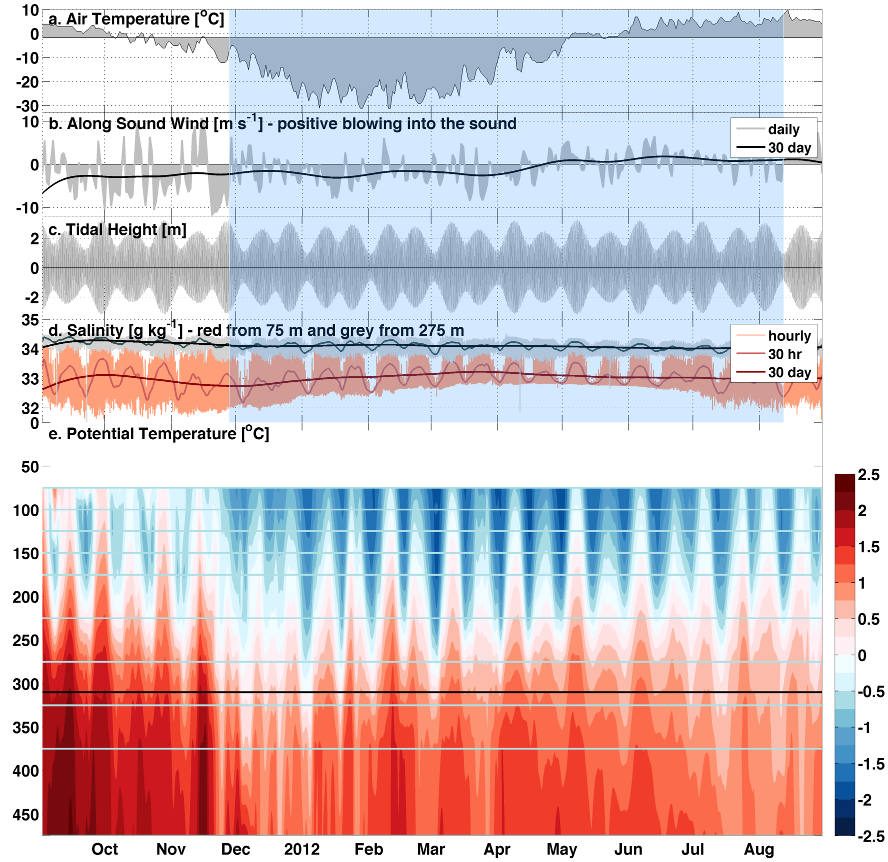

Figure 2.12: Time-series plots from the south mooring location. (a) NCEP reanalysis daily averaged air temperature at 2 m with a horizontal line at the freezing point of 32 g kg^{-1} water. (b) NCEP reanalysis daily average winds at 10 m rotated along the sound. (c) tidal height from Webtide model. (d) mooring salinity at 75 m (red) and 275 m (grey), lighter lines are hourly data, mid-tone lines have a 30 hr filter applied and darkest lines a 30 day filter. (e) mooring potential temperature time series. A 30 hour low pass filter has been applied to all data. Grey lines indicate instrument depths and the black line the depth of the sill.

lab package (Dewey, 1999). For a maximum tidal velocity of 0.3 m s^{-1} (maximum modelled tides at this location reached 0.18 m s^{-1}) the top of the mooring experienced a maximum vertical excursion of 4 m, which is less than 1% of water depth. Further confirmation that the mooring did not significantly move vertically comes from the bottom temperature sensor located at 1 m off the bottom (Figure 2.13b) that follows the same fluctuations as the sensors above. Therefore, it is assumed the observed fluctuations are not the result of instruments moving through different vertical layers in the water column.

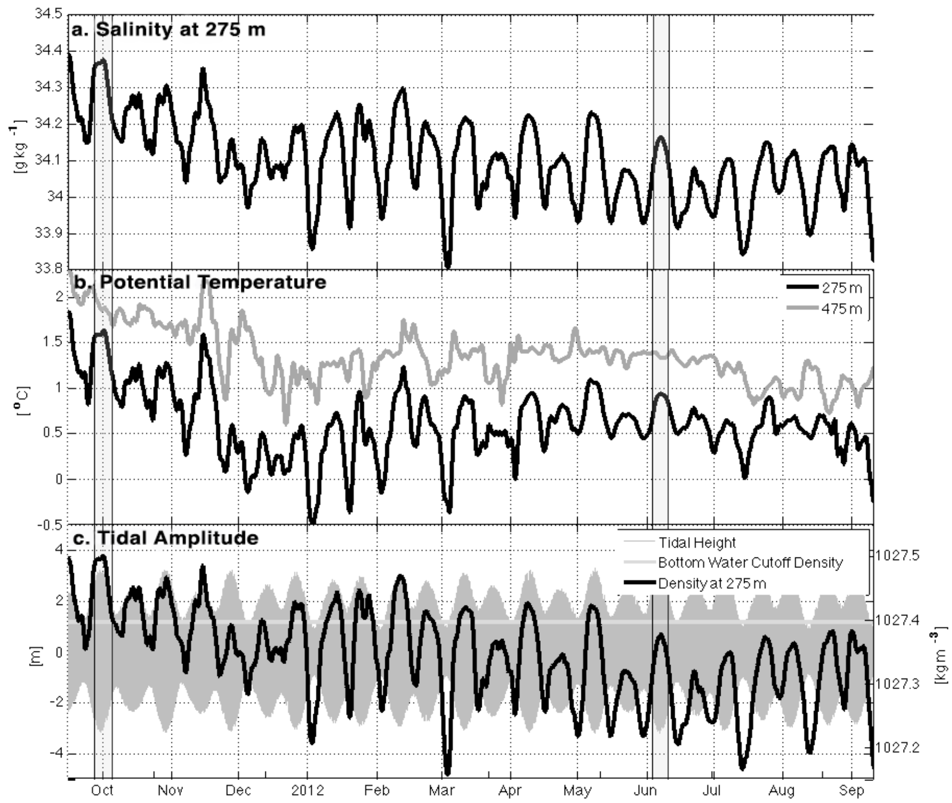

Figure 2.13: Temperature and salinity data from the south mooring at 275 and 475 m with tides from Webtide. (a) salinity at 275 m. (b) potential temperature from both 275 m and the bottom (475 m). (c) tidal height in grey is indicated on left axis and density in black on right. Light grey line marks the deep water threshold of 1027.4 kg m^{-3}. Highlighted period in September to October 2011 represents a time of deep-water renewal while the highlighted period in June 2012, no deep-water renewal occurs.

Deep Water Replenishment

In this section, we will show that deep water replenishment in Cumberland Sound occurred most often during spring tides in the fall of 2011. The 2011 and 2012 temperature-salinity curves from the sound were compared to the 2011 data extending out into the Labrador Sea (Figure 2.5a). No CTD casts were performed in the Labrador Sea in 2012. The south mooring CT sensor at 275 m, 200 m above the bottom (shown on Figure 2.5b), was situated to measure external water entering the sound. Over 2011-2012, the mooring water was of similar salinity, but colder than the summer CTD casts taken farther into the sound. Salinity at 275 m fluctuated following the spring-neap tides (Figure 2.13a). Compared to CTD casts from within the sound (Figure 2.4c), these fluctuations represent a depth range between 400-900 m, meaning that at 275 m, just above sill depth, water destined to fill most of the lower layers regularly passes.

Most of the year, water passing the mooring contained predominately BIC water, slightly cooler than the September 2011 BIC water denoted in light green in Figure 2.5b. At times, water passing the mooring, warmed and became denser, but never as warm and dense as the WGC water, suggesting mixed BIC/WGC water entered the sound. The densest water that passed the mooring matched water from 300 m in the BIC/WGC front (dark green lines in Figure 2.5b) and the deepest water in the sound. It is likely that this external water passing the mooring mixed with and cooled, or displaced, the deep water already in the sound resulting in the cooling observed between 2011 and 2012 (Figure 2.4b).

Over 2011-2012, density at 275 m decreased (Figure 2.13c). In general, water dense enough to become bottom water passed the mooring infrequently (bottom water cut off density of 1027.4 kg m^{-3}, Figure 2.13c) in pulses that were also warmer (Figure 2.13b). These warm pulses only reached a maximum of 2.5 °C, and never as warm as the 2.9 °C bottom temperatures measured in 2011. Although, these pulses of warm, dense bottom water occurred into May 2012, they were most frequent in the fall of 2011 and corresponded to spring tides (Figure 2.13c) suggesting stronger currents associated with these tides play an important role in mixing the front water and facilitating its entry into the sound. Water was generally less dense on the neap tides (Figure 2.13c) and water entering the sound was predominately BIC water. Overall, roughly 75% of the time water passing the mooring was not dense enough to become bottom water.

At the sound's mouth, maximum barotropic tidal velocities from the Webtide Model reached 0.18 m s^{-1} (Hannah et al., 2008). A rough determination of how far water moves on each tide, the horizontal tidal excursion (E), was calculated using:

$$E = U_o T \pi^{-1} \tag{2.2}$$

where U_o is the horizontal velocity and T is the tidal period. Maximum tidal excursion at the mouth of the sound was 2.6 km, much less than the shelf width (~300 km), suggesting tidal ventilation could not have acted alone to ventilate the deep water.

'Pulses' containing the densest and warmest water were observed September to November 2011 on the spring tides. An example spring tide from October 2011 is highlighted in Figure 2.13. Here water dense enough to be bottom water passes more frequently than during a comparable spring tide from June 2012, also highlighted (Figure 2.13). Considering the 30 hr filtered density for both time periods, water dense enough to be bottom water passed the mooring in November 2011 and not during June 2012. The fall is the time of peak currents for both the BIC and WGC. At this time, the BIC gets denser due to ice formation and further reduces the density difference with the WGC. This seasonal variability, suggests that deep water in the sound is the result of tidal mixing of the BIC and WGC at times when the variability in these currents allows the water to flow into the sound.

2.4 Discussion

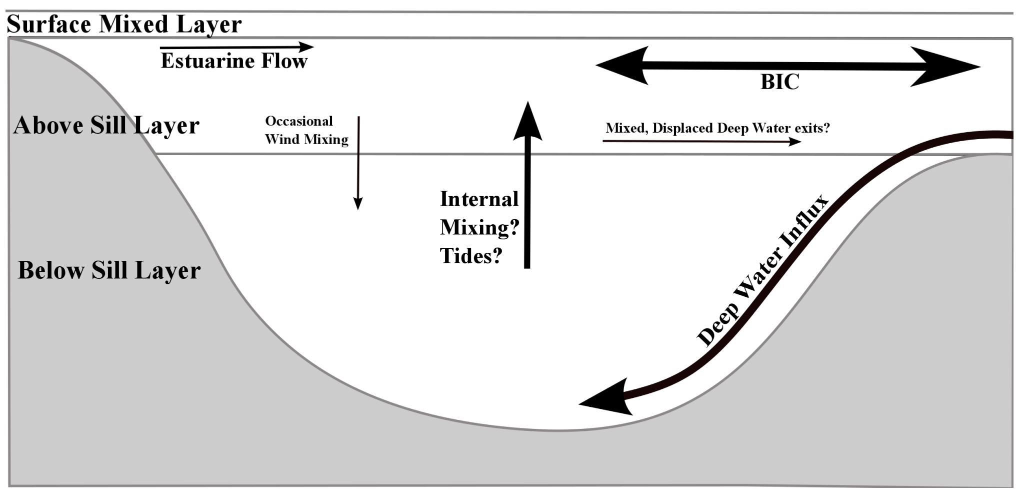

Figure 2.14: Schematic diagram illustrating some of the physical processes that occur through the year in Cumberland Sound. External influence includes: geostrophic incursion of the BIC dominating the characteristics of the above sill layer and deep water pulses of mixed BIC and WGC water replenishing the deep water. Observed internal processes include: estuarine flow and occasional wind mixing. A requirement for mid-depth processes, such as internal tides, remains to mix the displaced water and allow it to exit the sound.

Although Cumberland Sound is an isolated sub-Arctic embayment, the currents crossing the sound's mouth subject the interior to influences from water masses from across the sub-Arctic. A schematic of the identified physical processes in Cumberland Sound is shown in Figure 2.14. Above the sill, cold, fresh water from the BIC circulates through the sound. Below the sill, lower layers are replenished intermittently by a warm, saline mix of BIC and WGC water masses. Although, external physical processes dominated, the observations suggested several internal processes, including estuarine flow and wind mixing, are also present. However, it is postulated that the observed internal processes are incomplete and other unidentified physical processes that reach to the mid-water column are required to explain the observations (Figure 2.14). Pulses of dense water were observed entering the sound, destined to replenish the deepest regions. However, evidence of water leaving the deep areas was not observed. As dense water entering the sound displaces what is already there, a link must exist between the deepest layers and the layers above. Since most of Cumberland Sound below the sill is horizontally homogeneous, any deep water displaced upwards must cool and freshen, implying that mixing occurs in the mid-water column below the temperature minimum but well above the bottom. The fate of the displaced deep water has not yet been determined, but it is possible that it rises to just above the sill and is entrained below the BIC water leaving the sound.

Several internal processes may impact the mid-depth water in the sound, such as observed wind mixing and estuarine circulation, and not-observed sinking of dense water from ice formation and internal tides. Infrequent wind mixing events influenced water to depths greater than 200 m. Typically these events lasted a few days and were accompanied by strong winds that switched direction. One event was observed in the fall of 2011 and two in the fall of 2010. Over the entire sound, wind mixing events might reach deep enough to facilitate cooling of the displaced deep water. Estuarine flow is another potential mechanism bringing up deeper water. At the head of the sound, a fresh water plume was observed pushing out from a seasonal river source. At $\sim$150 m, a pocket of warmer water with higher salinity was observed beneath the fresh water plume above, perhaps drawn up from below. Not observed, but likely playing a role, is sinking cold, salty water that is rejected when ice forms. Finally, the mid-depth water is likely impacted by the strong tidal currents in the area. It is postulated that these currents get converted into strong internal tides within the sound. It is likely that a combination of all these processes facilitates the removal of displaced bottom water from the lower layers.

Changes within either the BIC or WGC have the potential to make a significant impact on the aquatic ecosystem of Cumberland Sound. For example, a significant freshening of the BIC from ice melt further north could increase the stratification above the sill and therefore potentially blocking the influx of dense bottom water into the sound. Within a few years the sound could become hypoxic and unable to support the current ecosystem. The likelihood of these changes occurring is difficult to determine. A freshening trend of 0.15 g kg^{-1} per decade has been observed in

Baffin Bay/Davis Strait (Steiner et al., 2013). One source of this fresh water is from melting glaciers in Greenland (Steiner et al., 2013). Between 1992-2010 the rate of discharge from Greenland's glaciers accelerated and is expected to keep accelerating (Rignot et al., 2011). Closer to Cumberland Sound, Hamilton and Wu (2013) predict the BIC will freshen by 0.4 g kg^{-1} by 2050. These predictions would strengthen stratification in the sound and increase the probability that replenishment would be cut off in the below-sill layer.

Alternately, if the BIC warmed or more WGC water entered the sound, bottom temperatures could rise slightly. Warmer water could change how fish use the area. For example, currently Greenland Halibut use Cumberland Sound as a foraging ground where they stay a few years before moving on (Peklova et al., 2012). To date, no evidence of spawning Greenland Halibut has been found in the sound (Kevin Hedges, pers. coms.) implying these fish leave to spawn. A known spawning ground exists in Davis Strait outside the sounds mouth in water warmer than 3 °C (Scott and Scott, 1988). Only a slight warming of Cumberland Sounds bottom water would result in water consistently above 3 °C, potentially changing the sound from a rich foraging ground to a spawning ground.

There is no other sub-Arctic site comparable to Cumberland Sound. Near by, only Frobisher Bay and Hudson Strait share similar widths as Cumberland Sound, are also in the flow path of the BIC and WGC, and have strong tidal currents, but neither provide a good comparison. Frobisher Bay, just south of the sound, is at most less than half the depth of Cumberland Sound and little previous work has been done here. Monitoring done in Hudson Strait (Straneo and Saucier, 2008) shows that a geostrophic flow through the strait occurs following the same pattern as Cumberland Sound; westward along the north shore and eastward along the south shore. However, Hudson Strait is part of a the larger Hudson Bay system (Straneo and Saucier, 2008) with much stronger tidal currents ($\sim$1 m s^{-1} in Hudson Strait vs $\sim$0.2 m s^{-1} in Cumberland Sound) preventing useful comparisons between the two locations.

Cumberland Sound is a complex and unique environment where influences from various sources have impacts down to the deepest depths. The water origins and important physical processes that define water within the sound have been identified. However, the internal processes have not been fully defined, nor has the impacts of changes to the BIC or WGC on the sound, leaving important questions unanswered for future study.

2.5 Conclusion

Water properties in Cumberland Sound are influenced by outside water of two different origins, the Baffin Island Current and the West Greenland Current. Above the sill, the cold Baffin Island Current follows a geostrophic pattern, bending into the sound. This water enters along the north shore, circulating the sound and leaves along the south shore, however at times this pattern is interrupted. The warm deep water is replenished from the recirculated arm of West Greenland Current occasionally flowing over the sill and down to a stable depth. This process is variable and occurs most frequently on spring tides. This influx of water prevents deep water hypoxia, allowing the deep-dwelling fish populations in the sound to thrive.

Chapter 3

On the Variability in Detection Ranges of Passive Acoustic Tags

Examining fish behaviour through passive acoustic tracking is a technique being employed more and more. Typically, research using this method focuses on detections without fully considering the influence of the environment. Here we linked the aquatic environment of Cumberland Sound with factors influencing the detection efficiency of fish tracking equipment and find multi-path signal interference to be a major issue. Cumberland Sound is a remote Arctic embayment where three species of deep-water fish are currently tracked. Detection ranges obtained through a series of year-long acoustic functionality experiments (range tests) are combined with two-dimensional ray tracing model results to examine the effect of both environmental and equipment related factors on detection ranges.

3.1 Introduction

How aquatic animals use their environment is an important question, but direct observations are difficult to obtain resulting in large data gaps. To fill these gaps a number of telemetric techniques have been developed. One method, passive acoustic animal tracking, is providing new information about how animals live in aquatic environments (Hussey et al., 2015; Lennox et al., 2017). In these studies, animals are surgically implanted with an acoustic transmitter, or 'tag', and receivers are deployed at critical locations where the animals might pass. When the tagged animal moves within the detection range of a receiver, its identity is recorded along with the time, creating an animal presence snapshot. Multiple detections of tagged animals provide information on movement and habitat use patterns, and inferences can be made about animal behaviours, such as migration patterns and predator/prey dynamics (Kessel et al., 2013). A review of studies from 1986 to 2012 found an exponential growth in the use of passive acoustic animal tracking (Kessel et al., 2013), causing this technique to be described as a 'revolution' (Hussey et al., 2015).

Passive acoustic telemetry is based on the following assumptions: 1. the experience of being tagged does not affect the behaviour of the animal being tracked, 2. equipment performance does not bias the data, and 3. the resulting detection data are representative of the animal's behaviour (Singh et al., 2009). Also, it is often assumed the rate of signal attenuation with distance is stable over space and time, something that generally is not true (Gjelland and Hedger, 2013).

Unfortunately, past studies typically do not fully consider passive acoustic tagging limitations. Kessel et al. (2013) found that researchers considered the variability of detection effectiveness in 42% of 378 studies evaluated, but only 18% discussed the influence of multiple external factors. However, reliable inferences about tagged animal behaviour can only be made in conjunction with an understanding of the dynamic nature of detection effectiveness for any particular study area (Payne et al., 2010; Kessel et al., 2013).

Determining how well an *in situ* passive acoustic telemetry system is able to detect tagged animals is critical for data interpretation. This includes quantifying the maximum detection range, that is, how far away from a tag the signal is reliably received. With the exception of occasional false detections (Simpfendorfer et al., 2015), one can be reasonably confident that a detection means a tagged animal is present. However, if no detections are recorded, one cannot be certain that no tagged animals are present because detection effectiveness is typically less than 100% and can change with environmental variability and equipment set up. Physical and technical limitations must be considered when interpreting detection data. The main issues impacting detection effectiveness are the environmental conditions, including ambient noise, multi-path interference, and the electrical and mechanical nature of the detection equipment. These issues are interconnected, and all play a role; thus, quantifying detection effectiveness requires addressing all of these factors.

As a tag's signal propagates from transmitter to receiver it is influenced by the local environment which can result in fluctuating detection effectiveness. First, the signal spreads geometrically as it propagates, causing the sound intensity to decrease at a rate of $1/r^2$ (spherical spreading) or $1/r$ (cylindrical spreading), where r is the range, depending on whether propagation is bottom/surface bounded. Further, propagating signals can be absorbed and/or scattered, or even blocked by obstacles (Medwin and Clay, 1998). In addition to the direct path, a signal may reflect off of boundaries resulting in the same signal following many paths between transmitter and receiver. These multi-path arrivals can interfere with the time coding of the signal used by the receiver to identify a specific tag and cause the receiver to fail to register a signal reception. Finally, the receiver must pick the signal out from the background noise, which also depends on the environmental conditions. Environmental factors change with time, further complicating data interpretation and making predictions about what factors impact detection effectiveness a difficult, site-specific problem (Huveneers et al., 2016; Ottera and Skilbrei, 2016).

The impacts of a changing environment on how tag signals are received are only beginning to be systematically examined. For example, Heupel et al. (2006) found that receivers located in adjacent estuarine and freshwater environments had a significant detection range difference, dropping from ∼800 m in the estuary to ∼600 m in freshwater. In another study, at different depths in a fjord, a combination of wave action and stratification resulted in detection ranges varying between 45 and 650 m (Finstad et al., 2005). Detection effectiveness was also found to vary due to turbulence and entrained bubbles (Thorstad et al., 2000). Clements et al. (2005) found that detection efficiency in shallow water (less than 21 m) was much greater for a flowing-water system than a static-water system, possibly due to background noise. This relates to the discussion by Kessel et al. (2015) of how low noise environments with a hard boundary (e.g. the water-air interface or the bottom) can result in short-range interference between different path signals, resulting in fewer than expected detections.

The optimum design and implementation of a passive acoustic animal tracking experiment is site-specific. In a recent study, Huveneers et al. (2016) found that receiver depth and orientation, along with time since deployment (potentially related to biofouling), had more influence on detection range than other environmental factors they considered (wind, precipitation, atmospheric pressure and water temperature). Detection ranges vary with tag transmitter power, with the detection ranges of lower-powered transmitters decreasing much faster than those of higher-powered tags (How and de Lestang, 2012). How a receiver is mounted on the mooring line can block incoming acoustic signals (Clements et al., 2005) and receiver performance can be negatively impacted by biofouling (Heupel et al., 2008; Ottera and Skilbrei, 2016; Huveneers et al., 2016).

A way to study these issues is to perform an acoustic functionality experiment, also known as a detection range test, at the study location. In such a test, a series of tags programmed to transmit at regular intervals are deployed at known ranges from a receiver. The purpose is to determine how effectively signals are recorded over time at different ranges to quantify the variability of the system (Singh et al., 2009). In addition, the impact of multi-path interference can be evaluated. These tests can also help to determine the optimum number of tags and the optimum receiver spacing, and can provide insight into possible causes of unexpected results (Singh et al., 2009).

Quantifying how receivers respond to local conditions through a detailed analysis of range test data can provide confidence in negative results (Udyawer et al., 2013). However, Kessel et al. (2013) found that although most of 378 acoustic tagging studies reviewed performed a range test, only 13% published the results. Additionally, the scope of these range tests varied from a single tag held in place for a few days to comprehensive testing with a series of tags deployed for the study period of up to a year (Kessel et al., 2013).

Another tool to examine both the effects of environmental factors and acoustic tracking geometry is acoustic modelling. Although acoustic models are widely used in other applications, they are only beginning to be applied to passive acoustic animal tracking studies. Melnychuk and Walters (2010) used an attenuation model to predict the number of fish that passed an array but were not detected. Gjelland and Hedger (2013) showed that the probability of detecting a tagged animal could be modelled using attenuation coefficients and general sound propagation theory. Huveneers et al. (2016) took a statistical approach by estimating the range at which detection probabilities drop below 50% from fitting detection data with a logistic or sigmoidal curve. How and de Lestang (2012) found a 3-parameter sigmoidal model provided the best fit. Despite these few reported studies, acoustic modelling as a tool to understand and interpret acoustic telemetry data is currently underused.

Here we investigate the environmental issues affecting the detection effectiveness of three range tests deployed in Cumberland Sound, Baffin Island, between 2011 and 2012. This work was conducted as part of an Ocean Tracking Network (OTN) study (Cooke et al., 2011) to monitor a commercially viable fish population in the sound (Peklova et al., 2012). The detection effectiveness at various ranges is evaluated and interpreted using a simple acoustic ray tracing model demonstrating the impact of multi-path interference. Even though the present analysis is focused on data from Cumberland Sound, the methodology from this work is applicable to passive acoustic telemetry studies in other locations.

3.2 Methods

3.2.1 Characteristics of transmitter tags and receiver arrays

The acoustic tags and receivers used in this study were manufactured by Vemco Ltd., Bedford, Nova Scotia, Canada, and are in wide use (Kessel et al., 2013). Different sizes of tags are available, creating a trade-off between tag size, battery life and power output. The tags chosen for a specific study depend on the target animal size and project data requirements; therefore, in any given scenario, multiple tag types may be used. In this study three types of tag (V9, V13 and V16) with a range of source levels were used (Table 3.1).

Tag Type	Frequency [kHz]	Power Output [dB re 1 μPa^2 Hz^{-1}]
V9	69	145-151
V13	69	147-153
V16	69	150-162

Table 3.1: Tag types used in this study. Frequency and power output are taken from the manufacture's website (http://vemco.com).

The basic operation of both animal tracking and range testing tags is the same. All tags transmit a unique acoustical time coded signal at a fixed frequency. The difference between fish and range test tags is the time intervals between transmissions. For fish tags, the signals are transmitted at random intervals to minimize the chance of two tags transmitting simultaneously within a receiver's range. In contrast, range test tags are programmed to transmit at a constant known interval. In this study, all tags were programmed with a fixed time interval between signal transmissions of between 1770 and 1830 s. Using a carrier frequency of 69 kHz, tag transmissions consist of two synchronization pulses followed by a unique identification (ID) code made up of a series of six pulses. Each pulse contains roughly 34 cycles of the carrier frequency, resulting in pulses ~5 ms long. The times between the various pulses form the ID code, with a total of seven digits. Each transmitted ID code is at least 1.9 s in duration.

When the VR2W-69 kHz receiver detects the first pulse it turns off (sleeps) for 260 ms to minimize interference from other signals and other tags. Following this delay the receiver turns back on and waits for the next pulse in the ID sequence. Once the second pulse is detected the receiver again sleeps for 260 ms before waiting for the third pulse. This process repeats for all eight pulses. The receiver then performs a checksum, or error check, to determine if a valid signal was detected. If a signal is validated, the date, time and ID code of the tag are stored in the receiver. Incomplete or non-existent ID codes may be detected for several reasons. The same signal following another path, a different signal or even noise of the right frequency to interfere with the signal can result in an invalid ID code or a false detection. It is also possible that a tagged animal can move through a region that blocks part of the signal (Simpfendorfer et al., 2008). Each receiver generates detection data summary statistics every 24 hours including the total number of pulses, the total number of synchronization intervals, and the number of checksum errors received per day. The total number of pulses divided by the total number of synchronizations should be equal to eight under ideal conditions. Any significant departure from eight indicates transmission collisions, path interference or significant ambient noise levels in the vicinity of the receiver.

3.2.2 Tag receiver deployments in Cumberland Sound

In support of fish tracking efforts in Cumberland Sound, three year-long range tests were performed from August 2011 to August 2012 (Figure 4.1). The aim was to determine the temporal variability and environmental dependence of detection ranges over a year in a range of water depths from 100-1000 m. To set the stage for acoustic propagation at the site, sound speed profiles were computed from the average of a set of summer 2011 and 2012 CTD (conductivity, temperature and depth) profiles (Figure 4.1b). At a depth of approximately 100 m there is a sound speed minimum, below which the sound speed increases steadily to the bottom creating an upward refractive acoustic environment. The shapes of the sound speed profiles were the same in the two years; note that both are summer profiles and winter conditions would be different. However, the speeds were lower in 2012 due to the colder water that year. A more detailed oceanographic discussion of the sound can be found in Bedard et al. (2015).

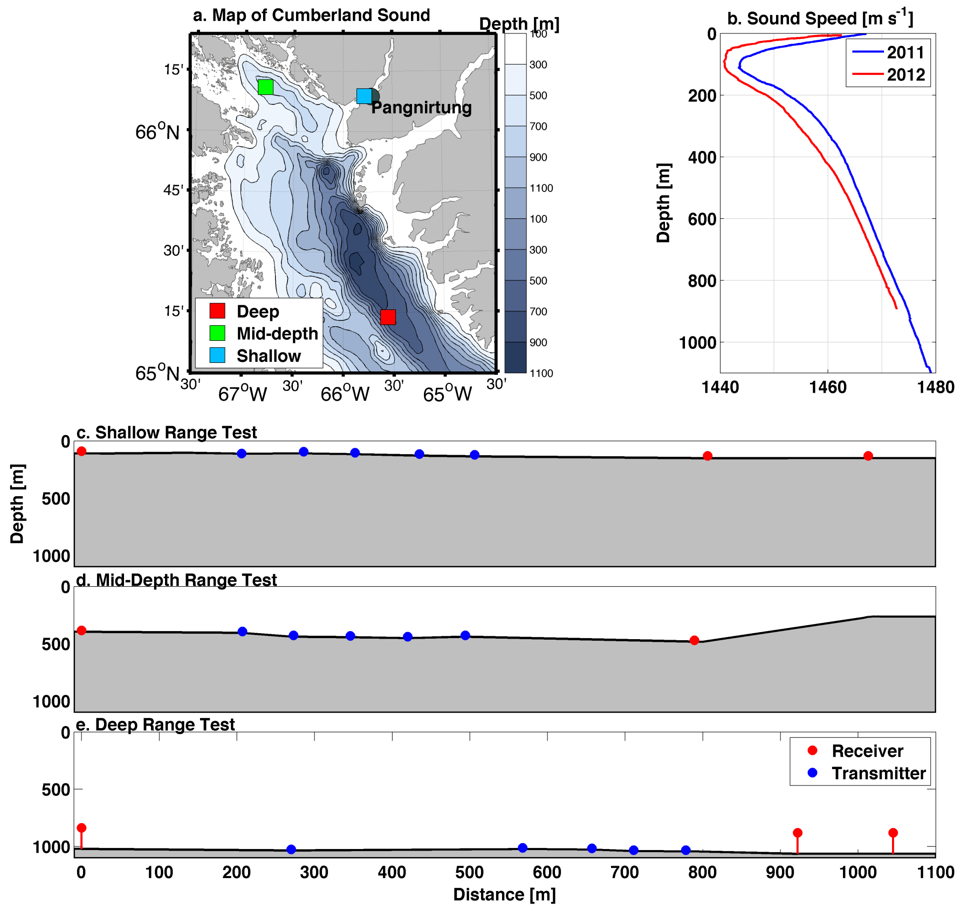

Figure 3.1: (a) Location of the acoustic receivers and transmitters in Cumberland Sound. Red square is the Deep Range Test, green square is the Mid-depth Range Test and the blue square is the Shallow Range Test. (b) Sound speed profiles for Cumberland Sound, blue for 2011 and red for 2012. (c-e) Layout of the three range tests where red dots indicate receiver moorings and the blue dots the transmitter moorings. The depth and distance scales are the same in all panels to allow comparison.

The range test layouts are summarized in Figure 4.1c-e and in Table 3.2. The first range test was conducted at a depth of 1000 m in the southern, deep-water region of the sound, and is referred to as the *Deep Range Test* (red square in Figure 4.1a). This test included both V16 and V13 tags. The second range test was conducted in ∼400 m of water in the northern end of Cumberland Sound and is referred to as the *Mid-depth Range Test* (green square in Figure 4.1a). This test was performed in a location with 10% slope to the sea floor and used all three tag types. The third test was conducted in ∼100 m of water inside Pangnirtung Fjord (blue square in Figure 4.1a), using all three tag types, and is referred to as the *Shallow Range Test*. Three

Range Test	Mooring Type	∼Instrument Depth [m]	∼Height Above Bottom [m]	Tags Used
Shallow	Receiver	100	20	
	Tag	100	10	V9, V13, V16
Mid-Depth	Receiver	400	13	
	Tag	400	10	V9, V13, V16
Deep	Receiver	1000	182	
	Tag	1000	10	V13, V16

Table 3.2: Receiver and tag depths for each range test. Mooring layouts can be found in Figure 4.1.

receiver moorings, each with a downward facing receiver, were deployed in as straight a line as possible at each site. The first receiver was set at a predetermined location, the second receiver at a horizontal distance of 800 m and the third receiver at 1000 m (Figure 4.1c-e). Between the first two receiver moorings, five shorter moorings with one of each type of tag used at the site were deployed at regular intervals. This combination resulted in a total of 15 tag-receiver ranges. Note, for the Mid-depth Range test the farthest receiver did not record any data and it was assumed to have failed. Each mooring consisted of a 100 kg anchor attached by a 2 m line to an acoustic release followed by a 12 m riser to a subsurface float. The receiver and tag depths for each range test are summarized in Table 3.2. The range test tags were attached ∼1.5 m below the subsurface float using stainless steel wire, with the tags positioned out from the mooring line and spaced ∼0.5 m apart to minimize contact and rubbing. Following the one-year deployment, all moorings were recovered, and the receiver's data were downloaded.

Due to the receiver/tag geometry chosen for these experiments, the acoustic signal from each tag was potentially received at three different receivers (except at the Mid-depth Range test where only two receivers functioned). Therefore, a check was performed to ensure that each tag was recorded on at least one receiver to confirm each tag performed as programmed. To minimize the possibility that a given recorded signal was the result of interference, a detected signal was only considered valid if two signals from a given tag were received in sequence on the same receiver. Signals which did not fulfil these requirements were removed from further analysis.

For all three range tests, the valid detections were summed daily. From these data the detection probability, D, was calculated by dividing the number of daily detections by the expected number of daily tag transmissions (48 for this study).

Detection probability was averaged monthly to allow for seasonal analysis.

Surface conditions and ambient noise

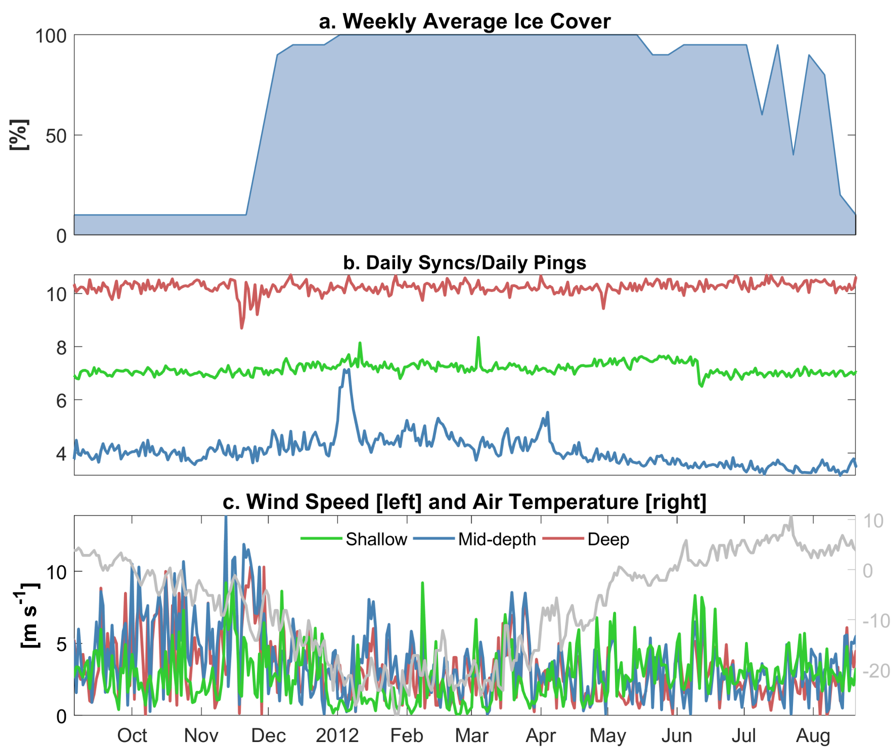

Figure 3.2: (a) Percent ice cover from the Canadian Ice Service weekly charts. (b) The ratio of the total number of pulses to the total number of synchronizations per day at each site; under ideal conditions this should be greater than 8. (c) Wind speed and air temperature from NCEP reanalysis at all three sites.

Due to its high latitude, Cumberland Sound experiences seasonal ice cover (Figure 3.2a). Weekly ice cover proportions from the Canadian Ice Service archives indicate that the sound had 50% ice cover by 28 November 2011 and 90% by 5 December. By 19 December 2011, fast ice began forming along the shores of the sound and by early January 2012, the sound contained primarily shore-fast ice. In May 2012, an open area formed midway along the south shore and cycled open and closed until the sound became ice-free. In the same month, at the north end of the sound, areas of reduced ice cover appeared then closed by early June. Ice began retreating in July leaving the sound mostly ice-free by late August.

Acoustic noise in the water column can potentially mask tag to receiver transmissions and therefore reduce the efficiency of a test range or tagging study. Farmer and Vagle (1988) established that a major component of the ambient noise field at kilohertz frequencies is produced by breaking waves generated by wind.

When the sound was ice-covered, internal ice processes and interactions with the air and water boundary layers become the primary sources of noise production (Carey and Evans, 2011). The resulting soundscape can have high variability. The rate of temperature change, duration and speed of the wind, tidal variations and currents, and how all these interact with the ice creates additional complexity making it difficult to estimate what the ambient noise levels might have been during the present study in the presence of ice. However, Milne et al. (1967) observed that wind and temperature change were the two main causes of high-frequency noise under ice.

3.2.3 Acoustic Ray-Tracing Model

To investigate and help interpret the acoustic range test data, a simple ray-tracing model was used. Ray-tracing (e.g., Clay and Medwin, 1977) provides a method to model sound propagation when the acoustic wavelength is much less than the water depth, changes in sound speed are negligible over several wavelengths, and the total ray path is much greater than the wavelength.

The ray-tracing model used was originally developed by Bowlin et al. (1992) then expanded to include boundary reflection losses as well as frequency dependent absorption by Erbe (2002). In the present simulations the bottom sediment composition was assumed to be a mixture of sand-silt-clay. Neither bottom scattering or sound propagation through sediment layers are included in the model. At the surface, the model can be run with either open ocean or solid ice cover losses (for a full discussion see Erbe (2002)). Sound speed profiles, which can be laterally-variable, and bathymetry are inputs to the model. The model calculates transmission losses between specified source and receiver locations. Using the nominal tag source levels (Table 3.1), the received levels at any receiver can be estimated for different sound speed profiles, bathymetries, bottom types and ocean surface scattering.

For this work, the ray tracing model was set-up using the sound speed profile from 2011 (Figure 4.1b) in 1 m increments and bathymetry from Figure 4.1c in 10 m increments. For each model run 10,000 rays were sent out between -89 and 89 degrees. The model was tested using extreme sound speed profiles with sources at different heights to ensure rays were refracted as expected.

3.3 Results

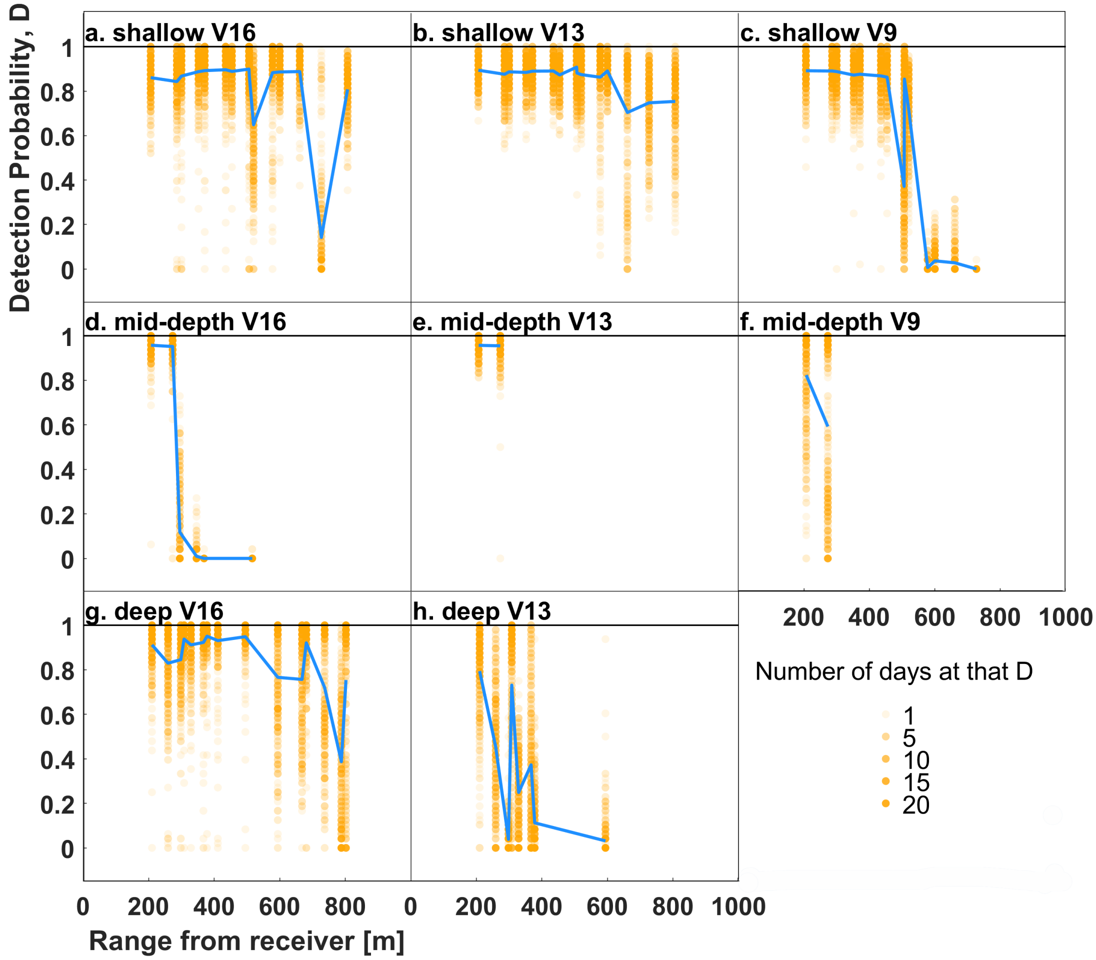

Figure 3.3: Daily detection probability, D, for all three range tests including all tag types in orange where the colour intensity indicates the number of days at that D value: more days are darker orange and fewer days are lighter where the aim was to highlight days with lower D. Blue line is the mean.

Daily detection probabilities, D, defined as the ratio of actual detections over the number of transmissions, for the three test ranges are shown in Figure 3.3 where darker circles indicate more data at that value. These results show data varied more between locations than between different tag types. Here, the maximum detection range is defined as the distance at which the probability of detection drops below 0.5.

This range varied with location and tag type. The V16 tags at both the shallow and deep sites, as well as the shallow V13 were detected over the longest ranges. Days with significantly fewer received tag IDs, or detection drop outs, are common in both the deep and shallow range tests, especially in the fall of 2011 (Figure 3.3). The number of observed dropouts is much lower in the mid-depth range test potentially a result of the overall detection ranges being significantly less (Figure 3.3d-f).

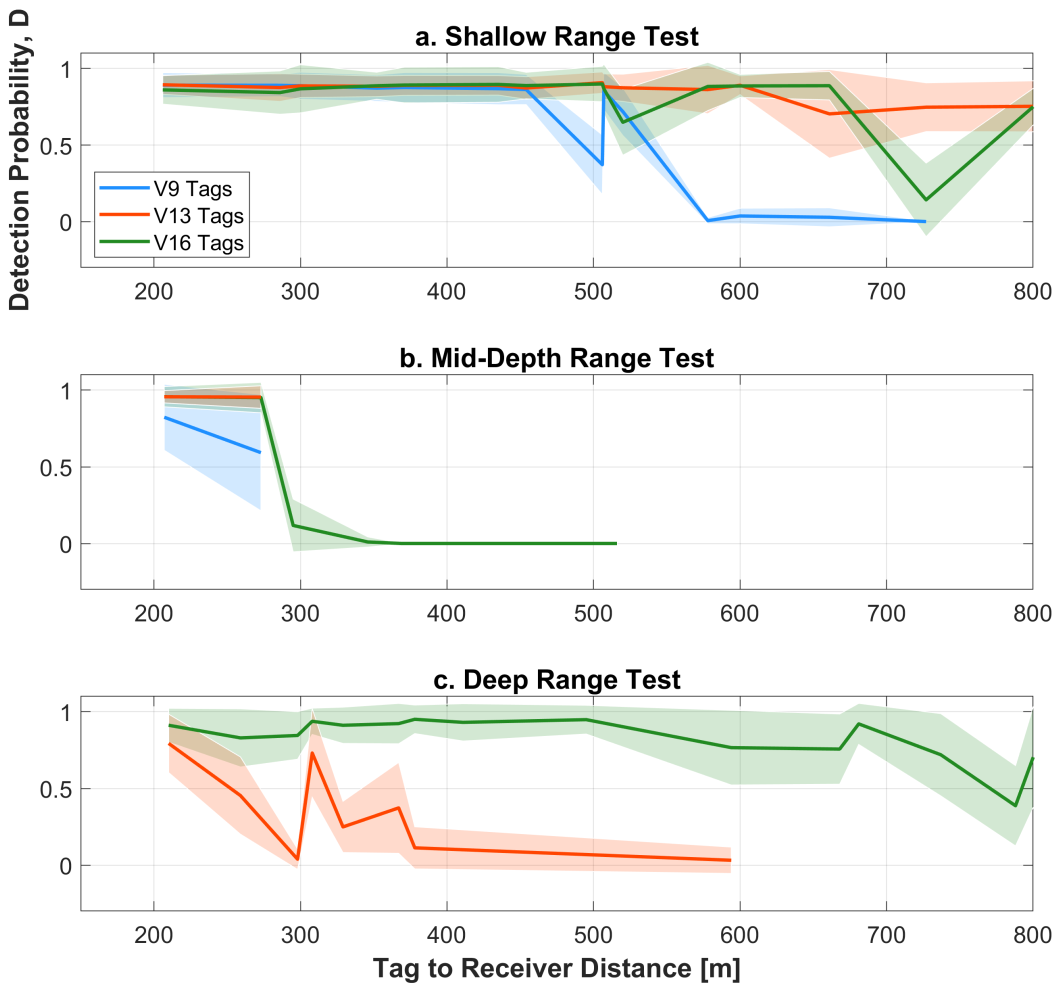

Figure 3.4: The mean curves of all received tag signals as a function of range for each test location (blue lines from Figure 3). Coloured bands indicate one standard deviation from the mean.

The average of all received tags for a single range test are plotted as solid lines in Figure 3.3. These curves are overlaid on the detection results for each location and tag type in Figure 3.3, then plotted separately in Figure 3.4 along with $\pm$ one standard deviation. For the Shallow Range Test the ranges at which D drops below

0.5 are ∼540 m, >800 m, and 700 m for the V9, V13, and V16 tags, respectively (Figure 3.4a). This differs from the Mid-Depth study where all 3 tag types have daily detection probability, D, below 0.5 beyond approximately 250 m (Figure 3.4b). For the Deep Test Range the D=0.5 ranges are ∼200 m and >800 m for the V13 and V16 tags (Figure 3.4c).

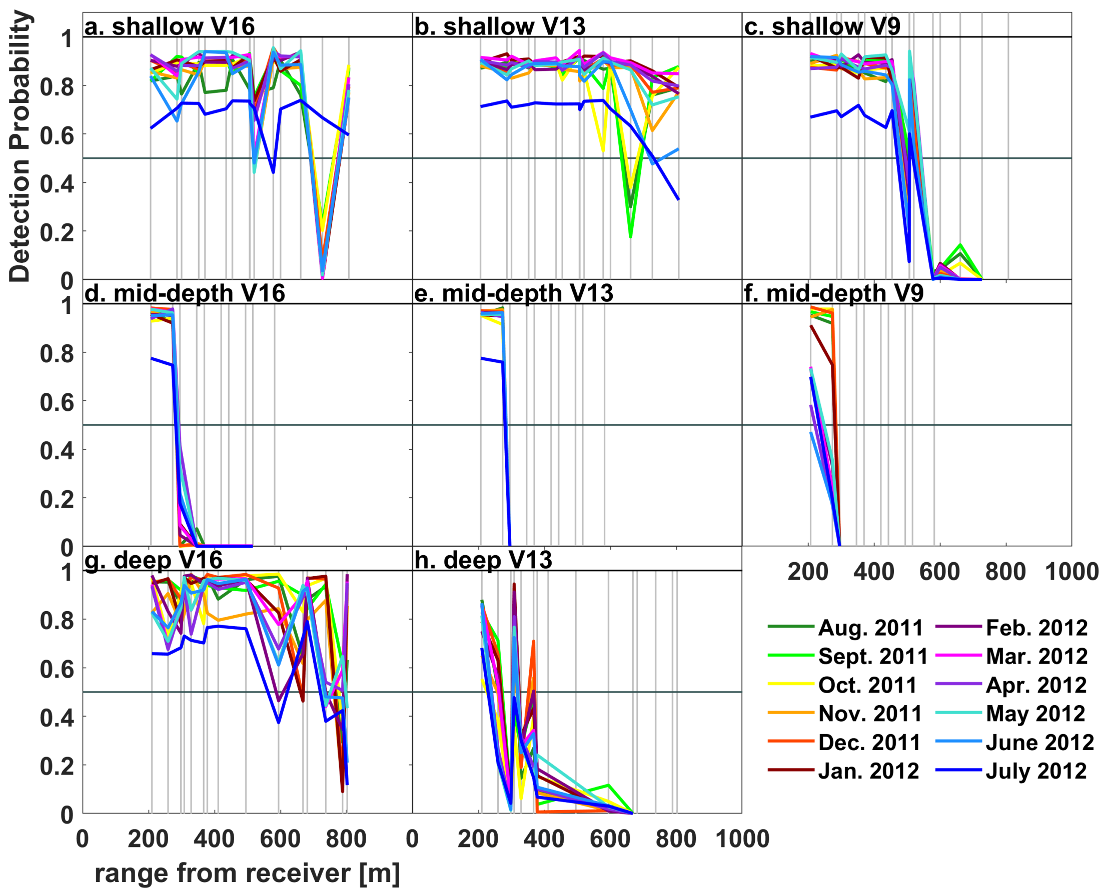

Figure 3.5: Monthly average range test results for all sites and tags. Thick grey horizontal line is the D=0.5 detection cut off and the thin, light grey vertical lines are the tag mooring distances from the receiver.

In both the deep and shallow range tests monthly averaged detections regularly drop to low values, with significant variability between months (Figure 3.5). For example, in the shallow V13 test at 661 m detection rates, D, drop below 0.5 only between August and October, 2011, staying above 0.5 for the rest of the study period (Figure 3.5b). These drop-outs do not occur at the same range between different tags at each test site. At the shallow site, the biggest drop out for the V16 tags occurred at 727 m (Figure 3.5a), for the V13 tags at 661 m (Figure 3.5b) and for the V9 tags at 506 m (Figure 3.5c). Similarly, in the Deep Range Test for the V13 tag at 270 m (Figure 3.5h) a drop out occurs without a corresponding drop in V16 receptions (Figure 3.5g). Possible explanations include: bottom features blocking the sound (unlikely as no features were detected with the depth sounder), mooring movement and multi-path signal interference. The lower detection probabilities measured in July 2012 were likely the result of the batteries failing in the tags.

One of the original objectives of these particular range tests was to evaluate the effect of water depth on detection range. The results show the most powerful tags (V16) both in the shallow and deep tests have detection ranges exceeding the maximum extent of the range test of 800 m; this suggests that the depth of either the tags or receivers are not an issue within this range, but it is unknown what effect depth may have at farther ranges. In the following sections each range test is discussed in more detail.

3.3.1 Shallow Range Test

The Shallow Range Test was conducted at an average depth of 100 m in Pangnirtung Fjord (Figure 4.1). Since the detailed bathymetry in the fjord is not well known, it is possible that there may be undocumented obstacles and minor bathymetric features. However, nothing significant was observed on the ship's echo-sounder while working in the area. The V16, V13 and V9 tags were tested over ∼800 m and the detection ranges were good at this site. With a few exceptions, the daily D values for the V16 tags remained above 0.8 out to the maximum extent of the test (807 m) (Figure 3.3a and 3.5a). At 727 m, D dropped to 0.2 at times between January and July 2012. In addition, a shorter range detection drop off occurred in May and early June and between 300 and 600 m primarily in the autumn of 2011. The V13 average detection rates were similar to the V16 rates with D>0.8 out to a range of ∼600 m (Figs. 3.3b and 3.5b). Farther out, the detection probability decreased to ∼0.7 to the maximum extent of the test. Again, detection drop outs occurred regularly between 550 m and 700 m in the autumn of 2011 and in June-July 2012. Finally, D>0.8 for all V9 tags closer than 500 m from a receiver (Figures 3.3c and 3.5c). Beyond that distance there was a significant drop in tag detections.

3.3.2 Mid-Depth Range Test

At the Mid-depth Range Test location, all three tag types were detected in a similar pattern (Figures 3.3d-f and 3.5d-f) with the V16 tags showing slightly better performance in Figure 3.4b where D is $\sim$0.4 at 290 m and $\sim$0.15 at 340 m. By separating the range test based on whether the acoustic signals had to travel up or down the 10% slope at the test site, the results shown in Figure 3.3d-f do not change significantly.

3.3.3 Deep Range Test

The Deep Range Test was conducted in the deepest part of Cumberland Sound at a water depth of 1000 m (Figure 4.1). This location is subject to strong tides and likely experiences occasional influxes of denser Davis Strait water (Bedard et al., 2015). Three receivers were positioned 184 m above the bottom while V13 and V16 tags were deployed 10 m above the bottom, creating the only range test with a significant depth difference between the tags and receivers. In general, more than 80% of the V16 tag transmissions were detected out to $\sim$600 m, but with significant variability as shown in Figure 3.3g and 3.5g. Most of the days with $D<0.5$ occurred in the autumn of 2011. At greater ranges the detection probability dropped, but on average remained above 0.6 out to the maximum range of 802 m.

The deep V13 range test produced the highest variability in D (Figure 3.3h and 3.5h). Also, the detection probability dropped from 0.8 to near 0 at ranges between 200 and 400 m, most easily observed in Figure 3.5h, intermittently over the year. An example of a significant drop followed by a gradual recovery is shown in Figure 3.6 for a tag located at 211 m from the reciever. The detection probability dropped from close to 1 to near 0 over a 2 day period between 10 and 12 October 2011. Over the same time frame, D at a range of 354 m, nearly 140 m further out, improved slightly. This time period corresponds to a time of deep water renewal (Bedard et al., 2015), when denser water entered the sound from outside and sank to the deepest depths. These renewal events occurred on spring tides in the fall of 2011. However, there was not any observed spring-neap cycle in the range test data, suggesting the two events may be unrelated.

The time intervals between pulses of improved detections (defined as periods when $D>0.1$) like those in Figure 3.6 were calculated over the entire year. These pulses were found to generally last less than 9 hours, with a mean time between them of days and therefore not related to any tidal frequencies in the sound.

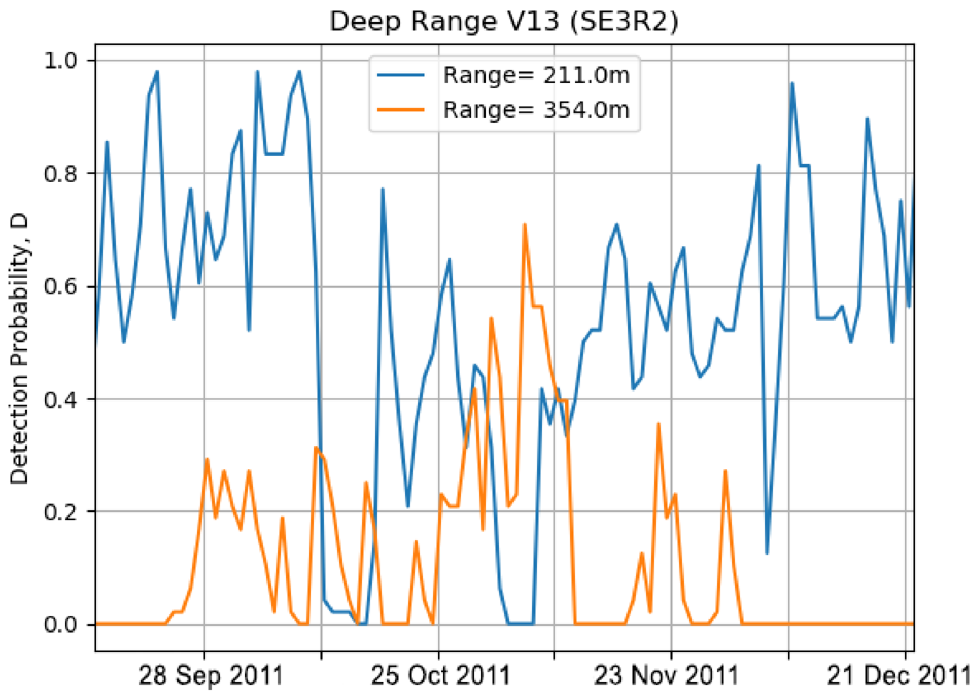

Figure 3.6: Detection probability at two ranges for the Deep V13 test. Blue line is for 211 m and the orange one for 324 m. Dates range between August to December 2011.

3.4 Discussion

The results presented above show both spatial and temporal variability in the detection probability in all three range tests. To facilitate interpretation of acoustic tag data it is important to understand the factors playing a role in defining the detection probability and its variability. To do this we used a simple two-dimensional ray-tracing model. Sound energy transmitted by a given tag is influenced by losses from spreading and frequency dependent scattering as well as losses due to molecular absorption as the signal travels to a receiver. The ray tracing model was configured with the tag-receiver configurations of the three range tests and the average of the two sound speed profiles shown in Figure 4.1b. Another factor that may impact results is focusing/defocusing of rays which is not considered here.

Figure 3.7 shows modelled received level as a function of range for the shallow range test. The three curves represent the range dependent received level when the mean source levels of each of the acoustic tags (Table 3.1) are used. From Figure

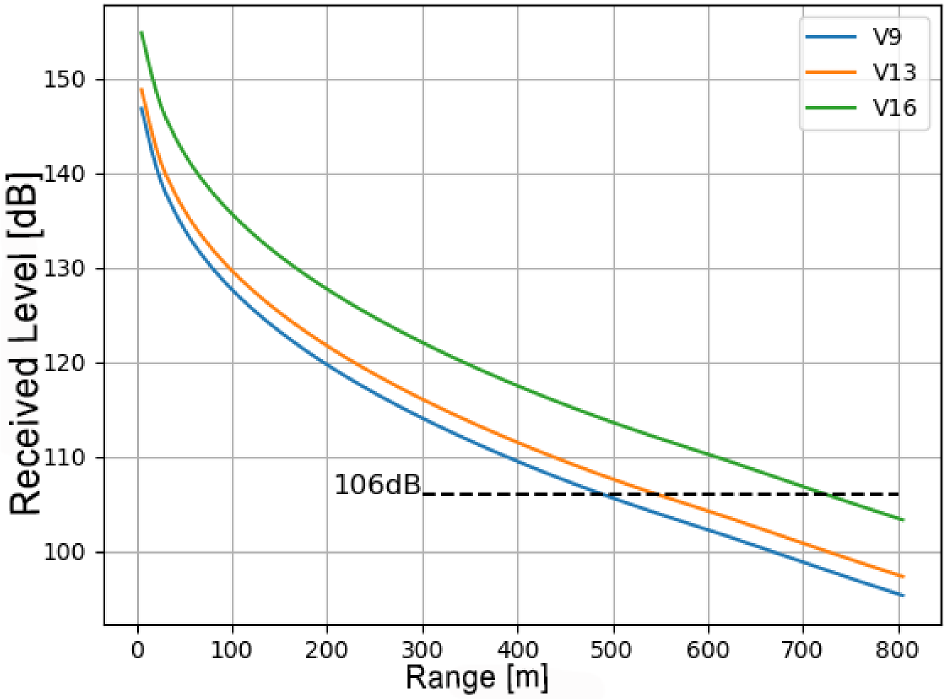

Figure 3.7: Received level as a function of range for the Shallow Range Test where the horizontal line at 106 dB is the observed detection threshold. Colours denote tag type: Blue for V9, orange for V13, and green for V16.

3.3a and c it is clear that for the V9 and V16 tags the maximum detection ranges, or ranges at which D=0.5, are approximately 500 m and 700 m, respectively. Using these ranges in Figure 3.7 it is possible to estimate that the detection threshold of the receivers is ∼106 dB re 1 μPa^2 Hz^{-1}. Assuming this detection threshold is also valid for the V13 tags, the results in Figure 3.7 show that the maximum range of the V13 tags is ∼550 m, which is a shorter range that observed in Figures 3.3, 3.4 and 3.5. Note, according to the tag manufacturer the tags have power outputs that can vary by as much as 12 dB (Table 3.1), potentially explaining some differences among the tag detection probabilities observed in this study.

The acoustic tags transmit coded signals at least 1.82 s in length, composed of eight 69 kHz pulses separated by a blanking period of 260 ms plus a delay associated with the particular ID. As stated previously, the receivers are programmed not to accept pulses arriving within the 260 ms blanking period, afterward there is a window when it is ready to accept the next pulse of the ID code. Ideally, all the pulses along a given acoustic path will make up the ID code transmitted by a given tag. However, if the signal following another path arrives at the receiver before the next direct path pulse, it would be recorded and the ID code would be compromised resulting in a missed detection or *mid-range gap* or a wrong tag ID recorded. The existence of a different path that could create a mid-range gap depends on the geometry and sound speed properties of a given site. As a given path becomes longer through reflections off surface and bottom interfaces, transmission losses due to reflection and scattering increase until the signal is too weak to be detectable at the receiver. Using the ray-tracing model it is possible to explore and compare the time delay and transmission losses experienced by different rays travelling between a tag and receiver.

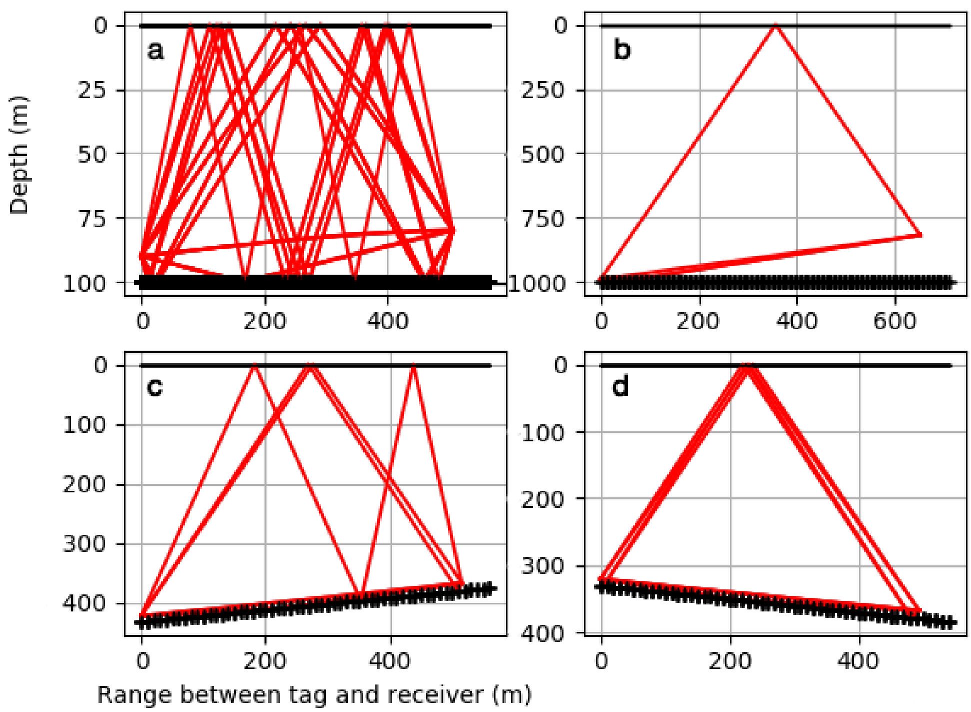

Figure 3.8: Model results showing possible paths between the tag and receiver for the four geometries used in this study. (a) Top left is the Shallow Range Test. (b) Top right is the Deep Range Test. (c) Bottom left is the Mid-depth Range Test up the 10% slope and (d) bottom right is the same depth but down the 10% slope.

A threshold of 20 dB between the direct path arrival and subsequent arrivals was set as the limit for detectable signals. i.e., if a secondary path signal was more than 20 dB below the direct path signal, it was discarded. This threshold was chosen based on the Shallow Range Test V9 result at a 500 m range (Figure 3.3c) because this test most closely follows the theoretical curves presented by the manufacturer.

Using this threshold, the detection range of the lowest power tag (V9) becomes 500 m (Figure 3.7) which is the same range given by the 'calm' setting on the Vemco range calculator for this tag (https://vemco.com/range-calculator/). Using the 20 dB threshold, Figure 3.8 shows all possible travel paths between tag and receiver for the four geometries used in this study, where the tag is at a range of 0 m and the receiver at the right in the figures. For the Shallow Range Test (Figure 3.8a) there is the direct, shortest, path, followed by bottom-reflected and surface-reflected paths, and then some source-surface-bottom-surface-receiver paths, etc. The maximum number of surface reflections is 3 and the maximum number of bottom reflections is 2. For the Deep Range Test (Figure 3.8b) there are only the direct path and one surface reflection path that are within our -20 dB criterion. Figure 3.8c and d are the Mid-Depth Range Tests with 10% up slope and 10% down slope, respectively.

The time delays between the direct path and all the secondary paths for the different tag-receiver combinations are shown in Figure 3.9. In the figure each diamond corresponds to the time delay between the direct path and secondary path, and the solid black horizontal lines show multiples of the 260 ms blank-out time. For the Shallow Range Test (Figure 3.9a), the pulses following the secondary paths all arrive significantly before the 260 ms blanking window. These pulses will therefore not interfere with the direct path pulses and will not be the cause of dropouts in the observed data.

The equivalent figure for the Mid-Depth Range Test (Figure 3.9b) shows the difference between arrival times for secondary paths and the direct path in the case the bottom is flat (blue diamonds), 10% downslope (red diamonds), and 10% upslope (green diamonds). In this case, there is a significant opportunity for secondary path pulses to arrive before the next direct path pulses since the delay is between 250 ms and 400 ms, with timing especially close to 260 ms at ranges greater than 300 m. We therefore argue that this interference is likely the cause of the very limited, and tag independent, detection range for this particular test range.

The Deep Range Test time differences are shown in Figure 3.9c. Here there are very few rays following a secondary path that meet the -20 dB requirement. However, the few that do have delay times close to two pulse detection windows as identified by the black line at 520 ms, at ranges greater than 500 m, and it is therefore possible that these secondary pulses could be detected, especially from the more powerful V16 tags and therefore help to explain the large variability in the detection probability (Figure 3.3g). It is worth noting that as the surface reflectivity increases and decreases due

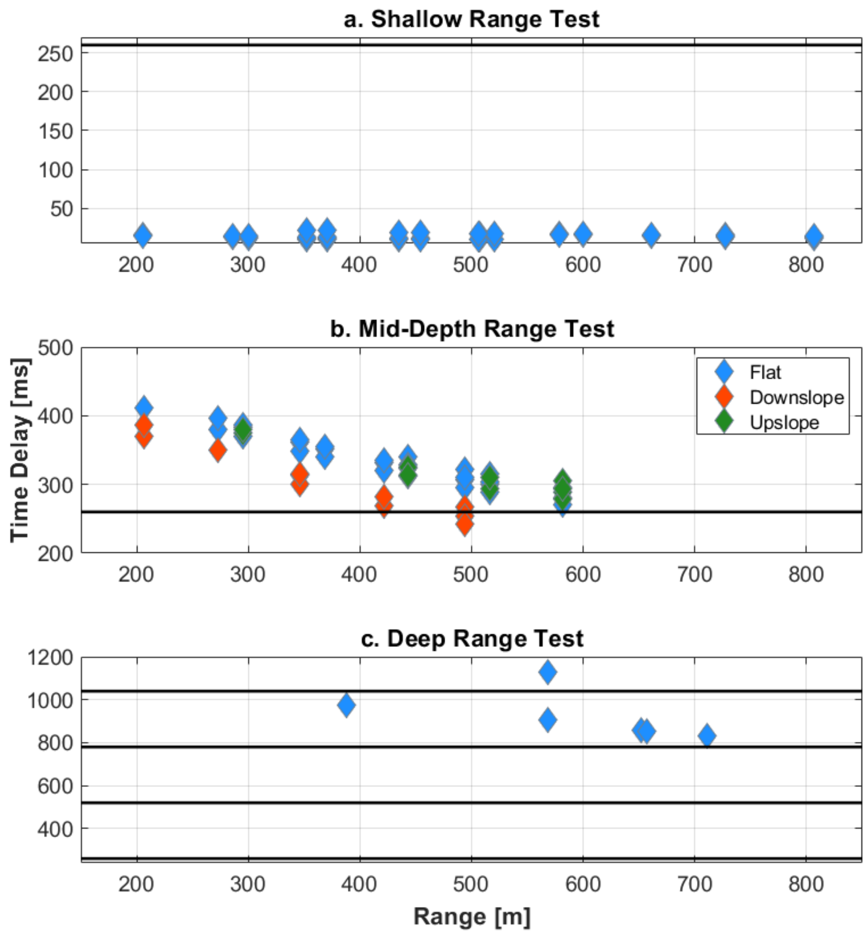

Figure 3.9: Time delays between the direct path and secondary paths shown in Figure 3.8 for all three range tests taken from Figure 3.7. Black lines indicate the end of the blanking period; the first line is 260 ms, the second 520 ms, the third, 780 ms and the fourth, 1020 ms.

to waves and ice, the signals from any given tag could move into and out of the 20 dB window in which such interference is assumed to be possible.

The ocean is a noisy place where every sound source impacts the noise level (Clay and Medwin, 1977) and noise in the environment can both improve and reduce the probability of detecting a tag's signal. There are many potential sources of noise at or near the tag frequency, including wind, and rain (Clay and Medwin, 1977). Additionally, in Arctic environments the constant motion of sea ice creates noise over various frequency ranges which is transmitted into the water column. Noise generated from thermal cracking of ice (Lewis and Denner, 1987) falls in the same frequency range as the tags. However, during this study, we did not observe any correlation between D and wind speed or sea ice, potentially due to the depths and short horizontal distances of the range tests. It would be expected that over longer ranges (i.e. $>$1 km), and especially for the shallow range test, that surface effects would have a greater impact.

An example where ambient noise may improve detection is the phenomenon of Close Proximity Detection Interference (CPDI) (Kessel et al., 2015); a consequence of multi-path collisions. CPDI creates a minimum effective detection range where, under the right conditions of low ambient noise and reflective boundaries, two paths of the same signal overlap at the receiver and a detection is not recorded. Although Kessel et al. (2015) did not discuss it, CPDI also requires a favourable sound speed profile and the right over-all geometry to have the same signal over two paths arrive at the right time to overlap. Kessel et al. (2015) showed this effect can lead to a misinterpretation of acoustical telemetry data and is more of an issue for higher powered tags because of the greater signal strength resulting in stronger signals following alternate paths.

For example, consider a system with two receivers and a target animal mostly stationary close to receiver 1 (example from Kessel et al., 2015). If the conditions were calm, the CPDI effect could be strong resulting in few detection at receiver 1 but many at receiver 2. An interpretation of these results could be that the animal is spending most of its time near receiver 2. While on a windy day when there is higher noise levels the CPDI effect would be reduced resulting in more detections at receiver 1 which could be interpreted to mean the animal is moving. This case highlights that ignoring the effect of CPDI could result in a misinterpretation of how an animal uses its environment.

All tags will have a maximum effective detection range; they may also have a minimum effective detection range and potentially regions of detection gaps mid-range. These gaps along with the minimum and maximum detection ranges may change as conditions change. The type of tag used does not provide any assurances mid-range gaps are avoided as these gaps were observed on all tag types used in this study, including the lowest power V9 tag, and they occurred to depths greater than 1000 m.

3.5 Conclusion

In passive acoustic tracking studies, every receiver has a maximum effective detection range and often a minimum detection range as well. In addition to these constraints, mid-range detection-gaps may also exist due to multi-path interference. Multi-path interference occurs when the geometry allows multiple paths of a tag's transmissions to overlap. The existence of this interference is an issue that can impact every passive acoustic telemetry study in some way as it is a function of how ID codes are coded, specifically their length, and the geometry combined with environmental conditions of a study site. In this study, mid-range gaps were observed for all tag types used including the lowest powered V9 tags, and occurred in water depths greater than 1000 m. It is important to note that these geometries may be different in different directions radiating out from the receiver along the horizontal plane. Additionally, these mid-range gaps, along with the minimum and maximum ranges, may change as oceanographic conditions change. An example could be when a front such as a salt wedge moves through the range of a receiver. A tagged fish on one side of the front may fall into a detection-gap, while a fish at the same range on the other side may not experience the same gap, as sound speed properties may be different due to the different conditions. Therefore, range tests may not find these gaps unless a tag is coincidentally deployed at one of these locations. Another important result was that no seasonality to the detection probability was observed.

Interpreting detection data without knowledge of detection ranges, especially mid-range gaps could lead to misleading conclusions impacting the validity of any quantitative analysis performed. Ultimately, wrong conclusions may be made about how animals use an area which can potentially lead to inappropriate conservation legislation. Several options exist to identify and deal with the impact of mid-range detection gaps. First, tags could be created with coding techniques that reduce the duration of each ID code, for example, using swept frequencies or phase coding techniques. Range test tags could be deployed for the duration of the study allowing for identification of mid-range detection gaps after a study is complete. Additionally, overlap between receivers should be designed for an entire study area especially if a quantitative study is planned to determine exact numbers of fish passing by. Two-dimensional ray tracing models, although somewhat simplistic, incorporate the factors that create multi-path interference. With some basic environmental data (i.e. sound speed profile and bathymetry), the geometries that most likely will result in multi-path interference can be identified.

Chapter 4

Underwater Soundscape of Cambridge Bay

A year-long study of the underwater soundscape of Cambridge Bay, Nunavut, was conducted over 2015. Unlike other Arctic locations considered to date, this site was louder when covered in ice with the loudest times occurring in April. Sounds of anthropogenic origin were found to dominate the soundscape with about ten times more snowmobile traffic on ice than open water boat traffic. The bay was quietest during the ice-break up in July, possibly because it was unsafe for both snowmobiles and boats. Over the course of the year precipitation, wind and ice noise were the other major contributors to the underwater soundscape and non-human biological sources were not significant.

4.1 Introduction

The underwater acoustic environment, or soundscape, of a marine habitat influences how an ecosystem functions (Staaterman et al., 2013). A soundscape combines environmental sounds, biological sounds from the local fauna (Bittencourt et al., 2016), as well as the sound of humans using the area. Since soundscapes change over multiple timescales (days, lunar cycles, seasons, etc.) in response to changing environmental conditions, long-term underwater acoustic recordings can capture natural acoustic rhythms and expose site-specific variability (Lillis et al., 2014). In addition, temporal patterns of marine habitat use can be revealed, including the impact of anthropogenic acoustic pollution (Rountree et al., 2006; Merchant et al., 2014). In Arctic regions, like Cambridge Bay, ambient sound levels show more seasonal variability than similar sites in the tropics (Haver et al., 2017).

The physical world creates sound through diverse mechanisms ranging from the flow noise of tides to the rumbling of earthquakes to meteorological activity. From above, wind and precipitation can contribute to an underwater soundscape. Wind noise typically peaks at a frequency around 500 Hz (Wenz, 1962), with higher wind speeds associated with broadband noise in the range of 0.1-10 kHz (Merchant et al., 2014). Different forms of precipitation on the water surface also add noise to the underwater environment. The sound of light rain peaks in the 15-25 kHz frequency band (Nystuen, 1986) while heavier rain generates sound energy down to frequencies of 500 Hz (Erbe et al., 2015). Both snowfall and rain on open water deposits tiny bubbles beneath the surface; when these bubbles collapse they emit sound between 50 and 200 kHz and can add up to 30 dB to underwater noise levels (Crum et al., 1999).

The presence of ice can make a radical difference to the soundscape through multiple mechanisms. Sea ice is a dynamic surface in near constant motion (Kinda et al., 2013) and as it moves sound is transmitted to the water below (Dyer, 1984). Ice colliding, rubbing, breaking and melting creates sounds over a wide frequency range from $<$10 Hz to $>$10 kHz (Erbe et al., 2015) with two main peaks. At 10-20 Hz, ice sounds originate from wind blowing over the surface, ridging, and internal fracturing (Dyer, 1984; Greene and Buck, 1977; Pritchard, 1984; Makris and Dyer, 1991). Sounds between $\sim$150-5000 Hz are generated from thermal cracking (Milne, 1972). Sea ice can dampen noise transmitted into the water column resulting in many regions being quieter when covered in ice than when ice free under certain conditions (for example: Insley et al. (2017)). Another sea ice effect is due to the rough nature of the underside of the ice which can limit long range sound propagation through the water column. The consequence of this scattering is that noise at frequencies $>$1 kHz is most likely produced locally (Diachok, 1976).

Marine life also contributes to the soundscape. From invertebrates, such as snapping shrimp, to marine mammals, to the more than 700 known species of soniferous fish, many underwater animals make noise (Luczkovich et al., 2008). For example, within a marine protected area in Brazil, fish choruses eclipsed other sources in the soundscape (Sanchez-Gendriz and Padovese, 2016) while in a study from the Adriatic Sea, fish and snapping shrimp sounds dominated (Pieretti et al., 2017). Migrating marine mammals can impact season variability of the soundscape; for example, in

Fram Strait, another Arctic location, fin whales created a louder environment when the region was ice free (Haver et al., 2017).

In many environments, anthropogenic noise can be a significant component of the soundscape. Anthropogenic noise can originate from sources located above, below or on the surface of the water or ice. Below the surface, sonars, explosions, submarines, remotely operated vehicles, scientific equipment such as acoustic Doppler current profilers or pumped conductivity temperature depth instruments, and other subsurface equipment can all contribute to a soundscape. On the surface, noise can be created by ships of all sizes by their propellers, engines and other internal workings. Snowmobiles or other vehicles operated on top of the ice also contribute. Even aircraft are a potential noise source in some locations. In the aquatic environment, anthropogenic noise is nearly ubiquitous and has been shown to cause a variety of negative effects on the fauna (Williams et al., 2015) by damaging an animal's hearing and/or forcing it to change behaviour (Tasker et al., 2010).

Many evaluations of coastal soundscapes have been performed (for example: Butler et al. (2016); Lillis et al. (2014); Bittencourt et al. (2016)); however, few have considered sites with seasonal ice cover (for example: Haver et al. (2017)). This paper provides a description of a year-long, continuous soundscape in Cambridge Bay, Nunavut, Canada, collected in 2015 using a hydrophone situated on the bottom in $\sim$9 m of water. This site is a remote Arctic location with a significant human presence. The local people are heavy users of the bay especially when it is ice covered. Here, we will evaluate how anthropogenic noise contributes to the underwater soundscape to provide a baseline for future measurements when natural sources or anthropogenic activities may change. For example, as ice conditions change, the Northwest Passage running through Dease Strait, at the mouth of Cambridge Bay, may be used more by shipping, potentially adding more summer noise to the bay's soundscape. To our knowledge, this is the first study looking at the impact of traffic both on ice and over open water in a remote Arctic location, as well as, perhaps, the first discussion of the underwater noise generated by snowmobiles.

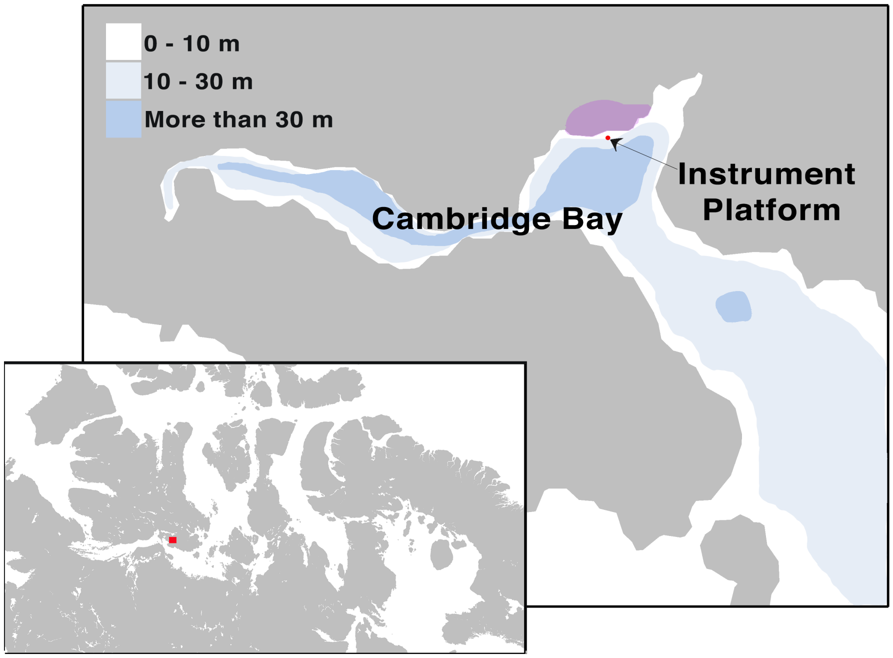

Figure 4.1: Map of Cambridge Bay where the community of the same name is highlighted in purple and the location of the underwater platform with a red dot. Bathymetry is taken from Gade et al. (1974). Inset map is of northern Canada with the location of Cambridge Bay denoted with a red square.

4.2 Methods

4.2.1 Location

Cambridge Bay, Nunavut, Canada (69.11°N, 105.05°W) is an Arctic location where an Ocean Networks Canada (ONC) cabled platform is located (Figure 4.1). The bay cuts into the southern side of Victoria Island (inset map of Figure 4.1) off Dease Strait with the community of Cambridge Bay located on its shore. The bay is part of the Canadian Arctic Archipelago (CAA), a region of islands and narrow straits where Pacific origin water passes through to the Atlantic (Prinsenberg and Bennett, 1989; McLaughlin et al., 2004; Rudels, 2012). The complex bathymetry of the bay can be simplified into two basins separated from Dease Strait by an 11 m sill. The outer basin has a maximum depth of 31 m, and a 20 m sill cuts off the inner basin. The focus of this study will be on the farthest inland section of the bay. The maximum depth of the eastern part is 86 m; it reaches 48 m in the centre and a maximum depth of 57 m in the western part.

Environmental conditions at the study site are typical for an Arctic location. Extreme annual variations in light levels combine with landfast ice that blankets the bay over the winter, reaching a maximum thickness of 2 m (McLaughlin et al., 2004). The meteorology in the western CAA, where Cambridge Bay is located, is similar to that found in the Beaufort Sea and varies with large-scale atmospheric fluctuations of the Arctic Oscillation (Barber and Hanesiak, 2004). In this region semi-diural tides have an average range of 0.4 m (Gade et al., 1974).

Gade et al. (1974) found that the heat budget of the bay was nearly locally balanced with little net exchange with outside water. The outside water in Dease Strait and Coronation Gulf are heavily influenced by the outflow of the MacKenzie River (Tully, 1952), which does not extend into the bay. Seasonal meltwater rivers discharge large amounts of fresh water to the bay over the short summer season, then are frozen over the rest of the year (McLaughlin et al., 2004). Salt exchanges are limited to summer months with the salt outflow due to entrainment with runoff being roughly balanced by an inflow at depth occurring after runoff ceases. During winter, the bay is virtually shut off from any fresh water discharge. As a result, estuarine circulation stops and bay circulation is governed by other processes, such as convection and tides.

Within Cambridge Bay, two systems of convective circulation were found by Gade et al. (1974). Salt rejection at the ice-water interface creates a homogenous upper layer under the ice. Deeper, the conditions become more complex. Where the water is shallow the upper layer convection reaches the bottom and the restricted circulation allows for an accumulation of rejected salty water. As a result, the density of water in the shallows exceeds the density in deeper waters and this salty, dense water flows down the slopes (Gade et al., 1974).

4.2.2 Environmental Data

All data used in this study were collected using ONC's instruments. The cabled platform was located at a depth of ∼9 m at a distance of 78 m from the shore at 69.1133°N, and 105.060°W (Figure 4.1). A Sea-Bird SeaCAT SBE19plus V2 Conductivity Temperature Depth (CTD) probe was located on the underwater platform and sampled at 1 Hz. On the same platform was an ASL Shallow Water Ice Profiler (SWIP), an upward-looking active sonar designed to measure ice draft in shallow water environments. Both instruments were exchanged for different ones of the same

Serial Number	Latitude [N]	Longitude [W]	Depth [m]	Deployment Dates
1288	69.11342	105.06129	8	1 January 2015 to 26 August 2015
1252	69.11268	105.06490	13	27 August 2015 to 31 December 2015

Table 4.1: Ocean Sonics icListen HF Hydrophone deployments and locations in Cambridge Bay covering 2015.

make and settings in late August 2015. Meteorological parameters were measured by a Lufft WS501 Weather Station located on shore (at 69.1139°N, and 105.060°W). This instrument made measurements every 60 s and remained in place for all of 2015.

4.2.3 Acoustic Recordings

Two hydrophone deployments occurred in 2015 (Table 4.1), and both hydrophones were calibrated by Ocean Networks Canada prior to deployment. Since the platform containing the hydrophones also contained other instruments, platform noise manifested as tonals at various frequencies which changed between deployments. Acoustic data were recorded continuously as wav files over frequencies up to 27.5 kHz for the first deployment and up to 8 kHz for the second at a sample rate of 64000 Hz. Spectra were computed using a Hann window with 50% overlap with 6400 samples per FFT window. All sound level measurements are reported as spectral levels in dB re 1 μPa^2 Hz^{-1}.

A number of data gaps occurred over the course of 2015. To quantify these gaps, the amount of data recorded per month is given in Table 4.2. From January to June most of the expected data were recorded, on average >95%. Rates dropped over the summer (July-August) to 60%. In September, less than 1% of the expected acoustic data were recorded (only about 8 hrs); therefore, this month will be omitted from further analysis. In November and December, recording rates increased again to an average of 86%. Unexpected power outages were generally responsible for the data gaps; the exception was a planned power outage for platform maintenance performed late August.

Month	Total number of files	Expected number of files	Percent data
January	8916	8928	>99
Febuary	7136	8064	95
March	8517	8928	95
April	8641	8640	>99
May	8214	8928	92
June	8638	8640	>99
July	5460	8928	61
August	5419	8928	61
September	37	8640	<1
October	4958	8928	56
November	7658	8640	87
December	7586	8928	85

Table 4.2: Expected and received data by month, where each file is five minutes in duration. The percentage of available data is included in the final column.

4.3 Results

4.3.1 Environmental Conditions

Over the course of the year, Cambridge Bay experienced extremes in light levels and temperature (Figure 4.2a and b) consistent with an Arctic environment. Global radiation ranged from zero during times of complete darkness in January and December, 2015, to >800 W m^{-2} around the summer solstice when daylight was continuous. Air temperature had an ∼60 °C range, from −40 °C in winter to 20 °C in summer (Figure 4.2b). Temperatures averaged below −20 °C from January into April, then again in October to the end of the year. The coldest temperatures were recorded mid-January through mid-February and temperatures only ranged above freezing May through September and into October. The warmest temperatures occurred in July and August.

Cambridge Bay has seasonal ice cover (Figure 4.2 and Figure 4.3a). In 2015, ice reached its maximum thickness of 1.78 m in mid-May, consistent with the thickness range of first year ice found in the Canadian Arctic Archipelago (McLaughlin et al., 2005). Over the next month, ice thickness rapidly decreased resulting in ice free conditions by the end of June. From mid-July to mid-October, the bay remained ice free. By mid-October ice began to form, increasing in thickness to the end of the year.

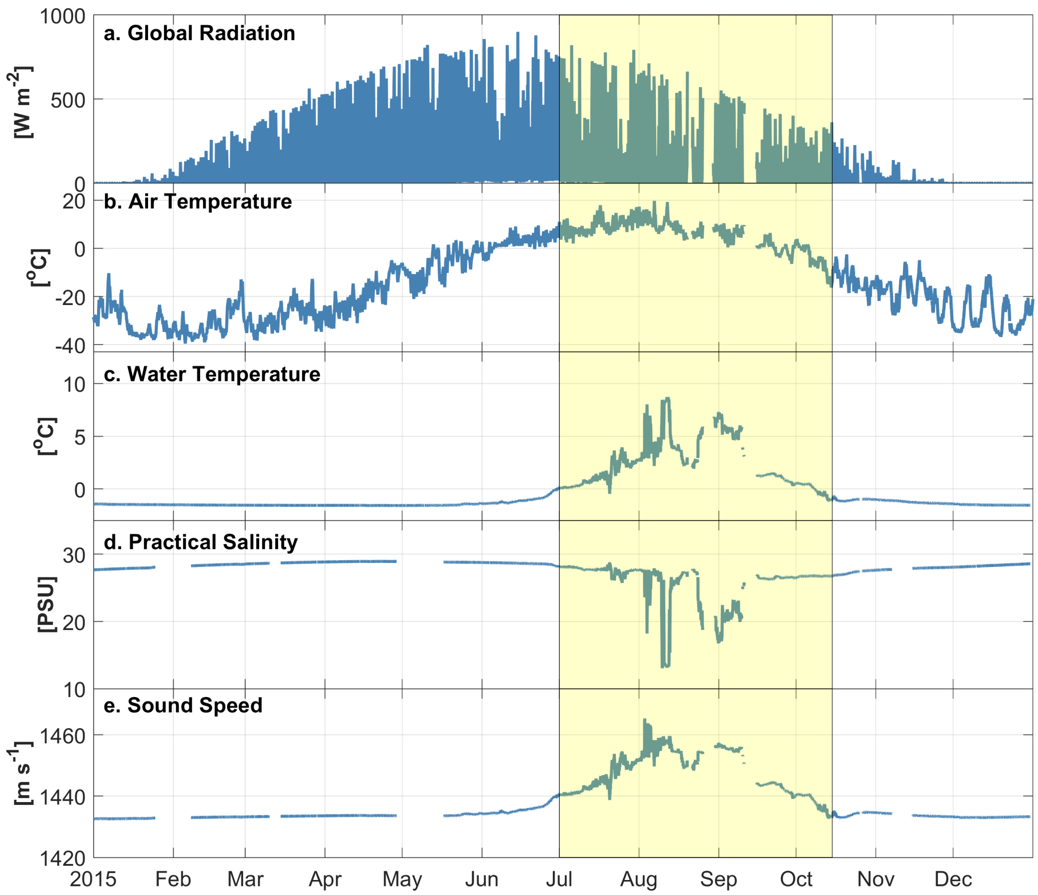

Figure 4.2: Environmental conditions in Cambridge Bay over 2015. The shore-based weather station recorded global radiation (a) and air temperature (b). Water temperature (c), practical salinity (d) and sound speed (e) are from the CTD on the underwater platform. Fifteen minute averaging was performed on all data and the ice free period from the SWIP is highlighted in yellow.

When the bay was covered in ice, water temperature remained at about -1.6 °C and salinity ranged between 28-29 PSU (Figure 4.2c and d). Under the ice, the sound speed hovered around ~1434 m s^{-1} (Figure 4.2e). When there was open water in the bay, both the water temperature and salinity had much wider ranges. Water temperature increased, peaking at 8.7 °C in August (Figure 4.2c) and salinity decreased to a minimum of 13.6 PSU (Figure 4.2d). Sound speed was also most variable during ice-free times, reaching a maximum of 1465 m s^{-1} early August (Figure 4.2e). The average windspeed was ~5 m s^{-1} (Figure 4.3c). Events with wind speeds approaching 20 m s^{-1} occurred in January, October and November. Although wind direction varied, the winds tended to be southeasterly especially in January, February, March and October.

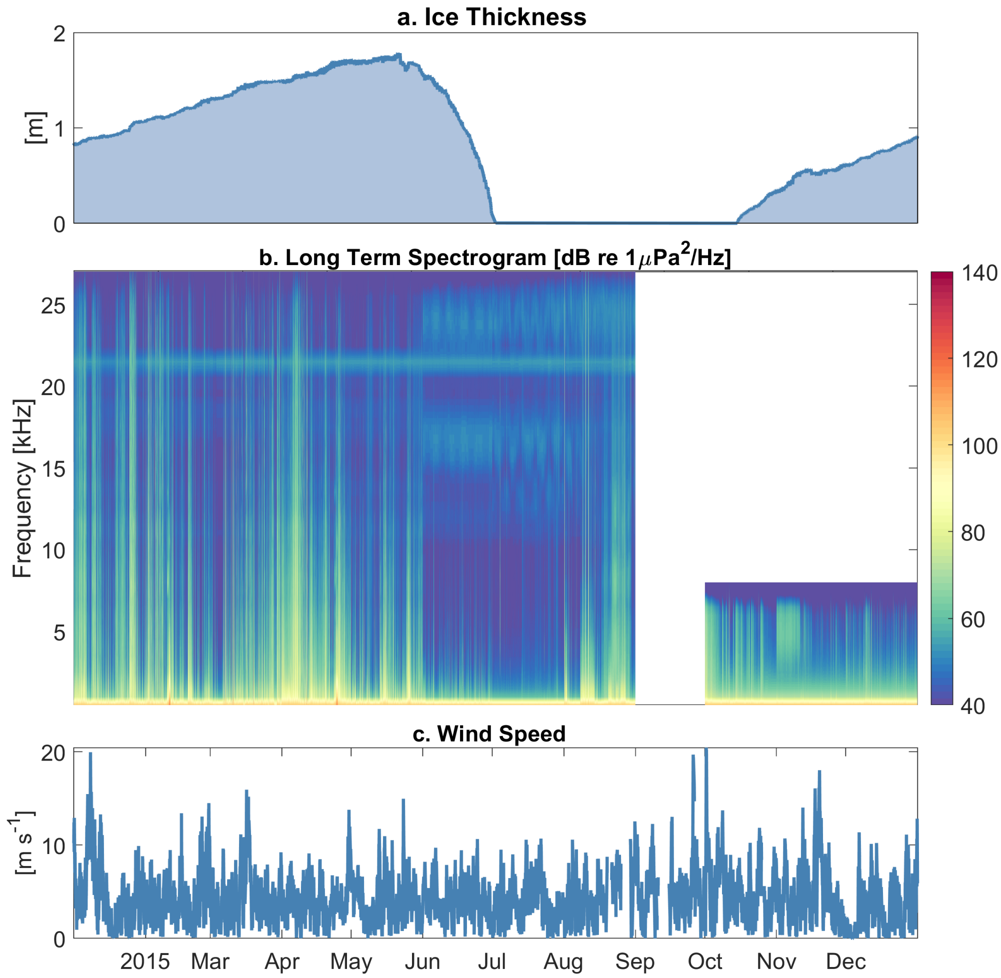

Figure 4.3: (a) Ice thickness in metres from the SWIP ice profiler. (b) Year long spectrogram created from the acoustic recordings with one hour averaging and 500 Hz frequency bins; colour bar denotes sound power intensity in dB re 1 μPa^2 Hz^{-1}. (c) Wind speed from the weather station.

4.3.2 Underwater Acoustic Environment

To characterize the soundscape of Cambridge Bay, the acoustic data are presented to highlight broad features first, then focus on details.

The power spectral density as a function of time for 2015 is shown in Figure 4.3b using one hour averaging and 500 Hz frequency bin size. Until August, the maximum frequency recorded was 27.5 kHz. During this time there was a persistent tonal at ~21 kHz likely caused by one of the other instruments co-located on the same platform. Unfortunately, when the hydrophone was replaced in August the maximum frequency recorded was reduced to 8 kHz for unknown reasons. To gain a better understanding

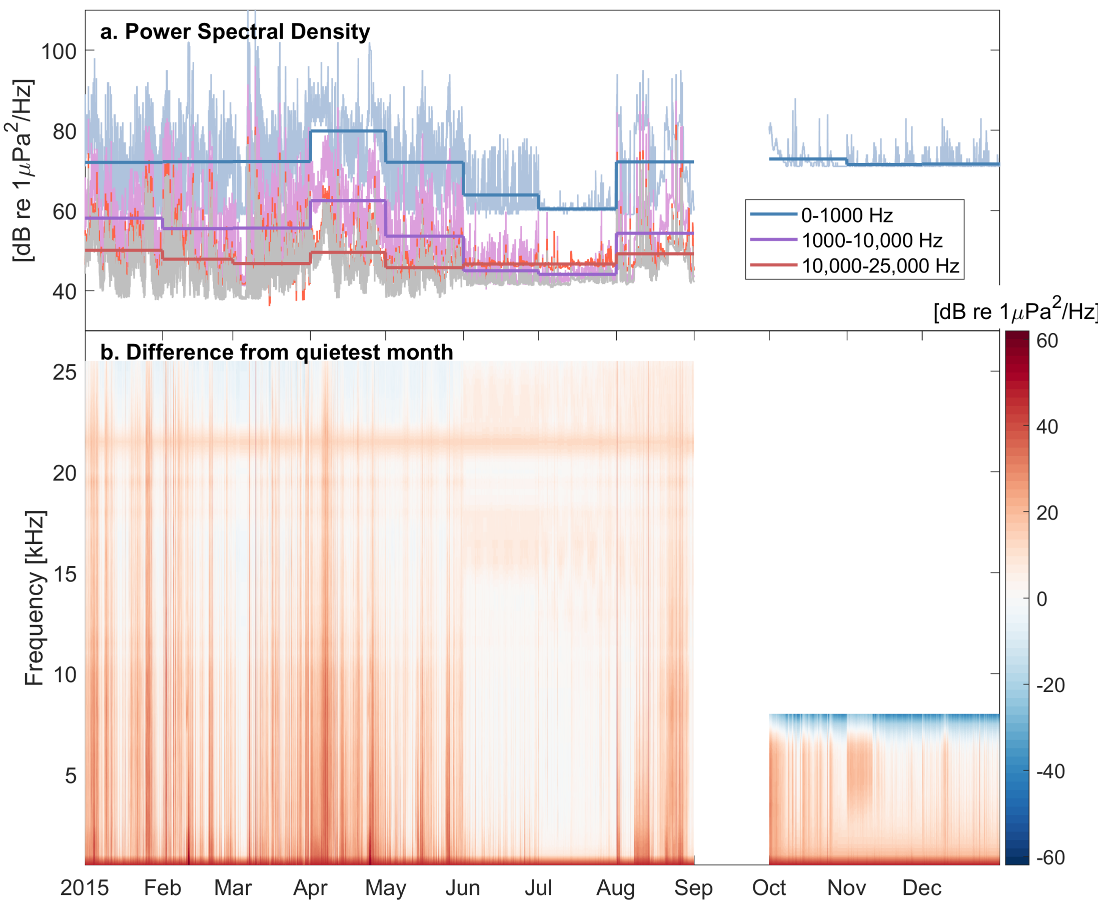

Figure 4.4: (a) Power spectral density in three frequency bands for 15-hour averages (thin lines) presented along with the monthly average of the band (thicker line). (b) Power spectral density with the 5$^{\text{th}}$ percentile of the spectral probability density of the quietest month (July 2015) removed over the full range of frequencies.

of the relative contribution of different frequency bands to the overall soundscape, the yearly-spectrogram was broken into three bands, 0-1, 1-10 and 10-25 kHz. Only the lowest frequency band was computed in the fall with the new, lower bandwidth. Each frequency band was averaged over 15 hours, then averaged over a calendar month (Figure 4.4a).

To present the noise level distribution over the full range of the recordings, spectral probability densities (SPD) were computed using normalized histograms over the full frequency range in 1-Hz intervals. Next, statistical variability was calculated and split into three power spectral density percentile bands where the n^{th} percentile gives the level that was lower $n\%$ of the time (Figure 4.5). The 50$^{\text{th}}$ percentile is the median (Figure 4.5b). The $\sim$21 kHz tonal identified in the year-long spectrogram showed up

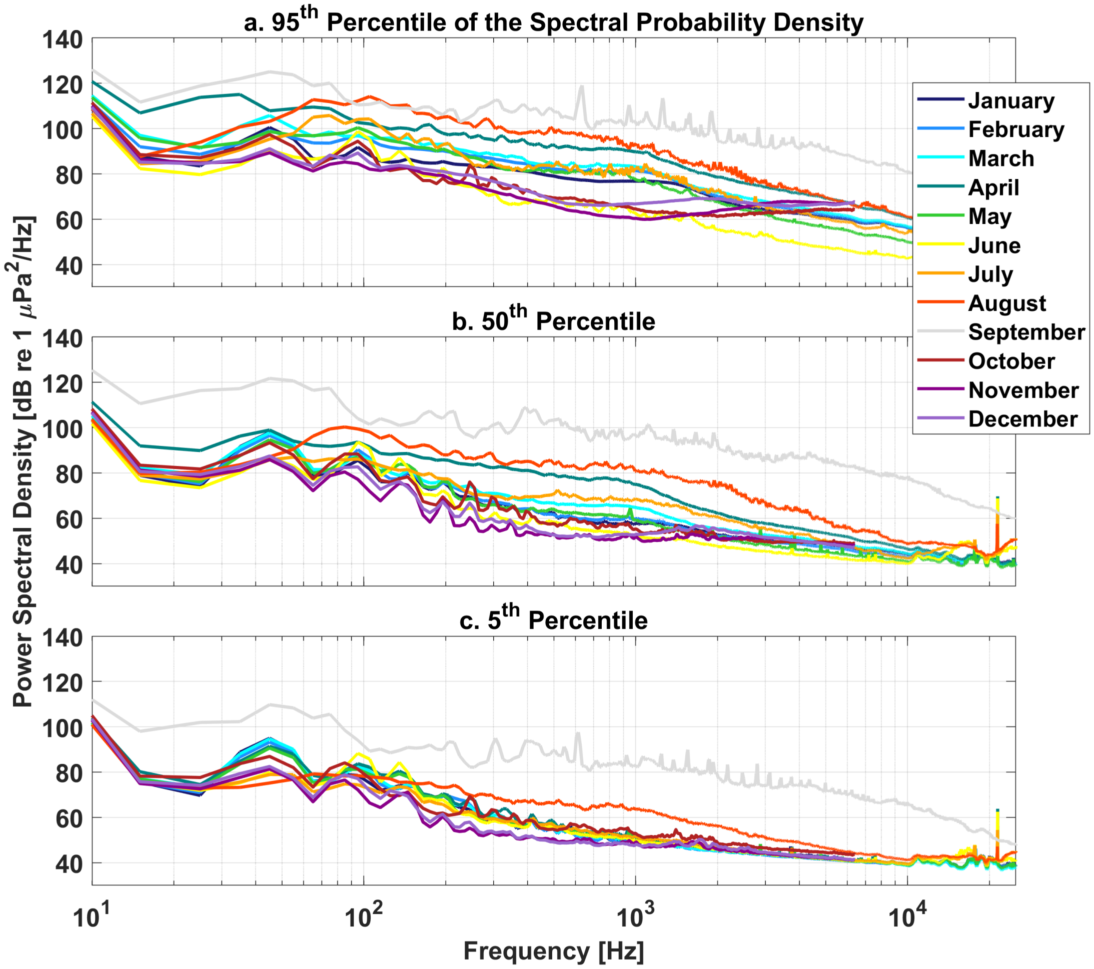

Figure 4.5: Monthly percentiles calculated from the spectral probability densities. September is greyed out as there were only 8 hours of data recorded that month.

as a spike in the SPD analysis (Figure 4.5). To look at how much louder the rest of the year was compared to the quietest month (July 2015), the 5$^{\text{th}}$ percentile of the SPD over the full range of frequencies was removed from the entire year and the remainder was plotted as a spectrogram (Figure 4.4b).

Over all frequencies, this analysis highlights that July was the quietest month and April was the loudest (Figure 4.4a). Below 1 kHz, ambient sound levels averaged around 70 dB reaching 100-110 dB at times (Figure 4.4a). This band was consistently louder than the higher frequencies (Figure 4.4a), peaking in April. The second loudest months were January and August. The 1-10 kHz band was next loudest, on average just below 60 dB, except during June and July when noise in this band dropped to ~45 dB which was quieter than the highest band. The loudest times in the middle band were the same as those for the lower band. The highest band was more consistent throughout the year with monthly averages ranging from 47-50 dB. Peaks occurred in April, August and January. In June, July and August 2015 there were harmonics around 17 and 24 kHz, likely originating from a 50 kHz sonar that started 29 May onboard a tug boat tied up at a near by dock. These harmonics are relatively quiet, reaching at most 50 dB.

A quiet period over the entire frequency range started in June (Figure 4.4a) corresponding to ice break-up. As noted above, July was the quietest month and also the first ice-free month of the year. During this quiet time, wind speeds did not exceed 10 m s^{-1} (Figure 4.3c). This quiet period could also have occurred because ice break up makes the bay dangerous for human transport, reducing the amount of anthropogenic noise, an issue which will be considered in the discussion. In addition to noise generated by the wind, the ice-free time included noise from the nearby dock from wave action and boats rubbing. There was also boat noise from engines and onboard equipment such at generators, pumps and sonars. A sub-set of a acoustic files were listened to. Occasional fish grunts were heard but, no marine mammal calls were identified.

4.4 Discussion

Simultaneous contributions from many sources make the underwater soundscape of Cambridge Bay complex. The most relevant sources are considered below.

4.4.1 Biological Sounds

Occasional fish sounds in the form of grunts were observed at frequencies between 120-380 Hz. However, it is unknown what species was calling, nor did the calls make a significant contribution to the soundscape. Over the course of 2015, no marine mammal calls were identified through either listening to the acoustic files or examining the spectrograms. This does not mean marine mammals were not present; however, their contribution to the soundscape was minimal. Overall, biological sources in Cambridge Bay were not a significant contributor to the underwater soundscape.

4.4.2 Physical Process Sounds

Of all the local physical processes, precipitation, wind and ice noise were the most significant sources. Tidal currents are another potential noise generating process (Urick, 1983); however, in Cambridge Bay, the noise generated was small likely because the tidal range was only 0.4 m; thus, tides were not considered as a major contributor to the soundscape.

Precipitation

Month	Precipitation [cm]
January	no data
Febuary	0.34
March	0.28
April	0.28
May	0.36
June	2.54
July	5.94
August	1.18
September	1.10
October	1.22
November	1.18
December	0.46

Table 4.3: Monthly precipitation for 2015 from http://climate.weather.gc.ca. Note, no data was available for January 2015.

To consider the contribution of precipitation to the soundscape of Cambridge Bay, data from the Government of Canada historical climate data repository was used as summarized in Table 4.3. Over 2015 there was ∼15 cm of precipitation. Note, no data was available for January 2015; however, it was likely low like the other winter months. Assuming snowfall on ice does not transfer much noise into the water column and that there was no rainfall on the ice, the period of open water would be the time precipitation would contribute the most sound. During ice-free times, precipitation would be expected to create a broad signal over a wide range of frequencies with a peak between 15-25 kHz (Nystuen, 1986). Over the ice-free period of 2015 a total of 10 cm of precipitation fell, with the most during a single day being <2 cm. From a visual inspection of the data, precipitation events were found to be intermittent; an

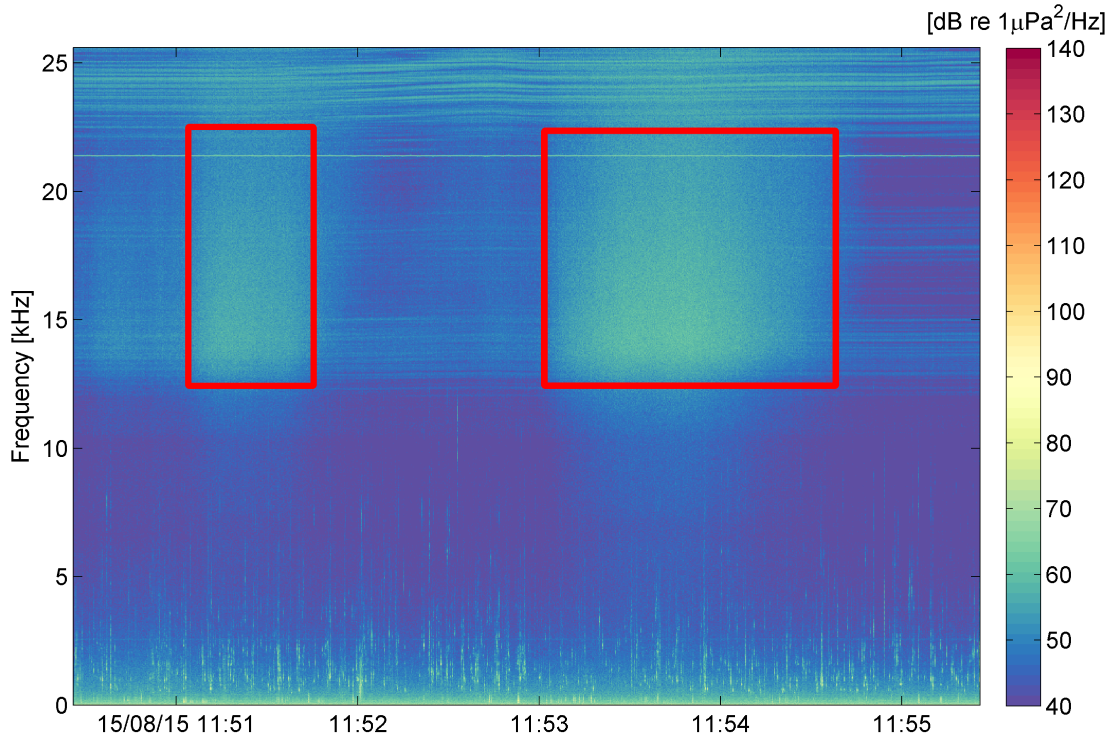

Figure 4.6: A five minute spectrogram from 15 August, 2015. The two intermittent rain events are highlighted with red boxes. The events peak between ∼14 and 15 kHz and reach at most 80 dB re 1 μPa^2 Hz^{-1}.

example is shown in Figure 4.6. This event reached a maximum of 62 dB re 1 μPa^2 Hz^{-1} at 15 kHz.

Wind noise

Wind is potentially a major contributor to the soundscape. Acoustical noise is transmitted into the water column by wind-generated breaking waves when there is no ice cover and through wind induced ice movement and blowing snow when there is ice cover. Alternately, the ice may act to insulate the water column from wind noise resulting in decreased noise (Greene, 1995; Insley et al., 2017). Here, wind noise will first be considered separate from the ice cover.

Wenz (1962) found that in shallow, open water wind generated noise can be loud, ranging from 80 dB re 1 μPa^2 Hz^{-1} up to 140 dB re 1 μPa^2 Hz^{-1} and occurs mostly a low frequencies, i.e. below 500 Hz. Thus the majority of wind noise is expected to fall in the lowest frequency band of up to 1000 Hz in Figure 4.4a. With the exception of April, throughout the year this band averages just above 70 dB re 1 μPa^2 Hz^{-1} with some daily spikes up to 110 dB re 1 μPa^2 Hz^{-1}. During the ice-breakup in June and ice-free period of July, sound in the lowest band dropped to the lowest levels of the year of below 65 dB re 1 μPa^2 Hz^{-1}.

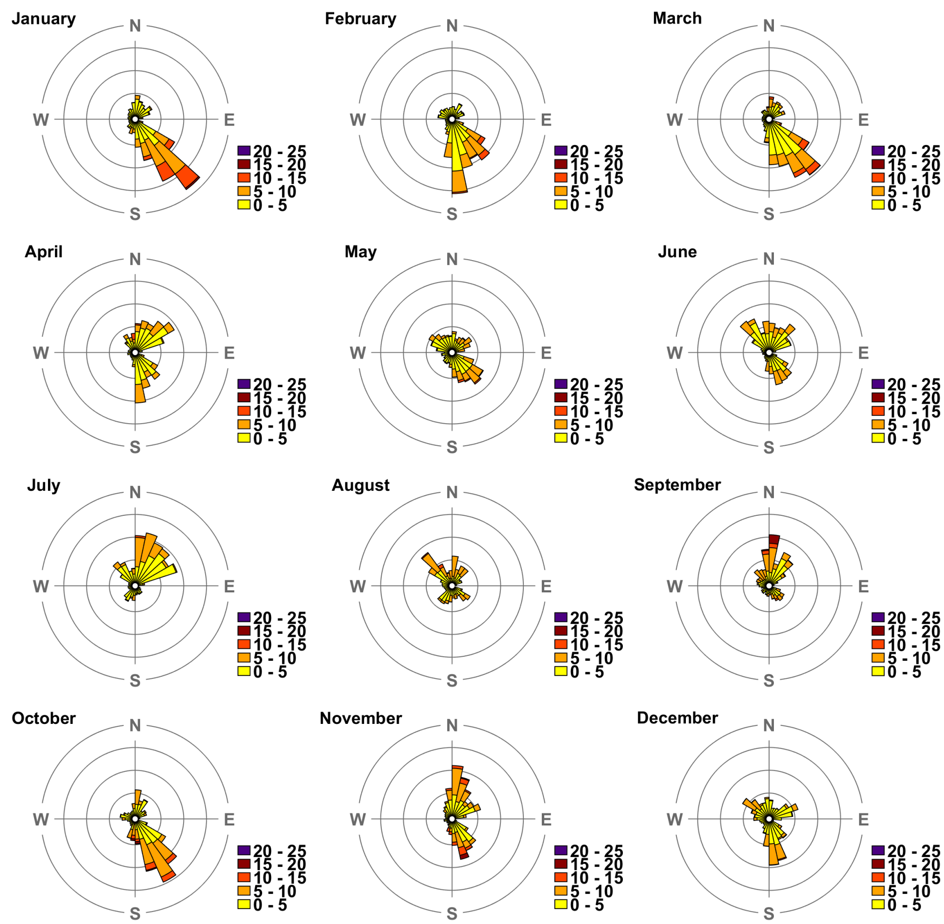

Figure 4.7: Winds presented by month in a wind rose format. The rings denote increasing percentage of the time the wind blew in that direction. From the inside going outward, the rings are 5, 10, 15, 20%. Colours denote wind speed in m s^{-1}.

Winds presented in a monthly wind rose format in Figure 4.7 show wind speed and direction each month. The lowest monthly average in the 0-1000 Hz frequency band occurred in July; this month had winds which averaged ~5 m s^{-1} which is the average wind speed of the year. However, July winds were predominantly northeastward which was an anomalous direction for the year (Figure 4.7). This was also the first full ice-free month and that likely also played a role in the low noise level. The lowest frequency band was loudest in April (Figure 4.4a), which was not a month with exceptionally high winds suggesting another source contributed to the soundscape at this time.

The strongest winds occurred in January, February, March and October (Figure 4.7), all months with ice cover. In early March, after 15-minute average wind speeds exceeded 15 m s^{-1} (Figure 4.3c) noise in the 0-1000 Hz band peaked at 110 dB re 1 μPa^2 Hz^{-1}, the loudest period of the year (Figure 4.4a) suggesting this wind event significantly increased underwater noise.

To quantify the amount of noise added to the water column by wind, a statistical analysis of the relationship between surface winds and the observed noise field developed by Vagle et al. (1990) was used (Figure 4.8). This approach relates the sound spectrum level, SSL(f), at frequency f in Hz, to the wind speed, U_{10}, in m s^{-1}, at an elevation of 10 m, as:

$$SSL(f) = 20\log_{10}(sU_{10} + b) - Q\log_{10}(8000/f) \tag{4.1}$$

In the equation Q is a unitless parameter incorporating how the SSL decreases as the frequency increases: here Q=−21 is used based on the slope of the average PSD over the year between 1 and 10 kHz. Parameters s and b are the slope and intercept of a linear fit between measured sound pressure and windspeed with s=58.87 and b=−80.94 used from Vagle et al. (1990).

Since the hydrophone was shallow, it is assumed there is negligible attenuation loss. This calculation was performed at 3 kHz. During the quietest month, July, noise measured was, in general, only slightly higher than the calculated wind-generated noise. This suggests wind generated noise dominated the soundscape at this time. In August, the measured sound ranged much higher, reaching above 80 dB re 1 μPa^2 Hz^{-1} at times. The calculated wind noise during this period did not exceed ~65 dB re 1 μPa^2 Hz^{-1} suggesting other sources contributed noise in addition to the wind such as noise from the boats tied up at the nearby dock.

Ice Noise

As the stresses on sea ice change, noise can be generated and transmitted to the water column below. Based on the proximity to shore, the assumption will be made that the ice cover on Cambridge Bay is land fast. To relate the soundscape to ice cover, ice thickness is plotted in Figure 4.3a. A noise peak has been reported for

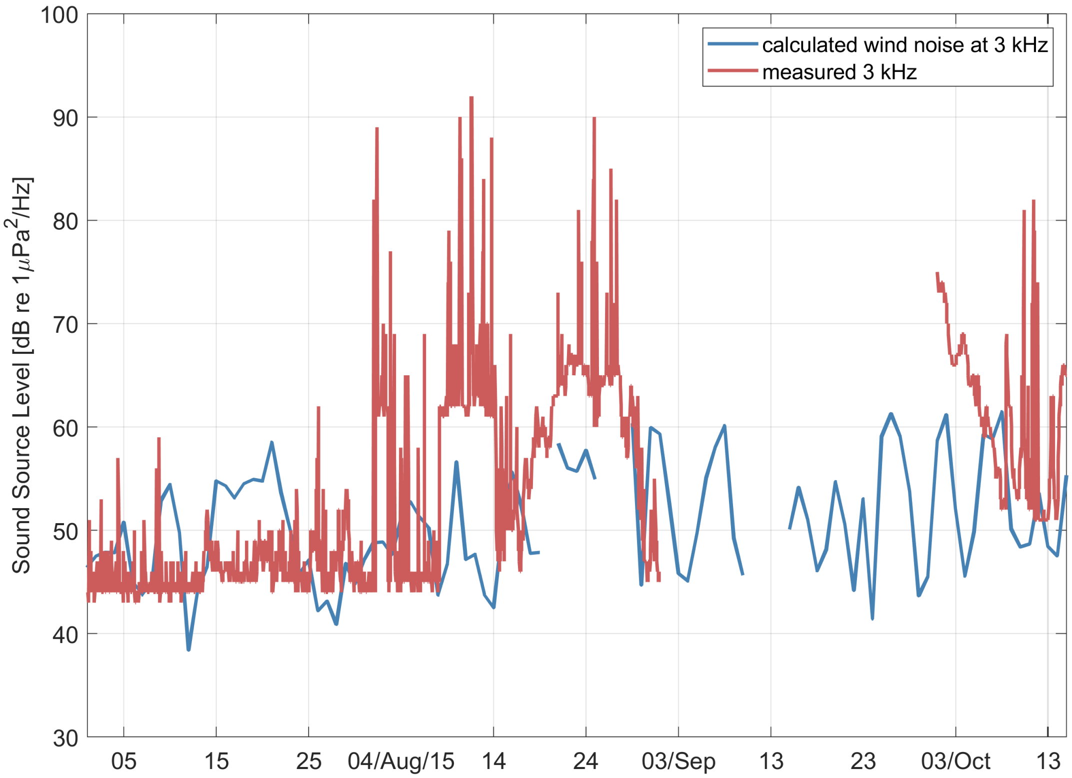

Figure 4.8: Daily average wind contribution to ambient noise calculated at 3 kHz based on averaged wind speed for the ice free period in blue. Red is the daily average in the 3 kHz frequency band.

ice-covered environments around 10-20 Hz from wind blowing over ice, ridging, ice cracking, and bending (Dyer, 1984; Greene and Buck, 1977; Pritchard, 1984; Makris and Dyer, 1991). By far, the lowest band (which includes 10-20 Hz) in Cambridge Bay is the noisiest; however, it retains similar noise levels during times of no ice. One major difference between the two time short-term variability, with times of ice cover being more variable most likely due to ice-related noise.

Date	Wind Speed [m s^{-1}]	Air Temperature [°C]	24 Hour Temperature Change [°C]	Number of Cracks
28 January 2015	10.2	−31.7	4.8	54
3 February 2015	3.27	−34	4.3	1
1 April 2015	6	−31	8.2	184

Table 4.4: Environmental parameters and the number of cracks over three 5-minute samples. For all sample times, water temperature remained relatively stable between −1.5 and −1.6 °C.

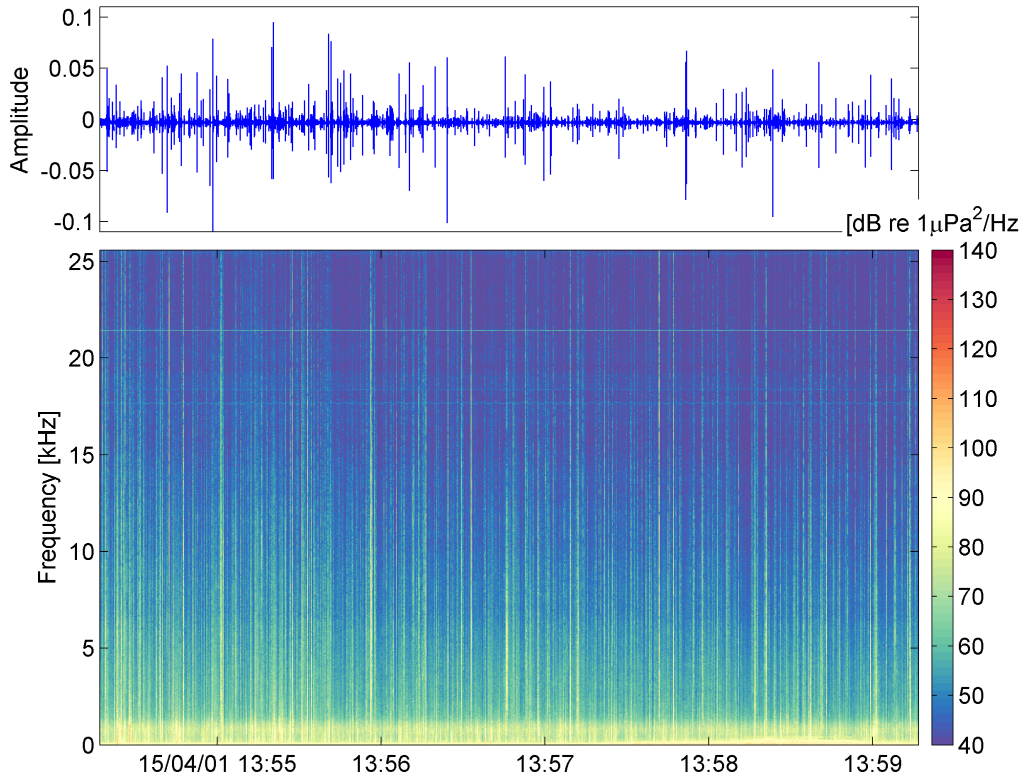

Figure 4.9: Ice cracking from 1 April 2015. Top panel is the waveform where the ice cracking manifests as spikes. The bottom panel is a five minute spectrogram where the PSD of the short ice cracking events reached a maximum of 87 dB re 1 μPa^2 Hz^{-1} at 5 kHz.

Thermal cracking of ice adds sound to the water column with a noise peak between 150-5000 Hz (Milne, 1972) as a series of short pulses where each pulse sounds like a 'pop'. Table 4.4 lists three 5-minute times where ice cracks were counted, together with the environmental conditions during these periods. An example of ice cracking from 1 April 2015 is shown in Figure 4.9 where a manual count found 184 cracks during the 5-minute period. For all three times, air and water temperatures were very similar; however, the change in air temperature over the 24 hours around the time with the most cracks on 1 April 2015 was 8.2 °C, almost double the other values presented in Table 4.4. The lowest windspeed on 3 February 2015 coincided with almost no cracking; although winds were stronger on 28 January 2015 than on 1 April 2015, this did not result in more cracking, suggesting the increased number in cracks were more related to temperature change, although this is an extremely small set of samples where multiple factors were in play.

4.4.3 Anthropogenic Sound

Vehicle noise dominated the anthropogenic component of the soundscape in Cambridge Bay, with ice cover being the deciding factor between boat or snowmobile use. Traffic noise in open shallow water typically falls in the frequency band between 10-1000 Hz and ranges from below 40 dB re 1 μPa^2 Hz^{-1} to as high as 100 dB re 1 μPa^2 Hz^{-1} (Wenz, 1962); this was also found to be true at Cambridge Bay for both open water and ice-covered conditions.

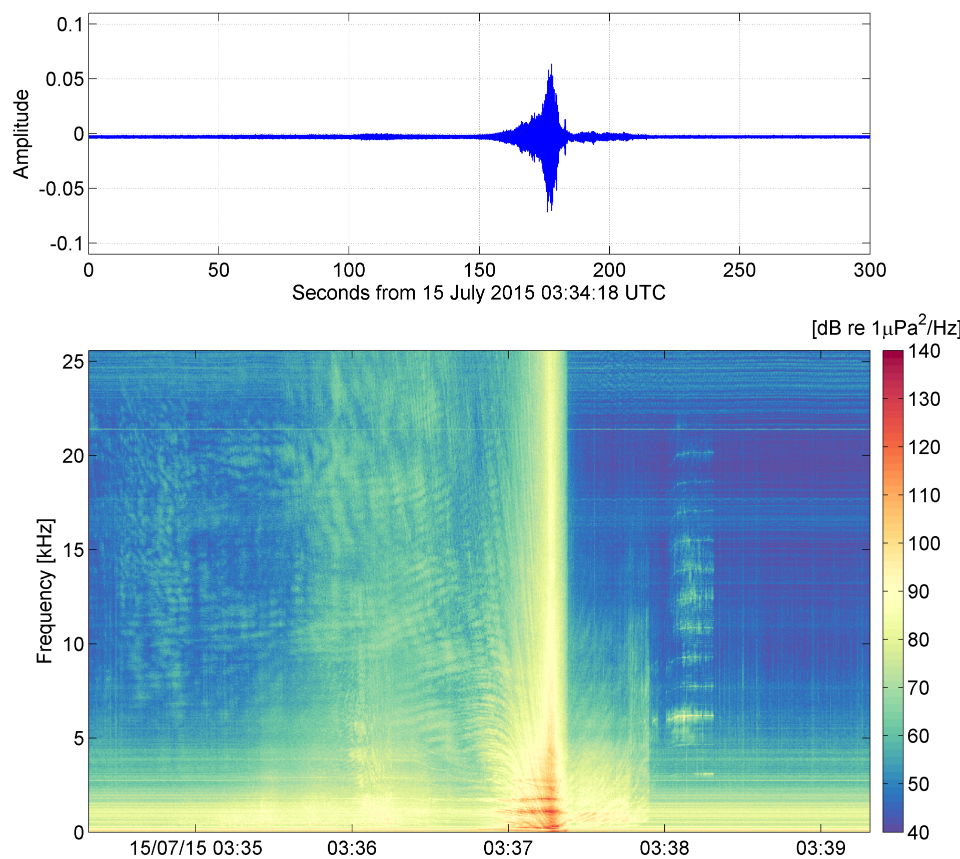

Figure 4.10: A typical underwater noise signature of a small boat as observed on 15 July 2015. Top panel shows the raw pressure signal of the passing boat. The bottom panel is a five minute spectrogram where the boat sounds reached a maximum of 145 dB re 1 μPa^2 Hz^{-1}.

During ice free times, boats generate sounds over a wide band of frequencies as a result of engine operation and propeller blade rotation (Figure 4.10). Typically, the boats in Cambridge Bay were small fishing vessels and pleasure craft. An additional noise contributor was a Norwegian tug boat tied along the dock a short distance from the hydrophone. At ~23:59 hrs UTC on 28 May 2015 a 50 kHz signal began and continued on until the fall (it is difficult to determine an exact end due to the data gaps in September). Several, less powerful, harmonics of this signal can be observed down to ~17 kHz (Figure 4.3b and 4.4b).

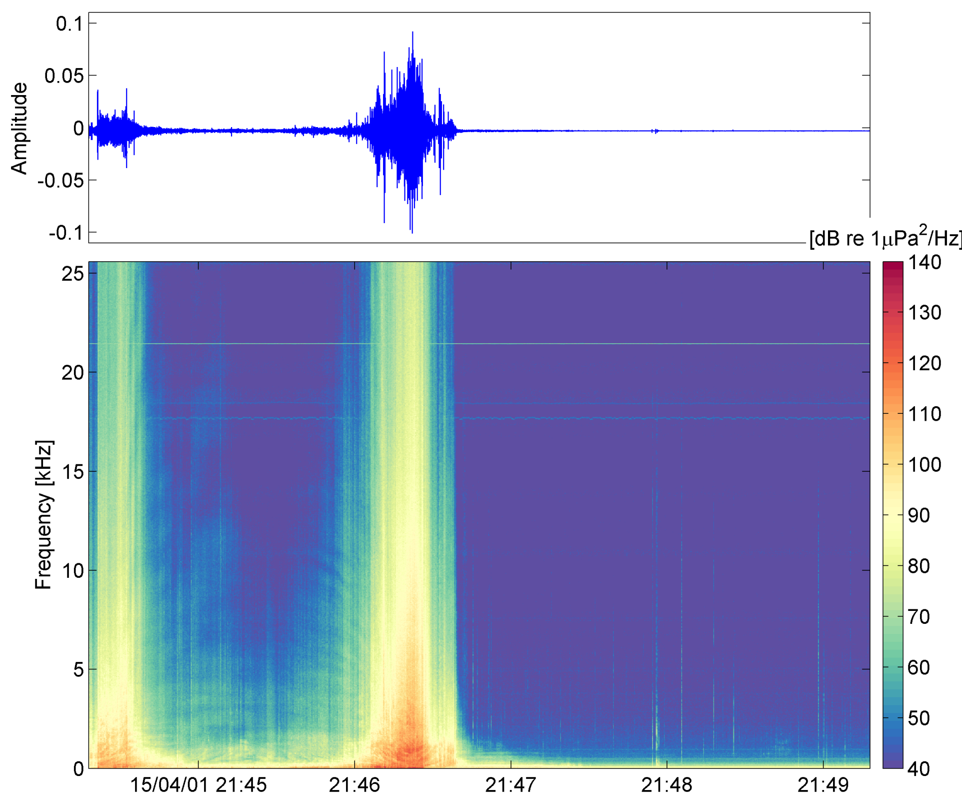

Figure 4.11: Underwater noise signatures from two snowmobiles observed on 1 January 2015. Top panel shows the raw pressure signal in arbitrary units. The bottom panel shows a five minute spectrogram where the snowmobile PSD reached 152 dB re μPa^2 Hz^{-1}.

Snowmobiles were operated when there was ice cover. These vehicles have similar combustion engine sounds as the small boats combined with the sound of the track and skis moving across the surface (Figure 4.11). It is possible a small portion of the vehicle traffic on the ice is other types of transportation such as trucks.

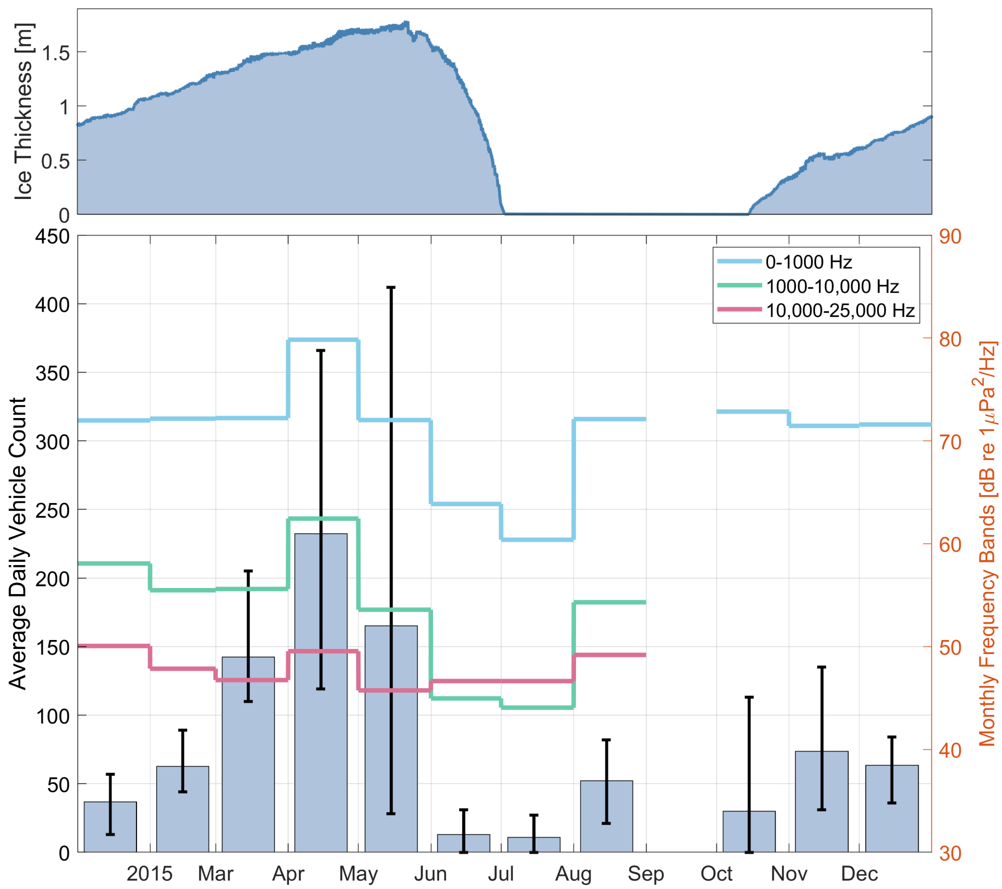

Figure 4.12: Top is the ice thickness on Cambridge Bay. Bottom are bars for the average number of vehicle passages (snowmobile or boat, depending on ice cover) counted over seven days of each month. Black lines are the error bars. Monthly frequency bands from 4.4a are included layered on top of the bottom panel with scale on the right side.

To make an assessment of how much vehicle traffic contributes to underwater noise in the bay, seven days were selected each month and analyzed manually. Lloyd's mirror interference patterns (for example see Figures 4.10 and 4.11) were counted where noise levels exceeded 90 dB re 1 μPa^2 Hz^{-1}, and the results were averaged together (Figure 4.12). Note, this method counts the same vehicle more than once if it passed over the hydrophone multiple times and the error is greater when multiple vehicles pass over close together as their signals merge potentially resulting in a lower estimate.

On the ice, traffic increased each month until reaching a peak in April (Figure 4.12). On a single Saturday that month >350 vehicle passages were counted; on average 100 more vehicles passed over the hydrophone than in either March or May. The significantly increased noise in the lowest frequency band (0-1000 Hz) in April (Figure 4.4a and 4.12) has already been shown not to be a direct result of winds. The increased vehicle traffic that month is almost certainly the source of the additional noise. In May, traffic levels were equivalent to those of April for the first part of the month, then dropped off as ice break up began, likely due to the dangerous conditions. The open water of June and July saw few boats. A possible reason for the quiet months of June and July (Figure 4.4a), especially during the ice break up, could be reduced traffic on the bay (Figure 4.12). Boat numbers increased dramatically in August to a maximum >80 in a single day. However, our results show that there were ten times the number of snowmobile passages than boats. These results suggest that sounds of anthropogenic origin, specifically vehicles, dominate the soundscape of Cambridge Bay, especially when there is ice cover.

4.4.4 Relative contributions of different sources

To characterize the contribution of the various sources discussed above, the major components of the soundscape in Cambridge Bay are presented in Figure 4.13. A baseline noise spectrum (purple line in Figure 4.13) was chosen from an ice-covered period with little wind and ice cracking. A five minute averaged noise spectrum from a period that includes the precipitation event shown in Figure 6 is plotted in green in Figure 4.13. These are both relatively quiet periods that have similar characteristics at mid-frequencies between 0.3 and 10 kHz. However, the ice-covered baseline spectrum is higher at the lowest frequencies, peaking at 60 Hz, than the ice-free time with precipitation. Above 10 kHz precipitation adds more noise.

Ice cracking added a moderate amount of noise into the water column during times of ice cover. Here, the period with ice-cracking (blue line in Figure 4.13) occurred 1 April 2015, when 184 cracks were recorded over a five minute period (Table 4.4). This period was louder than the ice-covered baseline period, peaking at ∼90 dB re 1 $\mu Pa^2\ Hz^{-1}$ at 60 Hz. Note, the ice-covered baseline spectrum also peaked around the same value, suggesting another ice-related source of the sound at this frequency. In the frequency band between 0.3-10 kHz, ice-cracking was ∼20 dB louder than the baseline and precipitation periods.

The contributions from both boats and snowmobiles were similar and, by far, the loudest contributors to the soundscape. Although these sources were intermittent, at

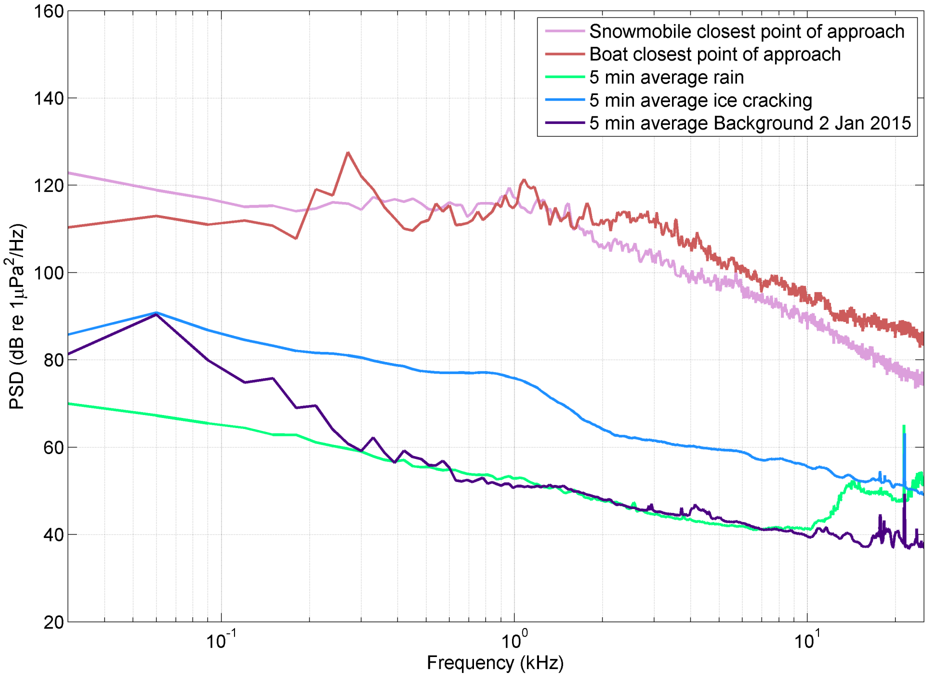

Figure 4.13: Relative contribution by frequency of the major contributors to Cambridge Bay's soundscape. Both the snowmobiles and boat contributions are taken from the closest point of approach of three vehicles averaged together. All others are an average over five minutes.

the closest point of approach both boats and snowmobiles had PSDs above 100 dB re 1 μPa^2 Hz^{-1} at frequencies up to 3 kHz. Above 3 kHz the noise levels begin to drop, but still remain above all the other major contributors to the soundscape. At times these PSDs exceeded 120 dB re 1 μPa^2 Hz^{-1}. The number of vehicles at different times (Figure 4.11) further confirmed that these sources dominated the soundscape at different times of the year especially when there was ice cover.

4.4.5 Comparison to other Arctic soundscapes

Shallow water soundscapes have been considered in many studies but none were found discussing the sound contribution of the passages of snowmobiles on the ice on the soundscape below. Furthermore, before the soundscape of Cambridge Bay can be compared to some of these other sites it is worth noting that environmental conditions, anthropogenic sources and site geometry can be vastly different between sites (Haxel et al., 2013).

Here we will consider the soundscapes of two other Arctic sites. In a study conducted near Sachs Harbour, $\sim$800 km from Cambridge Bay, ambient sound levels were lower during ice cover than during periods without ice. During January to March at this site noise levels dipped below the noise floor of the hydrophones used, that is, $<70 \pm 10$ dB re 1 μPa^2 Hz^{-1} (Insley et al., 2017). In the Beaufort Sea, under-ice noise was found to be $\sim 65 \pm 10$ dB re 1 μPa^2 Hz^{-1} at a frequency of 100 Hz (Kinda et al., 2013). In Cambridge Bay, noise at this frequency was >80 dB re 1 μPa^2 Hz^{-1} for both periods with significant ice cracking and periods with no ice cracking (Figure 4.13 blue and purple spectra) suggesting Cambridge Bay is overall a noisier site.

An acoustic survey of another Arctic location with seasonal ice cover, Fram Strait, was conducted in 2009-2010 (Haver et al., 2017). In general, this site was louder than Cambridge Bay, with median broadband sounds exceeding 100 dB re 1 μPa^2 Hz^{-1}. Like Cambridge Bay, Fram Strait experiences strong seasonal variability, but was found to be quieter in winter than in summer (Haver et al., 2017). In Fram Strait, biological sources, specifically fin whales, were the major reason for the seasonal variability. Although, marine mammals were not observed during the ice free period in Cambridge Bay, the biggest reason for the difference is likely the heavy use of snowmobiles. The anthropogenic source of much of the sound in Cambridge Bay suggests this site may have more in common with heavily trafficked sites in coastal areas despite the high latitude.

Another component that has not been captured in the current soundscape of Cambridge Bay, but is an issue in more southern locations (for example: Garrett et al. (2016)) is the sound of distant shipping. Diachok (1976) noted that scattering under ice prevents sound from propagating long distances, suggesting this is more likely to be present when there is open water. The nearby Dease Strait (Figure 4.1) provides a thoroughfare for transiting the Northwest Passage; as climate change reduces the amount of ice cover, this route may be used more, potentially adding more summer noise to the Cambridge Bay soundscape.

4.5 Conclusion

This may be the first study showing the contribution of snowmobiles to a marine soundscape. In 2015, the soundscape in Cambridge Bay was dominated by anthropogenic noise, which was louder when there was ice cover than during ice free periods. This seasonal variability was a significant factor as the bay was quietest during the ice-break up in July possibly because it was unsafe for both snowmobiles and boats. The ambient sound levels in the bay were driven by ice cover through controlling the types of vehicles using the bay (snowmobiles on ice and boats on open water). Although the observed source levels of both boats and snowmobiles were similar, in 2015 there were in total ten times more snowmobile passages than boats. The abundance of snowmobiles passages relative to boats explains why the bay was louder when there was ice cover.

Over the course of the year, precipitation, wind and ice noise were other important contributors to the underwater soundscape. Biological noise was not a significant sound source and the relationship between wildlife presence and anthropogenic sounds is unknown.

Chapter 5

Conclusion

The objective of this thesis was to gain an understanding of the link between Arctic coastal oceanography and the local soundscape on the detection range of acoustically-tagged fish to give context to biological behaviour recorded. The intent was to do this through determining what oceanographic processes define the underwater environment and what sources dominate the soundscape. Then, by looking at how these physical processes and sounds impact tag effectiveness within this environment.

Here, we explored the oceanographic processes within the Arctic coastal embayment of Cumberland Sound, then evaluated the functionality of passive acoustic fish tracking tags in use there. In the sound, both oceanographic, and acoustic tag range data were collected in situ, and combined with a simple ray-tracing model. Due to reasons external to this project, it became impossible to obtain acoustic recording in Cumberland Sound, so the underwater soundscape of another Arctic coastal site, Cambridge Bay was described.

The following sections highlight the important results.

5.1 Oceanography of Cumberland Sound

Cumberland Sound is a large embayment on the southeast coast of Baffin Island that opens to Davis Strait. The fish population thriving at the deepest depths demonstrate that hypoxic conditions do not exist. Conductivity and temperature verses depth profiles were collected during three summer field seasons (2011-2013) and two moorings were deployed during 2011-2012. Within the sound, salinity increased with increasing depth while water temperature cooled reaching a minimum at roughly 100 m. Below

100 m, the water became both warmer and saltier. Temperature-salinity curves for each year followed a similar pattern, but the entire water column in Cumberland Sound cooled from 2011 to 2012, then warmed through the summer of 2013.

Even though the sound's maximum depth is over a kilometre deeper than its sill, water in the entire sound is well oxygenated. A comparison of water masses within the sound and in Davis Strait shows that, above the sill, the sound is flooded with cold Baffin Island Current water following an intermittent geostrophic flow pattern entering the sound along the north coast and leaving along the south. Below the sill, replenishment is infrequent and includes water from both the Baffin Island Current and the West Greenland Current. Deep water replenishment occurred more frequently on spring tides, especially in the fall of 2011. Although the sound's circulation is controlled by outside currents, internal water modifying processes are presumed to occur such as estuarine flow and wind-driven mixing.

5.2 Detection Range Variability of Passive Acoustic Tags

Passive acoustic tracking is a technique gaining in popularly to quantify fish movement and is being used to make fishery management decisions. Typically, research using this method focuses on detections without fully considering the influence of the environment. In Cumberland Sound there are three species of deep-water fish being currently tracked. Detection ranges obtained through a series of year-long acoustic functionality experiments (range tests) were combined with two-dimensional ray tracing model results to examine the effect of environmental factors on detection ranges. Multi-path signal interference emerged as a major issue interrupting the continuity of detection ranges.

Every receiver has a maximum effective detection range and often a minimum detection range as well. In addition to these constraints, mid-range detection-gaps may also exist due to multi-path interference. Multi-path interference occurs when the geometry allows multiple paths of a tag's transmissions to overlap. The existence of this interference is an issue that can impact every passive acoustic telemetry study in some way as it is a function of how ID are coded, specifically their length, and the geometry combined with environmental conditions of a study site.

Mid-range gaps were observed for all tag types used in this study. It is important to note that site geometry may be different in different directions radiating out from the receiver along the horizontal plane. Additionally, these mid-range gaps, along with the minimum and maximum ranges, may change as oceanographic conditions change. Therefore, range tests may not find these gaps unless a tag is coincidentally deployed at one of these locations. Interpreting detection data without knowledge of detection ranges, especially mid-range gaps could lead to misleading conclusions impacting the validity of any quantitative analysis performed. Ultimately, wrong conclusions may be made about how animals use an area which can potentially lead to inappropriate conservation legislation.

Several options exist to identify and deal with the impact of mid-range detection gaps. Range test tags could be deployed for the duration of the study allowing for identification of mid-range detection gaps after a study is complete. Additionally, overlap between receivers should be designed for an entire study area especially if a quantitative study is planned to determine numbers of fish passing by. Two-dimensional ray tracing models, although somewhat simplistic, incorporate the factors that create multi-path interference. With some basic environmental data (i.e. sound speed profile and bathymetry), the geometries most likely to result in multi-path interference can be identified. A reasonable first step to identify if multi-path interference may be an issue at a site, would be to assume minimal refraction over the range test and calculate travel times for different paths based on straight lines.

5.3 Cambridge Bay Soundscape

Finally, the marine soundscape in Cambridge Bay was evaluated over 2015 and it was found that noise of anthropogenic origin dominated. The site was louder when there was ice cover than during the ice free periods. This seasonal variability was a significant factor as the bay was quietest during the ice-break up in July possibly because it was unsafe for both snowmobiles and boats. The ambient sound levels in the bay were driven by ice cover through controlling the types of vehicles using the bay (snowmobiles on ice and boats on open water). Although the observed source levels of both boats and snowmobiles were similar, in 2015 there were in total ten times more snowmobile passages than boats. The abundance of snowmobiles passages relative to boats explains why the bay was louder when there was ice cover. Over the course of the year, precipitation, wind and ice noise were other important contributors to the underwater soundscape. Biological noise was not found to be a significant sound source.

5.4 Future Directions

The previously undocumented link between the physical environment and the observed variability of detection ranges of passive acoustic tags through multi-path interference will allow biological studies using this technique to better understand their results. A natural followup would be to include impacts of the soundscape on detection ranges.

Although, we were unable to link the soundscape of Cumberland Sound with the range test results, the Cambridge Bay soundscape indicated at how important this connection can be. The Cambridge Bay acoustic data coincided with a range test of the same tags used in Cumberland Sound. Unfortunately, the range test data set proved to be unusable as it was heavily contaminated by a nearby ship running a 50 kHz sonar from May until September. This corrupted range test does prove an important point—sounds within an environment, even when they are not at the exact frequency of the tag used (69 kHz), can profoundly impact the results. This is an area that should be investigated further.

Bibliography

Bacle, J., Carmack, E., and Ingram, R. G. (2002). Water column structure and circulation under the North Water during spring transition: April-July 1998. *Deep-Sea Research II*, 49:4907–4924.

Barber, D. and Massom, R. (2007). *Polynyas: Windows to the world*, chapter The role of sea ice in Arctic and Antarctic polynyas, pages 1–54. Elsevier Oceanographic Series 74.

Barber, D. G. and Hanesiak, J. M. (2004). Meteorological forcing of sea ice concentrations in the southern Beaufort Sea over the period 1979 to 2000. *Journal of Geophysical Research: Oceans*, 109(C6).

Bedard, J. M., Vagle, S., Klymak, J. M., Williams, W. J., Curry, B., and Lee, C. M. (2015). Outside influences on the water column of Cumberland Sound, Baffin Island. *Journal of Geophysical Research: Oceans*, 120:5000–5018.

Bendat, J. S. and Piersol, A. G. (2010). *Random Data: Analysis and Measurement Procedures, 4th Edition*. Wiley Series in Probability and Statistics.

Bittencourt, L., Barbosa, M., Secchi, E., Jr, J. L.-B., and Azevedo, A. (2016). Acoustic habitat of an oceanic archipelago in the Southwestern Atlantic. *Deep Sea Research Part I: Oceanographic Research Papers*, 115:103–111.

Bowlin, J., Spiesberger, J., Duda, T., and Freitag, L. (1992). Ocean Acoustical Ray-Tracing Software RAY. Technical report, Woods Hole Oceanographic Institution Technical Report.

Butler, J., Stanley, J. A., and IV, M. J. B. (2016). Underwater soundscapes in near-shore tropical habitats and the effects of environmental degredation and habitat restoration. *Journal of Experimental Marine Biology and Ecology*, 479:89–96.

Carey, W. M. and Evans, R. B. (2011). *Ocean Ambient Nosie: Measurement and Theory*. Springer Science and Business Media.

Carmack, E. (2007). The alpha/beta ocean distinction: A perspective on freshwater fluxes, convection, nutrients and productivity in high-latitude seas. *Deep-Sea Research II*, 54:2578–2598.

Carmack, E. and Wassmann, P. (2006). Food webs and physical-biological coupling on pan-Arctic shelves: Unifying concepts and comprehensive perspectives. *Progress in Oceanography*, 71:446–477.

Clay, C. and Medwin, H. (1977). *Acoustic Oceanography: Principles and Applications*. John Wiley & Sons, New York.

Clements, S., Jepsen, D., Karnowski, M., and Schrek, C. (2005). Optimization of an acoustic telemetry array for detecting transmitter-implanted fish. *North American Journal of Fisheries Management*, 25:429–436.

Cooke, S., Iverson, S., Stokesbury, M., Hinch, S., Fisk, A., VanderZwaag, D., Apostle, R., and Whoriskey, F. (2011). Ocean Tracking Network Canada: a network approach to addressing critical issues in fisheries and resource management with implications for ocean governance. *Fisheries*, 36 (12):583–592.

Cooper, L., Cota, G., Pomeroy, L., Grebmeier, J., and Whitledge, T. (1999). Modification of NO, PO, and NO/PO during flow across the Bering and Chukchi shelves: Implications for use as Arctic water mass tracers. *Journal of Geophysical Research*, 104(C4):7827–7836.

Crum, L. A., Pumphrey, H. C., Roy, R. A., and Prosperetti, A. (1999). The underwater sounds produced by impacting snowflakes. *The Journal of the Acoustical Society of America*, 106(4):1765–1770.

Cuny, J., Rhines, P., and Kwok, R. (2005). Davis Strait volume, freshwater and heat fluxes. *Deep-Sea Research I*, 52:519–542.

Cuny, J., Rhines, P., Niler, P., and Bacon, S. (2002). Labrador Sea Boundary Currents and the fate of the Irminger Sea Water. *Journal of Physical Oceanography*, 32:627–647.

Curry, B., Lee, C., Petrie, B., Moritz, R., and Kwok, R. (2014). Multiyear Volume, Liquid Freshwater, and Sea Ice Transports through Davis Strait, 2004-10. *Journal of Physical Oceanography*, 44:1244–1266.

Dayton, P., Mordida, B., and Bacon, F. (1994). Polar Marine Communities. *Integrative and Comparative Biology*, 34 (1):90–99.

Dewey, R. (1999). Mooring Design and Dynamics:a Matlab package for designing and analyzing oceanographic moorings. *Marine Models Online*, 1:103–157.

Diachok, O. I. (1976). Effects of sea-ice ridges on sound propagation in the Arctic Ocean. *The Journal of the Acoustical Society of America*, 59(5):1110–1120.

Dunbar, M. (1958). Physical Oceanographic Results of the "Calanus" Expedition in Ungava Bay, Frobisher Bay, Cumberland Sound, Hudson Strait and Northern Hudson Bay, 1949-1955. *Journal of the Fisheries Research Board of Canada*, 15 (2):155–201.

Dupont-Prinet, A., Vagner, M., Chabot, D., and Audet, C. (2013). Impact of hypoxia on the metabolism of Greenland halibut (Reinhardtius hippoglossoides). *Canadian Journal of Fisheries and Aquatic Sciences*, 70:461–469.

Dyer, I. (1984). The song of sea ice and other Arctic Ocean melodies. In Dyer, I. and Chryssostomidis, C., editors, *Arctic Policy and Technology*, pages 11–37. Hemisphere, New York.

Erbe, C. (2002). An algorithm to predict zones of impact on marine mammals around underwater industrial noise. Technical report, Canadian Coast Guard, Central and Arctic Region. pages: 43.

Erbe, C., Verma, A., McCauley, R., Garvilov, A., and Parnum, I. (2015). The marine soundscape of Perth Canyon. *Progress in Oceanography*, 137:38–51.

Farmer, D. M. and Vagle, S. (1988). Observations of high-frequency ambient sound generated by wind. In Kerman, B., editor, *Natural Mechanisms of Surface Generated Noise*, page 639. Kluwer.

Finstad, B., Okland, F., Thornstad, E., Bjorn, P., and McKinley, R. (2005). Migration of hatchery-reared atlantic salmon and wild anadromous brown trout post-smolts in a norwegian fjord system. *Journal of Fish Biology*, 66 (1):86–96.

Fratantoni, P. and Pickart, R. (2007). The Western North Atlantic Shelfbreak Current System in Summer. *Journal of Physical Oceanography*, 37:2509–2533.

Gade, H. G., Lake, R. A., Lewis, E. L., and Walker, E. R. (1974). Oceanography of an Arctic bay. *Deep-Sea Research*, 21:547–571.

Garrett, J. K., Blondel, P., Godley, B. J., Pikesley, S. K., Witt, M. J., and Johanning, L. (2016). Long-term underwater sound measurements in the ship noise indicator bands 63 Hz and 125 Hz from the port of Falmouth Bay, UK. *Marine Pollution Bulletin*, 110:438–448.

Gjelland, K. and Hedger, R. (2013). Environmental influence on transmitter detection probability in biotelemetry: developing a general model of acoustic transmission. *Methods in Ecology and Evolution*, 4:665–674.

Gladish, C., Holland, D., and Lee, C. (2015). Oceanic Boundary Conditions for Jakobshavn Glacier. Part II: Provenance and Sources of Variability of Disko Bay and Ilulissat Icefjord Waters, 1990-2011. *Journal of Physical Oceanography*, 45:33–63.

Greene, C. R. (1995). Ambient noise. In Richardson, W. J., Greene, C. R., Malme, C. I., and Thomson, D. H., editors, *Marine mammals and noise*, pages 87–100. Academic Press, San Diego.

Greene, C. R. and Buck, B. M. (1977). Arctic noise measurement experiments using Nimbus 6 data buoys. *U. S. Navy Journal of Underwater Acoustics*, 27:827–838.

Hamilton, J. and Wu, Y. (2013). Canadian Technical Report of Hydrography and Ocean Science 282: synopsis and trends in the physical environment of Baffin Bay and Davis Strait. Technical report, Ocean and Ecosystem Sciences Division, Maritimes Region, Fisheries and Oceans Canada.

Hannah, C., Dupont, F., Collins, A., Dunphy, M., and Greenberg, D. (2008). Revisions to a modelling system for tides in the Canadian Arctic Archipelago. *Canadian Technical Report of Hydrography and Ocean Science*, 259:1–62.

Haver, S. M., Klinck, H., Nieukirk, S. L., Matsumoto, H., Dziak, R. P., and Miksis-Olds, J. L. (2017). The not-so-silent world: Measuring Arctic, Equatorial, and Antarctic soundscapes in the Atlantic Ocean. *Deep Sea Research Part I: Oceanographic Research Papers*, 122:95–104.

Haxel, J. H., Dziak, R. P., and Matsumoto, H. (2013). Observations of shallow water marine ambient sound: The low frequency underwater soundscape of the central Oregon coast. *The Journal of the Acoustical Society of America*, 133(5):2586–2596.

Heupel, M., Reiss, K., Yeiser, B., and Simpfendorfer, C. (2008). Effects of biofouling on performance of moored data logging acoustic receivers. *Limnology and Oceanography: Methods*, 6:327–335.

Heupel, M., Semmens, J., and Hobday, A. (2006). Automated acoustic tracking of aquatic animals: scales, design and deployment of listening station arrays. *Marine and Freshwater Research*, 57 (1):1–13.

Hofmann, A., Peltzer, E., Walz, P., and Brewer, P. (2011). Hypoxia by degrees: Establishing definitions for a changing ocean. *Deep-Sea Research I*, 58:1212–1226.

How, J. and de Lestang, S. (2012). Acoustic tracking: issues affecting design, analysis and interpretation of data from movement studies. *Marine & Freshwater Research*, 63:312–324.

Hu, X. and Myers, P. (2013). A Lagrangian view of Pacific water inflow pathways in the Arctic Ocean during model spin-up. *Ocean Modelling*, 71:66–80.

Hussey, N., Kessel, S., Aarestrup, K., Cooke, S., Cowley, P., Fisk, A., Harcourt, R., Holland, K., Iverson, S., Kocik, J., Flemming, J. M., and Whoriskey, F. (2015). Aquatic animal telemetry: A panoramic window into the underwater world. *Science*, 348 (6240).

Huveneers, C., Simpfendorfer, C., Kim, S., Semmens, J., Hobday, A., Pederson, H., Stieglitz, T., Vallee, R., Webber, D., Heupel., M., Peddermors, V., and Harcourt, R. (2016). The influence of environmental parameters on the performance and detection range of acoustic receivers. *Ecology and Evolution*, 7(7):825–835.

Insley, S. J., Halliday, W. D., and de Jong, T. (2017). Seasonal Patterns in Ocean Ambient Noise near Sachs Harbour, Northwest Territories. *Arctic*, 70(3):239–248.

Jones, E., Anderson, L., and Swift, J. (1998). Distribution of Atlantic and Pacific waters in the upper Arctic Ocean: Implications for circulation. *Geophysical Research Letters*, 25(6):765–768.

Jones, E., Swift, J., Anderson, L., Lipizer, M., Civitarese, G., Falkner, K., Kattner, G., and McLaughlin, F. (2003). Tracing Pacific water in the North Atlantic Ocean. *Journal of Geophysical Research*, 108 (C4).

Kalnay, E., Kanamitsu, M., Kistler, R., Collings, W., Deaven, D., Gandin, L., Iredell, M., Saha, S., White, G., Woollen, J., Zhu, Y., Chelliah, M., Ebisuzaki, W., Higgins, W., Janowiak, J., Mo, K., Ropelewski, C., Wang, J., Leetmaa, A., Reynolds, R., Jenne, R., and Joseph, D. (1996). The NCEP/NCAR 40-Year Reanalysis Project. *Bulletin of the American Meteorological Society*, pages 427–471.

Kessel, S., Cooke, S., Heupel, M., Hussey, N., Simpfendorfer, C., Vagel, S., and Fisk, A. (2013). A review of detection range testing in aquatic passive acoustic telemetry studies. *Reviews in Fish Biology and Fisheries*. online only.

Kessel, S., Hussey, N., Webber, D., Gruber, S., Young, J., Smale, M., and Fisk, A. (2015). Close proximity detection interference with acoustic telemetry: the importance of considering tag power output in low ambient noise environments. *Animal Biotelemetry*, 3:5.

Kinda, G. B., Simard, Y., Gervaise, C., Mars, J. I., d'Heres, M., and Fortier, L. (2013). Under-ice ambient noise in Eastern Beaufort Sea, Canadian Arctic, and its relation to environmental forcing. *The Journal of the Acoustical Society of America*, 134(77):77–87.

Kumlien, L. (1879). *Contributions to the Natural History of Arctic America, Made in Connection with the Howgate Polar Expedition, 1877-78*. Bulletin of the United States National Museum. Washington, D.C.

Lennox, R. J., Aarstrup, K., Cooke, S. J., Cowley, P. D., Deng, Z. D., Fisk, A. T., Harcourt, R. G., Heupel, M., Hinch, S. G., Holland, K. N., Hussey, N. E., Iverson, S. J., Kessel, S. T., Kocik, J. F., Lucas, M. C., Flemming, J. M., Nguyen, V. M., Stokesbury, M. J. W., Vagle, S., Vanderzwaag, D. L., Whoriskey, F. G., and Young, N. (2017). Envisioning the future of aquatic animal tracking: Technology, science, and application. *BioScience*, 67:884–896.

Lewis, J. K. and Denner, W. W. (1987). Arctic ambient noise in the Beaufort Sea: Seasonal space and time scales. *Journal of the Acoustical Society of America*, 82(3):988–997.

Lillis, A., Eggleston, D. B., and Bohnenstiehl, D. R. (2014). Estuarine soundscapes: distinct acoustic characteristics of oyster reef compared to soft-bottom habitats. *Marine Ecology*, 505:1–17.

Lique, C., Treguier, A., Blanke, B., and Grima, N. (2010). On the origins of water masses exported along both sides of Greenland: A Lagrangian model analysis. *Journal of Geophysical Research*, 115:C05019.

Luczkovich, J. J., Mann, D. A., and Rountree, R. A. (2008). Passive acoustics as a tool in fisheries science. *Transactions of the American Fisheries Society*, 137(2):533–541.

Makris, N. C. and Dyer, I. (1991). Environmental correlates of Arctic ice-edge noise. *The Journal of the Acoustical Society of America*, 90(6):3288–3298.

McLaughlin, F., Carmak, E., Ingram, R., Williams, W., and Michel, C. (2004). *The Sea, Volume 14*, chapter Oceanography of the Northwest Passage, pages 1211–1242. Harvard University Press.

Medwin, H. and Clay, C. (1998). *Fundamentals of Acoustical Oceanography.*

Melling, H. (2002). Sea ice of the northern Canadian Arctic Archipelago. *Journal of Geophysical Research*, 107 (C11).

Melnychuk, M. and Walters, C. (2010). Estimating detection probabilities of tagged fish migrating past fixed receiver stations using only local information. *Canadaian Journal of Fisheries and Aquatic Sciences*, 67:641–658.

Merchant, N. D., Pirotta, E., and Thompson, T. R. (2014). Monitoring ship noise to assess the impact of coastal developments on marine mammals. *Marine Pollution Bulletin*, 78(1-2):85–95.

Michel, C., Ingram, R., and Harris, L. (2006). Variability in oceanographic and ecological processes in the Canadian Arctic Archipelago. *Progress in Oceanography*, 71:379–401.

Milne, A. R. (1972). Thermal tension cracking in sea ice: A source of under-ice noise. *Journal of Geophysical Research*, 77:2177–2192.

Milne, A. R., Ganton, J. H., and McMillin, D. J. (1967). Ambient noise under sea ice and further measurements of wind and temperature dependence. *The Journal of the Acoustical Society of America*, 41.

Myers, P., Donnelly, C., and Ribergaard, M. (2009). Structure and variability of the West Greenland Current in Summer derived from 6 repeat standard sections. *Progress in Oceanography*, 80:93–112.

Myers, P. and Ribergaard, M. (2013). Warming of the Polar Water Layer in Disko Bay and Potential Impact on Jakobshavn Isbrae. *Journal of Physical Oceanography*, 43:2629–2640.

Nystuen, J. A. (1986). Rainfall measurements using underwater ambient noise. *The Journal of the Acoustical Society of America*, 79:972–982.

Ottera, H. and Skilbrei, O. (2016). Influence of depth, time and human activity on detection rate of acoustic tags: a case study on two fish farms. *Journal of Fish Biology*, 88:1229–1235.

Payne, N., Gillanders, B., Webber, D., and Semmens, J. (2010). Interpreting dial activity patterns from acoustic telemetry: the need for controls. *Marine Ecology Progress Series*, 419:295–301.

Peklova, I., Hussey, N., Hedges, K., Treble, M., and Fisk, A. (2012). Depth and temperature preferences of the deepwater flatfish Greenland halibut Reinhardtius hippoglossoides in an Arctic marine ecosystem. *Marine Ecology Progress Series*, 467:193–205.

Pieretti, N., Martire, M. L., Farina, A., and Danovaro, R. (2017). Marine soundscape as an additional biodiversity monitoring tool: A case study from the Adriatic Sea (Mediterranean Sea). *Ecological Indicators*, 83:13–20.

Prinsenberg, S. and Bennett, E. (1989). Vertical Variations of Tidal Currents in Shallow Land Fast Ice-Covered Regions. *Journal of Physical Oceanography*, 19:1268–1278.

Pritchard, R. S. (1984). Arctic Ocean background noise caused by ridging of sea ice. *The Journal of the Acoustical Society of America*, 75(2):419–427.

Rignot, E., Velicogna, I., van der Broke, M., Monaghan, A., and Lenerts, J. (2011). Acceleration of the contribution of the Greenland and Antarctic ice sheets to sea level rise. *Geophysical R*, 38:L05503.

Rountree, R. A., Gilmore, R. G., Goudey, C. A., Hawkins, A. D., Luczkovich, J. J., and Mann, D. A. (2006). Listening to fish. *Fisheries*, 31(9):433–446.

Rudels, B. (2012). Arctic Ocean circulation and variability - advection and external forcing encounter constraints and local processes. *Ocean Science*, 8:261–286.

Sanchez-Gendriz, I. and Padovese, L. R. (2016). Underwater soundscape of marine protected areas in the south Brazilian coast. *Marine Pollution Bulletin*, 105:65–72.

Scott, W. and Scott, M. (1988). *Atlantic Fishes of Canada*. Canadian Bulletin of Fisheries and Aquatic Sciences No. 219.

Simpfendorfer, C., Heupel, M., and Collins, A. (2008). Variation in the performance of acoustic receivers and its implication for positioning algorithms in a riverine setting. *Canadian Journal of Fisheries and Aquatic Sciences*, 65:482–492.

Simpfendorfer, C., Huveneers, C., Steckenreuter, A., Tattersall, K., Hoenner, X., Harcourt, R., and Heupel, M. (2015). Ghosts in the data: false detection in VEMCO pulse position modulation acoustic telemetry monitoring equipment. *Animal Biotelemetry*, 3:55.

Singh, L., Downey, N., Roberts, M., Webber, D., Smale, M., van den Berg, M., Harding, R., Engelbrecht, D., and Blows, B. (2009). Design and calibration of an acoustic telemetry system subject to upwelling events. *African Journal of Marine Science*, 31 (1):355–364.

Staaterman, E., Rice, A. N., Mann, D. A., and Paris, C. B. (2013). Soundscapes from a Tropical Eastern Pacific reef and a Caribbean Sea reef. *Coral Reefs*, 32:553.

Steiner, N., Azetsu-Scott, K., Galbraith, P., Hamilton, J., Hedges, K., Hu, X., Janjua, M., Lambert, N., Larouche, P., Lavoie, D., Loder, J., Melling, H., Merzouk, A., Meyers, P., Perrie, W., Peterson, I., Pettipas, R., Scarratt, M., Sou, T., Starr, M., Tallmann, R., and van der Baaren, A. (2013). Climate Change Assessment in the Arctic Basin Part 1: Trends and Projections - A Contribution to the Aquatic Climate Change Adaptation Services Program. Technical report, Fisheries and Oceans Canada, Science Branch, Pacific Region.

Straneo, F. and Saucier, F. (2008). The outflow from Hudson Strait and its contribution to the Labrador Current. *Deep-Sea Research I*, 55:926–946.

Tang, C., Ross, C., Yao, T., Petrie, B., DeTracey, B., and Dunlap, E. (2004). The circulation, water masses and sea-ice of Baffin Bay. *Progress in Oceanography*, 63:183–228.

Tasker, M. L., Amundin, M., Andre, M., Hawkins, A., Lang, W., Merck, T., Scholik-Schlomer, A., Teilmann, J., Thomsen, F., Werner, S., and Zakharia, M. (2010). Marine Strategy Framework Directive. Task Group 11 Report - Underwater noise and other forms of energy. Technical report, Institue for Environment and Sustainabiliy.

Thomas, D. N., Fogg, G. E., Convey, P., Fritsen, C. H., Gili, J. M., Gradinger, R., Laybourn-Parry, J., Reid, K., and Walton, D. W. H. (2008). *The Biology of Polar Regions*. Oxford University Press.

Thorstad, E., Okland, F., Rowsell, D., and McKinley, R. (2000). A system for automated recording of fish tagged with coded acoustic transmitters. *Fisheries Management and Ecology*, 7 (4):281–294.

Tully, J. P. (1952). Oceanographic Data of the Western Canadian Arctic Region, 1935-37. *Journal of Fisheries Research Board of Canada*, 8(5):378–382.

Udyawer, V., Chin, A., Knip, D., Simpfendorfer, C., and Heupel, M. (2013). Variable response of coastal sharks to severe tropical storms; environmental cues and changes in space use. *Marine Ecology Progress Series*, 480:171–183.

Urick, R. J. (1983). *Principles of Underwater Sound*. McGraw-Hill, New York.

Vagle, S., Large, W. G., and Farmer, D. M. (1990). An Evaluation of the WOTAN Technique of Inferring Oceanic Winds from Underwater Ambient Sound. *Journal of Atmospheric and Oceanic Technology*, 7:576–595.

Wenz, G. M. (1962). Acoustic Ambient Noise in the Ocean: Spectra and Sources. *The Journal of the Acoustical Society of America*, 34(12):1936–1956.

Williams, R., Wright, A. J., Ashe, E., Blight, L. K., Bruintjes, R., Canessa, R., Clark, C. W., Cullis-Suzuki, S., Dakin, D. T., Erbe, C., Hammond, P. S., Merchant, N. D. N. D., O'Hara, P. D., Purser, J., Radford, A. N., Simpson, S. D., Thomas, L., and Wale, M. A. (2015). Impact of anthropogenic noise on marine life: Publication patterns, new discoveries, and future directions in research and management. *Ocean & Coastal Management*, 115:17–24.